IAEA HUMAN HEALTH REPORTS No. 9

Quantitative Nuclear Medicine Imaging: Concepts, Requirements and Methods

IAEA
International Atomic Energy Agency

IAEA HUMAN HEALTH SERIES PUBLICATIONS

The mandate of the IAEA human health programme originates from Article II of its Statute, which states that the "Agency shall seek to accelerate and enlarge the contribution of atomic energy to peace, health and prosperity throughout the world". The main objective of the human health programme is to enhance the capabilities of IAEA Member States in addressing issues related to the prevention, diagnosis and treatment of health problems through the development and application of nuclear techniques, within a framework of quality assurance.

Publications in the IAEA Human Health Series provide information in the areas of: radiation medicine, including diagnostic radiology, diagnostic and therapeutic nuclear medicine, and radiation therapy; dosimetry and medical radiation physics; and stable isotope techniques and other nuclear applications in nutrition. The publications have a broad readership and are aimed at medical practitioners, researchers and other professionals. International experts assist the IAEA Secretariat in drafting and reviewing these publications. Some of the publications in this series may also be endorsed or co-sponsored by international organizations and professional societies active in the relevant fields.

There are two categories of publications in this series:

IAEA HUMAN HEALTH SERIES

Publications in this category present analyses or provide information of an advisory nature, for example guidelines, codes and standards of practice, and quality assurance manuals. Monographs and high level educational material, such as graduate texts, are also published in this series.

IAEA HUMAN HEALTH REPORTS

Human Health Reports complement information published in the IAEA Human Health Series in areas of radiation medicine, dosimetry and medical radiation physics, and nutrition. These publications include reports of technical meetings, the results of IAEA coordinated research projects, interim reports on IAEA projects, and educational material compiled for IAEA training courses dealing with human health related subjects. In some cases, these reports may provide supporting material relating to publications issued in the IAEA Human Health Series.

All of these publications can be downloaded cost free from the IAEA web site:

http://www.iaea.org/Publications/index.html

Further information is available from:

Marketing and Sales Unit
International Atomic Energy Agency
Vienna International Centre
PO Box 100
1400 Vienna, Austria

Readers are invited to provide their impressions on these publications. Information may be provided via the IAEA web site, by mail at the address given above, or by email to:

Official.Mail@iaea.org.

QUANTITATIVE NUCLEAR MEDICINE IMAGING: CONCEPTS, REQUIREMENTS AND METHODS

The following States are Members of the International Atomic Energy Agency:

AFGHANISTAN
ALBANIA
ALGERIA
ANGOLA
ARGENTINA
ARMENIA
AUSTRALIA
AUSTRIA
AZERBAIJAN
BAHRAIN
BANGLADESH
BELARUS
BELGIUM
BELIZE
BENIN
BOLIVIA
BOSNIA AND HERZEGOVINA
BOTSWANA
BRAZIL
BULGARIA
BURKINA FASO
BURUNDI
CAMBODIA
CAMEROON
CANADA
CENTRAL AFRICAN REPUBLIC
CHAD
CHILE
CHINA
COLOMBIA
CONGO
COSTA RICA
CÔTE D'IVOIRE
CROATIA
CUBA
CYPRUS
CZECH REPUBLIC
DEMOCRATIC REPUBLIC OF THE CONGO
DENMARK
DOMINICA
DOMINICAN REPUBLIC
ECUADOR
EGYPT
EL SALVADOR
ERITREA
ESTONIA
ETHIOPIA
FIJI
FINLAND
FRANCE
GABON
GEORGIA
GERMANY
GHANA
GREECE
GUATEMALA
HAITI
HOLY SEE
HONDURAS
HUNGARY
ICELAND
INDIA
INDONESIA
IRAN, ISLAMIC REPUBLIC OF
IRAQ
IRELAND
ISRAEL
ITALY
JAMAICA
JAPAN
JORDAN
KAZAKHSTAN
KENYA
KOREA, REPUBLIC OF
KUWAIT
KYRGYZSTAN
LAO PEOPLE'S DEMOCRATIC REPUBLIC
LATVIA
LEBANON
LESOTHO
LIBERIA
LIBYA
LIECHTENSTEIN
LITHUANIA
LUXEMBOURG
MADAGASCAR
MALAWI
MALAYSIA
MALI
MALTA
MARSHALL ISLANDS
MAURITANIA
MAURITIUS
MEXICO
MONACO
MONGOLIA
MONTENEGRO
MOROCCO
MOZAMBIQUE
MYANMAR
NAMIBIA
NEPAL
NETHERLANDS
NEW ZEALAND
NICARAGUA
NIGER
NIGERIA
NORWAY
OMAN
PAKISTAN
PALAU
PANAMA
PAPUA NEW GUINEA
PARAGUAY
PERU
PHILIPPINES
POLAND
PORTUGAL
QATAR
REPUBLIC OF MOLDOVA
ROMANIA
RUSSIAN FEDERATION
RWANDA
SAN MARINO
SAUDI ARABIA
SENEGAL
SERBIA
SEYCHELLES
SIERRA LEONE
SINGAPORE
SLOVAKIA
SLOVENIA
SOUTH AFRICA
SPAIN
SRI LANKA
SUDAN
SWAZILAND
SWEDEN
SWITZERLAND
SYRIAN ARAB REPUBLIC
TAJIKISTAN
THAILAND
THE FORMER YUGOSLAV REPUBLIC OF MACEDONIA
TOGO
TRINIDAD AND TOBAGO
TUNISIA
TURKEY
UGANDA
UKRAINE
UNITED ARAB EMIRATES
UNITED KINGDOM OF GREAT BRITAIN AND NORTHERN IRELAND
UNITED REPUBLIC OF TANZANIA
UNITED STATES OF AMERICA
URUGUAY
UZBEKISTAN
VENEZUELA
VIET NAM
YEMEN
ZAMBIA
ZIMBABWE

The Agency's Statute was approved on 23 October 1956 by the Conference on the Statute of the IAEA held at United Nations Headquarters, New York; it entered into force on 29 July 1957. The Headquarters of the Agency are situated in Vienna. Its principal objective is "to accelerate and enlarge the contribution of atomic energy to peace, health and prosperity throughout the world".

IAEA HUMAN HEALTH REPORTS No. 9

QUANTITATIVE NUCLEAR MEDICINE IMAGING: CONCEPTS, REQUIREMENTS AND METHODS

INTERNATIONAL ATOMIC ENERGY AGENCY
VIENNA, 2014

COPYRIGHT NOTICE

Marketing and Sales Unit, Publishing Section
International Atomic Energy Agency
Vienna International Centre
PO Box 100
1400 Vienna, Austria
fax: +43 1 2600 29302
tel.: +43 1 2600 22417
email: sales.publications@iaea.org
http://www.iaea.org/books

Printed by the IAEA in Austria
January 2014
STI/PUB/1605

IAEA Library Cataloguing in Publication Data

Quantitative nuclear medicine imaging : concepts, requirements and methods. — Vienna : International Atomic Energy Agency, 2014.
p. ; 24 cm. — (IAEA human health series, ISSN 2074–7667 ; no. 9)
STI/PUB/1605
ISBN 978–92–0–141510–3
Includes bibliographical references.

1. Nuclear medicine. 2. Imaging systems in medicine. 3. Radioisotopes — Therapeutic use. 4. Cancer — Imaging. I. International Atomic Energy Agency. II. Series.

IAEAL 13–00857

FOREWORD

The absolute quantification of radionuclide distribution has been a goal since the early days of nuclear medicine. Nevertheless, the apparent complexity and sometimes limited accuracy of these methods have prevented them from being widely used in important applications such as targeted radionuclide therapy or kinetic analysis. The intricacy of the effects degrading nuclear medicine images and the lack of availability of adequate methods to compensate for these effects have frequently been seen as insurmountable obstacles in the use of quantitative nuclear medicine in clinical institutions. In the last few decades, several research groups have consistently devoted their efforts to the filling of these gaps. As a result, many efficient methods are now available that make quantification a clinical reality, provided appropriate compensation tools are used. Despite these efforts, many clinical institutions still lack the knowledge and tools to adequately measure and estimate the accumulated activities in the human body, thereby using potentially outdated protocols and procedures.

The purpose of the present publication is to review the current state of the art of image quantification and to provide medical physicists and other related professionals facing quantification tasks with a solid background of tools and methods. It describes and analyses the physical effects that degrade image quality and affect the accuracy of quantification, and describes methods to compensate for them in planar, single photon emission computed tomography (SPECT) and positron emission tomography (PET) images. The fast paced development of the computational infrastructure, both hardware and software, has made drastic changes in the ways image quantification is now performed. The measuring equipment has evolved from the simple blind probes to planar and three dimensional imaging, supported by SPECT, PET and hybrid equipment. Methods of iterative reconstruction have been developed to allow for more consistent compensation for physical effects and imaging system limitations. On these grounds, quantitative imaging is now a broad field of work for the scientific community, and its current translation to the clinical environment can be undertaken with confidence, for better and more accurate diagnostic and therapeutic applications using consistent and well validated protocols.

This publication complements previous efforts of the IAEA related to activity measurement and quantification. The quantitative measurement of tissues and other biological samples is addressed in Technical Reports Series No. 454. The quality control requirements of current PET and SPECT imaging equipment are addressed in IAEA Human Health Series No. 1 and No. 6, respectively. This report does not cover the fields addressed by these publications.

The IAEA gratefully acknowledges the special contribution of the drafting committee, including I. Buvat (France), E.C. Frey (United States of America), A.J. Green (United Kingdom) and M. Ljungberg (Sweden). The IAEA officers responsible for this publication were S. Palm and G.L. Poli of the Division of Human Health.

EDITORIAL NOTE

This report does not address questions of responsibility, legal or otherwise, for acts or omissions on the part of any person.

Although great care has been taken to maintain the accuracy of information contained in this publication, neither the IAEA nor its Member States assume any responsibility for consequences which may arise from its use.

The use of particular designations of countries or territories does not imply any judgement by the publisher, the IAEA, as to the legal status of such countries or territories, of their authorities and institutions or of the delimitation of their boundaries.

The mention of names of specific companies or products (whether or not indicated as registered) does not imply any intention to infringe proprietary rights, nor should it be construed as an endorsement or recommendation on the part of the IAEA.

The authors are responsible for having obtained the necessary permission for the IAEA to reproduce, translate or use material from sources already protected by copyrights.

The IAEA has no responsibility for the persistence or accuracy of URLs for external or third party Internet web sites referred to in this book and does not guarantee that any content on such web sites is, or will remain, accurate or appropriate.

CONTENTS

1. INTRODUCTION 1

2. QUANTITATIVE TASKS 1

2.1. Quantitative indices 2
2.1.1. Counts 2
2.1.2. Relative quantification from count ratios 2
2.1.3. Activity 3
2.1.4. Activity concentration 3
2.1.5. Per cent injected activity 3
2.1.6. Functional and metabolically active volumes 3
2.1.7. SUV 4
2.1.8. Kinetic parameters 4
2.2. Reliability of quantitative measures 5
2.2.1. Accuracy 5
2.2.2. Precision 5
2.2.3. Root mean square error 6
2.3. Common issues affecting quantitative imaging 6
2.3.1. Natural background 6
2.3.2. Radioactive decay 6
2.3.3. Noise 7
2.3.4. Photon attenuation 8
2.3.5. Scatter 9
2.3.6. Motion 10
2.3.7. Resolution and partial volume 11
2.3.8. Count rate problems 13
2.3.9. Recovery of 3-D information 15
2.3.10. Region and volume definition 18
2.3.11. Calibration 18
2.4. Validation 18

3. QUANTIFICATION WITH WHOLE BODY PROBES 19

3.1. Background 19
3.2. Radioactive decay 19
3.3. Noise 19
3.4. Attenuation 19
3.5. Scatter 20
3.6. Motion 20
3.7. Resolution and partial volume 20
3.8. Recovery of 3-D information 20
3.9. Count rate problems 20
3.10. Calibration 20

4. QUANTITATIVE PLANAR IMAGING 21

4.1. Collimator selection 21
4.2. Attenuation correction 22
4.2.1. Patient thickness 22
4.2.2. Transmission measurement 22
4.3. Scatter 24
4.3.1. Effective attenuation coefficient 24
4.3.2. Energy window based scatter correction methods 24
4.3.3. The buildup function method 25
4.4. Resolution and partial volume 26
4.5. Recovery of 3-D information 26
4.6. Count rate problem 26
4.7. Noise 27
4.8. Region and volume definition 27
4.9. Motion 27
4.10. Calibration 27

5. QUANTITATIVE SPECT OR SPECT/CT IMAGING 27

5.1. Tomographic reconstruction 27
5.2. Photon attenuation 28
5.3. Scatter 30
5.4. Resolution and partial volume 32
5.5. Resolution compensation 33
5.6. Partial volume correction 34
5.7. Recovery of 3-D information 35
5.8. Count rate problems 35
5.9. Noise 35
5.10. Region and volume definition 36
5.11. Motion 36
5.12. Calibration 36

6. QUANTITATIVE PET OR PET/CT IMAGING 38

6.1. Tomographic reconstruction 39
6.2. Photon attenuation 40
6.3. Scatter 42
6.4. Resolution and partial volume 43
6.5. Recovery of 3-D information 43
6.6. Count rate problems 43
6.7. Noise 44
6.8. Region and volume definition 44
6.9. Motion 45
6.10. Calibration 47

7. QUANTITATIVE IMAGING PROTOCOLS 47

7.1. Need for protocols 47
7.2. Expertise and training requirements 47
7.2.1. Specification 47
7.2.2. Execution 48

7.3. Elements 48
7.3.1. Procedural 48
7.3.2. Technical 48
7.3.3. Quality assurance and quality control 49
7.4. Validation 49

REFERENCES 51

ABBREVIATIONS 59
CONTRIBUTORS TO DRAFTING AND REVIEW 61

1. INTRODUCTION

Over the past 15 years, there has been a great deal of progress in the development of methods for accurately quantifying nuclear medicine images. However, propagation of these methods into clinics has been slow. The purpose of this publication is to review the state of the art in image quantification and provide a background for medical physicists and physicians who wish to quantify activity distributions of radiopharmaceuticals used in nuclear medicine. While this publication is largely self-contained, some understanding of basic nuclear medicine physics concepts is assumed.

Nuclear medicine images can be used for either detection tasks, such as identifying perfusion defects, or quantitative tasks, such as estimating ejection fraction, standardized uptake values (SUVs) or organ absorbed dose. Obtaining images that are suitable for quantitative tasks often requires additional processing compared with those used for visual interpretation. This additional processing often results in improved resolution and contrast and reduced artefacts. These improvements in the image will often, but not always, translate directly to improved performance on detection tasks. For example, the development of attenuation correction methods for cardiac single photon emission computed tomography (SPECT) has improved detection of myocardial perfusion defects, while at the same time providing images which are quantitatively more accurate.

Many current applications that involve quantification of nuclear medicine images use relative quantification only. These applications often involve ratios of image intensity values. The underlying assumption is that the effects of physical factors such as attenuation and scatter cancel out. In reality, this assumption often does not hold. This is because the magnitudes of these physical factors are both spatially varying and patient dependent. Computing relative values from images that have been processed to provide improved quantification will result in reduced spatial variance and patient dependence, even for applications where relative quantification is sufficient.

Another advantage of using images that are quantitative in an absolute sense is to provide improved consistency. For example, some diagnostic procedures involve the use of diagnostic thresholds derived from normal databases; absolute quantification in creation and use of these databases will ensure that reference values derived from databases are consistent across centres, imaging equipment and time, and are independent of patient variability.

In addition to the potential for improving image quality and relative quantification, there are several applications of nuclear medicine that require images that are quantitatively accurate in an absolute sense. Two such increasingly important applications are targeted radiotherapy treatment planning and advanced kinetic analysis.

Achieving absolute quantification requires appropriate equipment, software and human resources. The level of these requirements depends on the imaging task. For example, quantifying activity in a tumour in the lungs requires more sophisticated resources than quantifying whole body activity. However, detailed knowledge of the requisite levels of resources is not widely available or appreciated.

This publication is organized as follows: in Section 2, the quantitative tasks encountered in nuclear medicine imaging are explored, together with figures of merit that can be used to characterize the reliability of quantification. The common issues affecting quantification accuracy are also reviewed. Sections 3, 4, 5 and 6 then address in detail quantification issues when attempting quantification using whole body probes, planar imaging, SPECT or SPECT/CT (the latter refers to a SPECT scanner used with a conventional computed tomography scanner) and PET or PET/CT, respectively. Section 7 discusses the need for quantification protocols and the requirements to put them into practice.

This publication uses a number of acronyms and abbreviations. While these are introduced in the text, a list of all the acronyms and abbreviations used is provided at the end of this publication.

2. QUANTITATIVE TASKS

The term ‘quantitative measurement’ is open to different interpretations in different contexts. This publication is concerned with how we can determine numerical values (relative or absolute) for the uptake or distribution of radionuclides in patients. The list below may not be exhaustive but demonstrates the range of meanings seen in the literature.

2.1. QUANTITATIVE INDICES

In all nuclear medicine studies, the aim is to answer a clinically relevant question for a particular patient. Many different types of question can be asked, and the need for compensation methods and postprocessing methods is therefore highly dependent on the question and thus on the type of answer required. Answering these questions involves using the information obtained from the nuclear medicine procedure to perform a task.

There are two general classes of tasks: classification and quantitative tasks. Classification tasks involve placing the patient into one of several discrete classes. The most basic classification task is a detection or binary classification task where patients are placed in one of two groups. For example, in fluorodeoxyglucose (FDG) PET cancer imaging, patients are identified as having cancerous or benign tumours based on FDG metabolism in the tumour. Some classification tasks involve more than two diagnostic classes: rest–stress myocardial perfusion imaging patients are identified as having normal perfusion or fixed or reversible perfusion defects.

Quantitative tasks, on the other hand, involve extracting a numerical value or values from data obtained in a nuclear medicine procedure. Examples and definitions of important quantitative tasks are given below, and they include the SUV in FDG imaging, the total activity in an organ or tumour or object of interest, the ejection fraction in the heart and the transit time through the stomach.

Classification tasks often, but not always, involve the qualitative interpretation of information obtained from nuclear medicine procedures. Qualitative interpretation means that an observer uses experience or other knowledge to evaluate the information and make the classification decision. Classification tasks can, however, be performed on the basis of quantitative values obtained from images: for example, in the diagnosis of cancer based on a strict SUV threshold.

The focus of this publication is on quantitative tasks. As a result, issues important in qualitative interpretation of images or the subsequent use of quantitative values to perform classification are not addressed.

A variety of types of quantitative values can be extracted from nuclear medicine images. This section provides a basic description of these values.

2.1.1. Counts

In non-imaging (probe) measurements, a counter attached to the probe sums the number of photons detected in a time interval. Total counts or counts per second are generally recorded.

In planar single photon imaging, the numbers of photons detected by a scintillation camera as falling inside the defined acceptance energy window at a position corresponding to a pixel in the image are termed ‘counts’. By analogy, the signal intensity of photons assigned to each voxel in a non-calibrated reconstructed image is often termed ‘number of counts’. However, this is a poor choice of terminology since the values are not directly counted. This is especially true when various compensations are applied in the process of generating the image.

2.1.2. Relative quantification from count ratios

The number of counts in a certain area in the image is calculated for a region of interest (ROI) or volume of interest (VOI) defined by the user. The sum of the counts is assumed to be a proportional measure of a clinically relevant factor.

2.1.2.1. ROIs in a single image

Count ratios for several ROIs can be used to detect differences in activity uptakes. An example is the comparison of activity uptake between the left and right kidneys.

2.1.2.2. ROIs over time

Activity uptake over time (dynamic studies) can be important in addressing the biokinetics of a particular organ or tissue. It is assumed that a normal tissue follows a certain time–activity curve (TAC) and that a change in the shape of the curve reveals clinically relevant changes in the functional behaviour of the organ. In many cases, it is assumed that the physical issues discussed below cancel out, but this is not always the case. For example, the left

and right kidneys may be located at different depths and the count difference therefore may not only be a function of the activity uptake. Examples are the determination of differential kidney clearance and dosimetric studies to obtain cumulated activity over a time period.

2.1.2.3. Comparison to normal database

Counts in ROIs can be compared with corresponding data from ROIs in images of patients that have been classified as normal based on other independent methods. Examples of studies using normal databases are the scoring of myocardial perfusion defects and regional cerebral blood flow measurements. It is important here that the particular patient study is measured using the same conditions as were used when creating the normal database.

2.1.3. Activity

Activity is a measure of the number of nuclear transformations occurring per unit of time. According to the International System of Units (SI), the unit for activity is the becquerel (Bq), defined as one transition per second, and is measured in reciprocal seconds (s^{-1}). The older standard, the curie (Ci), is still in common usage and 1 Ci = 3.7×10^{10} Bq. The goal of quantitative nuclear medicine is to determine the absolute activity in a given volume, e.g. a patient, an organ or a tumour, or per unit volume (e.g. kBq/mL), by external measurement of the radiation emitted by the patient.

If a parallel hole collimator is used, then the measured count rate of a radioactive source located in air and within the field of view of the camera is independent of the source-to-collimator distance. This is the same in PET after a built-in normalization matrix has been applied. This means that a single calibration factor (cps/MBq) can be used to convert a number of counts into an activity value regardless of the location of the ROI in the image. However, if the source is located within an attenuating patient, then the count rate will be dependent on the media. Therefore, if the aim for a particular study is to measure the activity in absolute units (MBq or mCi), then compensation for photon interactions in the patient is necessary.

2.1.4. Activity concentration

The activity in a source in air can be accurately determined from the counts in an ROI that is large enough to completely cover the image of the source. However, when aiming to determine the activity concentration (MBq/mL), a 3-D tomographic modality generally is required. Under certain conditions, 2-D activity measurements can be combined with an additional modality to obtain the volume of the source (e.g. CT studies of tumour sizes). Because of the limited system resolution, compensation is needed by, e.g., recovery coefficients or image based partial volume correction (PVC) methods. In the literature, compensation for many physical effects is termed correction even though full correction may not be possible. In this publication, these terms are used interchangeably.

2.1.5. Per cent injected activity

Activity uptake expressed as percentage of injected activity is sometimes a convenient measure. However, it is necessary to measure residual activity (such as the syringe and associated tubing) after administration, and to correct for physical decay.

2.1.6. Functional and metabolically active volumes

Nuclear medicine imaging can give information about functional volumes (such as ejection fraction) or metabolically active volumes or volumes with impaired metabolism (such as tumour volume with increased metabolic activity in PET, or cardiac defect extent in SPECT).

Functional volumes (mostly end systolic, end diastolic and stroke volumes in cardiac imaging) are indirectly estimated through activity measurement, assuming the measured signal intensity is proportional to the blood volume in the left ventricle cavity. In other words, measuring such volume does not involve actual volume delineation. The accuracy of these functional volume estimates is thus directly related to the accuracy of activity measurement.

PET or PET/CT scans are increasingly used as an adjunct to define treatment planning in radiotherapy and for patient monitoring. For these specific applications, the metabolically active volumes are relevant to help define the treatment plan or assess whether a tumour responds to therapy [1].

Unlike functional volume, the metabolically active (or inactive) volume is defined as the volume with increased (or decreased) uptake with respect to surrounding activity, which is expressed in mL, and which requires actual volume delineation. The motivation for measuring such volumes is that they do not necessarily match anatomical volumes as seen from CT or magnetic resonance (MR) images (metabolic changes generally precede anatomical changes and thus bear useful and early diagnostic or prognostic information). Given the mediocre spatial resolution of SPECT and PET images, the accurate delineation of metabolically active regions is a great challenge, for which there is not yet a unique and satisfactory solution. For instance, in PET imaging of tumours with increased glucose metabolism, many methods have been proposed to delineate tumour volumes. Most of them are based on considering that all voxels with an activity value greater than a given threshold belong to the tumour. This threshold can be expressed as an absolute uptake value, or as a function of the maximum uptake or mean uptake calculated in the tumour. The background activity can also be accounted for to set the threshold [2]. There is currently no consensus on which method should be preferred and this is an active area of research [3].

2.1.7. SUV

SUV is the most commonly used index for the quantification of tumour uptake in PET or PET/CT scans. The SUV is defined as the ratio of the tumour uptake (kBq/mL) divided by the injected activity (kBq) normalized by the dilution volume (mL) at the time of imaging. Assuming the patient has a volumetric density of 1 g per mL, the SUV is usually calculated using:

$$\mathrm{SUV} = \frac{\text{tumour uptake (kBq/mL)}}{\text{injected dose (kBq)/patient weight (g)}} \cdot \frac{\mathrm{mL}}{\mathrm{g}} \tag{1}$$

SUV is a unit-less quantity. If the tracer is distributed uniformly throughout the patient, then the SUV would be 1 everywhere. Any departure from 1 indicates a non-uniform distribution of the tracer in the patient body.

Although the patient volume is often approximated as equal to the patient weight, other normalization factors have been proposed [4–9]. Similarly, there is no single way to assess the tumour uptake (e.g. different regions can be used). SUV therefore does not refer to a unique and standard definition. The ways the numerator and denominator are calculated can significantly affect the SUV estimate.

Despite numerous definitions, SUV has been found to be a useful index (although often not reproducible from one centre to another). Indeed, by including a normalization term accounting for the injected activity and patient volume, it improves the comparison of values across patients to a greater extent than if no normalization was performed. For instance, by looking at PET images in SUV units, patient images can be compared on the same colour scale, even if the normalization is not perfect.

2.1.8. Kinetic parameters

Dynamic PET or PET/CT and SPECT or SPECT/CT enable the estimation of physiologically meaningful parameters, such as the influx constant K_i, which is proportional to the metabolic glucose rate, or the myocardial blood flow ($\mathrm{mL \cdot min^{-1} \cdot g^{-1}}$). Such estimates require the acquisition of an image series over time, an estimate of the arterial input function and a kinetic model. The kinetic parameters are then estimated by fitting the measured activity concentration over time in specific regions to the kinetic model. Such absolute quantification is rarely performed in a clinical setting, however, owing to its high level of requirements (including lengthy dynamic imaging protocols, assessment of the arterial input function and software to fit the measured data to a kinetic model). A detailed discussion of kinetic analysis is beyond the scope of this publication although it usually requires accurate quantification of the individual frames.

2.2. RELIABILITY OF QUANTITATIVE MEASURES

It is highly desirable that quantitative measures used for diagnosis or therapy treatment planning be reliable. Two fundamental concepts related to the reliability of a measure are accuracy and precision, which characterize the two components in the error in a measurement procedure. Sometimes, it is useful to have an overall measure of reliability.

2.2.1. Accuracy

The accuracy of a measurement procedure is the degree to which the mean (the average of many such measurements) differs from the true measurement. Common measures of accuracy are the bias, b, and relative error:

$$b = E\{m_i - t \mid i\} = \bar{m} - t$$
$$\text{Relative error} = \frac{b}{t} \tag{2}$$

where m_i is the ith measurement, t is the true value (and is assumed not to be zero), $\bar{m}$ is the mean measurement over the set of acquisitions $\{i\}$, and $E\{m_i \mid i\}$ is the expectation value operator, which takes the mean of set of measurements, $\{m_i\}$, over all measurements. Note that in this, the measurement of the same value is repeated many times.

In nuclear medicine applications, it is often more relevant to take the average over a population of patients or in one patient imaged at different times where the true value is expected to differ. In this case, it is useful to define the ensemble bias, b_{Ensemble}:

$$b_{\text{Ensemble}} = E\{m_j - t_j | j\} = \bar{m} - \bar{t} \tag{3}$$

where j represents measurements over a population of patients or the same patient at different times, t_j is the true value for measurement j, and $\bar{t}$ is the mean of the true values. Since many of the factors that affect bias are patient dependent, a complete evaluation of a quantitative imaging method should be performed with respect to an ensemble that represents the patients to be imaged.

2.2.2. Precision

Precision describes the spread of a series of measurements around the mean. Common measures of precision are the standard deviation, σ, and the coefficient of variation, COV:

$$\sigma = \sqrt{E\left\{(m_i - \bar{m})^2 | i\right\}}$$
$$\text{COV} = \frac{\sigma}{\bar{m}} \tag{4}$$

where the symbols have the same meanings as in the previous equations. Once again, it is more relevant to talk about the ensemble precision, meaning the spread in precision over a population of patients or the same patient at different times. We thus define the ensemble standard deviation as:

$$\sigma_{\text{Ensemble}} = \sqrt{E\left\{(m_j - \bar{m}_j)^2 | j\right\}} \tag{5}$$

In this expression, $\bar{m}_j$ represents the mean of the value over many measurements if the same patient had been imaged many times. Again, a complete evaluation of a quantitative imaging method should include the evaluation of the ensemble standard deviation over a relevant patient population.

Often good precision is as or more important than good absolute accuracy of a quantitative measurement used for diagnosis and treatment.

2.2.3. Root mean square error

In optimizing or comparing quantitative procedures, it is often useful to have a single measure of the reliability. One such measure is the root mean square error (RMSE), given by:

$$\mathrm{RMSE} = \sqrt{b^2 + \sigma^2} = E\left\{\left(m_i - t\right)^2 | i\right\} \tag{6}$$

Note that this gives the squares of the bias and standard deviation equal weights. Once again, we can define the associated ensemble quantity averaged over a patient population:

$$\mathrm{RMSE}_{\mathrm{Ensemble}} = \sqrt{b^2_{\mathrm{Ensemble}} + \sigma^2_{\mathrm{Ensemble}}} = \sqrt{E\left\{\left(m_j - t_j\right)^2 | j\right\}} \tag{7}$$

2.3. COMMON ISSUES AFFECTING QUANTITATIVE IMAGING

There are a number of physical, instrumentation and patient dependent factors that must be addressed when performing quantitative tasks with images obtained from a nuclear medicine study.

2.3.1. Natural background

Natural radioactivity, patients in neighbouring rooms or corridors and residual radioactivity can result in background radiation. For low count studies, this can have a significant contribution to measured data and result in degraded quantitative information if not compensated for. Compensation for natural background radioactivity can be accomplished by acquiring images either before or after imaging patients, or both. If these count rates are too high, it indicates that cleanup, additional shielding or other remedial action should be taken. In any event, the resulting background images or counts can be subtracted from those in the patient measurements, possibly after scaling, to account for differences in acquisition time.

2.3.2. Radioactive decay

By definition, radionuclides undergo radioactive decay resulting in reduced activity as a function of time. For quantitative tasks it is important to account for this effect. For example, to calculate the percentage of injected activity in an organ, one needs to decay correct the measured activity in organs relative to the time of injection and the injected activity from the time the syringe was measured in the dose calibrator. Similarly, for dynamic studies, it is often desirable to remove the effects of physical decay by decay compensating back to the injection time. Decay compensation can be accomplished by scaling the image or data by a factor given by a decay factor, DF:

$$\mathrm{DF} = e^{-\lambda t} \tag{8}$$

where λ is the decay constant for the radionuclide (equal to $\ln 2/T_{1/2}$, where $T_{1/2}$ is the half-life of the radionuclide) and t is the time difference between the time for which the counts are decay corrected to and the time of the measurement. For acquisitions that are long compared to the half-life of the radionuclide, it may be necessary to use decay correction factors that take into account decay during measurement.

2.3.3. Noise

In nuclear medicine, noise results from the random nature of the radioactive decay process. Each atom of a radionuclide has the same probability of decay, which is independent of time, and the probability of decay for each atom is independent of other atoms. Thus, for a large number of atoms, the decay is governed by Poisson statistics. The probability, P_N, of N decays from a source having an activity A in a time t is:

$$P_N = \frac{m^N e^{-m}}{N!} \tag{9}$$

where $m = At$ is the mean number of counts. Note the number of counts, N, is an integer while the mean number of counts may be any value. Figure 1 shows the shape of the Poisson distribution for several different values of m. Note that for low counts the distribution is significantly asymmetrical. Also, unlike the normal distribution, it is zero for $m \leq 0$ and $N \leq 0$. If the mean count is m, the variance in the number of counts, σ_m^2, is:

$$\sigma_m^2 = m \tag{10}$$

Thus, the COV is:

$$\text{COV} = \frac{\sigma_m}{m} = \frac{1}{\sqrt{m}} \tag{11}$$

Thus, lower fractional noise can be obtained when the mean number of counts increases, i.e. for higher activities or longer counting times.

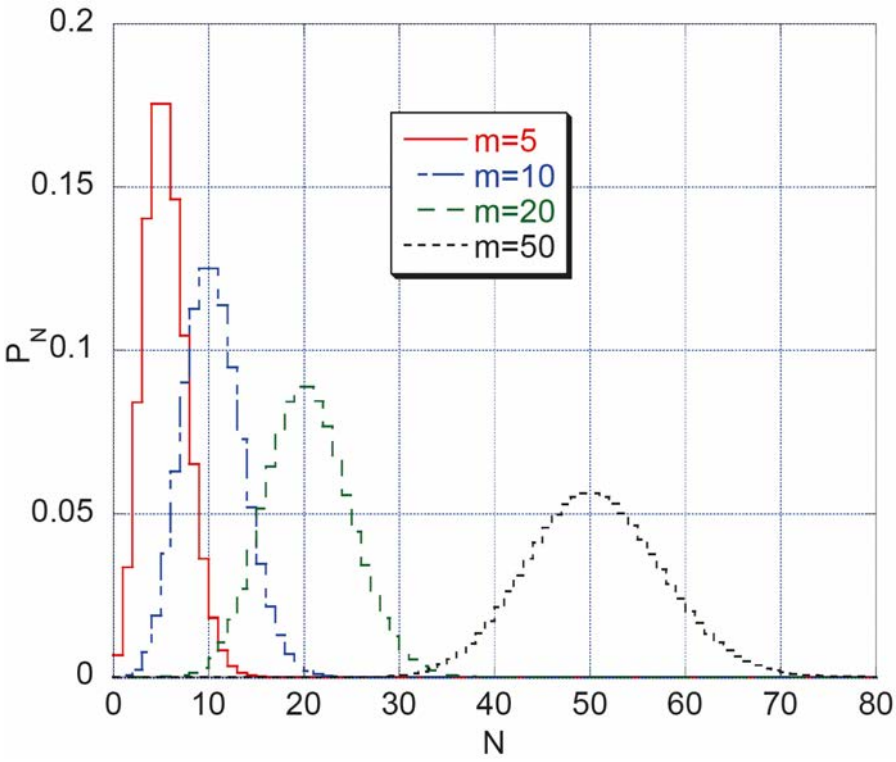

FIG. 1. Plot of Poisson probability of recording N counts for several values of mean counts, m.

Since the detection probabilities are random and independent, the number of counts recorded by radiation detectors in nuclear medicine systems is also governed by the Poisson distribution. So, if the mean number of recorded counts is m, the probability distribution, variance and COV are given by the same expressions above. Also note that the pixel values in the projection data are independent random variables. Thus, for unprocessed projection images, the variance in an ROI is equal to the sum of the mean counts in the region. The standard deviation (the square root of the variance) is often approximated by the square root of the number of counts in a pixel or region.

However, image processing operations such as low pass filtering and tomographic image reconstruction result in noise correlations. This means that the noise in neighbouring pixels (or voxels) is related and thus that the variance of the sum of voxel values in a tomographic image is no longer equal to the sum of the mean voxel values. The noise correlations can be described by the covariance matrix, Σ, which is given by:

$$\sum_{ij} = E\left\{\left(x_i - \mu_i\right)\left(x_j - \mu_j\right)\right\} \tag{12}$$

where Σ_{ij} is the covariance for voxel i with respect to voxel j, $E\{\ \}$ represents the expectation over many noise realizations, x_i and x_j are the voxel values in voxels i and j, respectively, and μ_i and μ_j are the mean voxel values for voxels i and j, respectively. Note that the covariance matrix is symmetrical about the diagonal and that the diagonal elements are the variance. Estimating the covariance for processed images is non-trivial, especially for images reconstructed iteratively. In addition, the covariance matrix for 3-D images is very large (of the order of the total number of voxels squared).

As discussed above, the variance of the projection data is related to the mean number of counts. Thus, the variance is proportional to the sensitivity of the imaging system, the activity of the source and the acquisition duration (see Fig. 2). It is also affected by factors that change the number of photons counted including attenuation, scatter, count rate losses, etc.

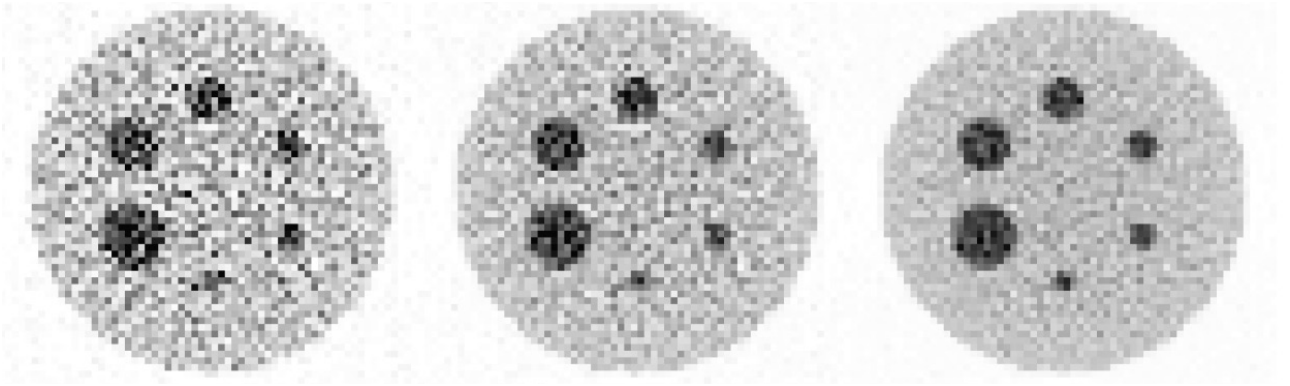

FIG. 2. The images show the dependence of noise on acquisition duration. PET images reconstructed using (left to right) 10, 30 and 90 million coincidences.

2.3.4. Photon attenuation

The effect of photon attenuation is essentially the reduction of photon fluence between two points due to photon interaction. This type of interaction is photoelectric absorption, Compton and coherent scattering and, if the photon energy is high enough, pair production.

The attenuation can be described by the exponential function:

$$N = N_0 e^{-\frac{\mu(h\nu,Z)}{\rho}\rho \cdot d} \tag{13}$$

where N is the measured count rate in an ROI, N_0 is the expected count rate in a non-attenuation environment, $\mu(hv,Z)/\rho$ is the mass attenuation coefficient, ρ is the density and d is the thickness of the attenuator, as indicated in Fig. 3. $\mu(hv,Z)/\rho$ depends on the photon energy hv and the composition of the attenuator expressed in terms of the atomic number Z. Photon attenuation implies that activity cannot be determined at various locations inside a patient using only one calibration factor (cps per MBq).

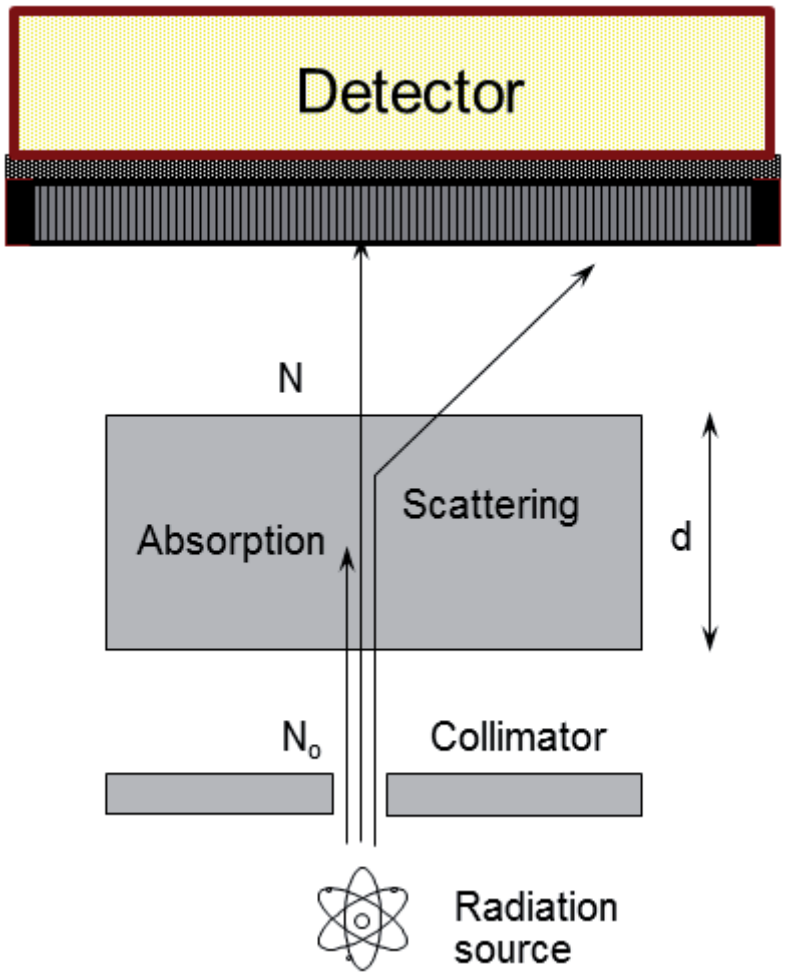

FIG. 3. The attenuation of photons reduces the count rate. The extent of the attenuation depends on the thickness of the attenuator, the tissue composition and the energy of the incident photon.

2.3.5. Scatter

Because of the limited energy resolution of scintillators used in the imaging devices, a relatively large energy window is needed to maintain good counting statistics. Some photons that are scattered in small angles (representing small energy losses) in the patient will therefore have a chance to be detected within the energy window. This detection will lead to potential difficulties in quantifying activity and a poorer contrast, since these photons carry incorrect information about the point of emission of the photon. The scatter contribution depends on several factors, such as photon energy, source distribution and tissue composition, in addition to camera specific parameters, such as energy resolution and window setting.

Figure 4 illustrates the differences between the real imparted energy distribution in a NaI(Tl) gamma camera and the distribution measured from the chain of energy conversion to scintillation light and light amplification through the photomultipliers. The distributions are of photons emitted from an object containing a radionuclide emitting 140 keV photons. The errors associated with the measurement of the energy signal create a broad distribution of measured energies for each input energy. The error is usually expressed by the full width at

half maximum (FWHM) of the peak expressed as a percentage of the true energy. As shown on the right, a rather broad energy window is needed to collect the 140 keV photons. Included in the illustration is also the scatter that 'leaks' into the main energy window and results in the scatter contribution to the image. For a 140 keV ($^{99}Tc^{m}$) acquisition the scatter to total ratio is in the order of 30–40% for common commercial scintillation cameras and their energy resolution is in the order of 9–12% FWHM at 140 keV and about 15% for the LSO crystals used in PET.

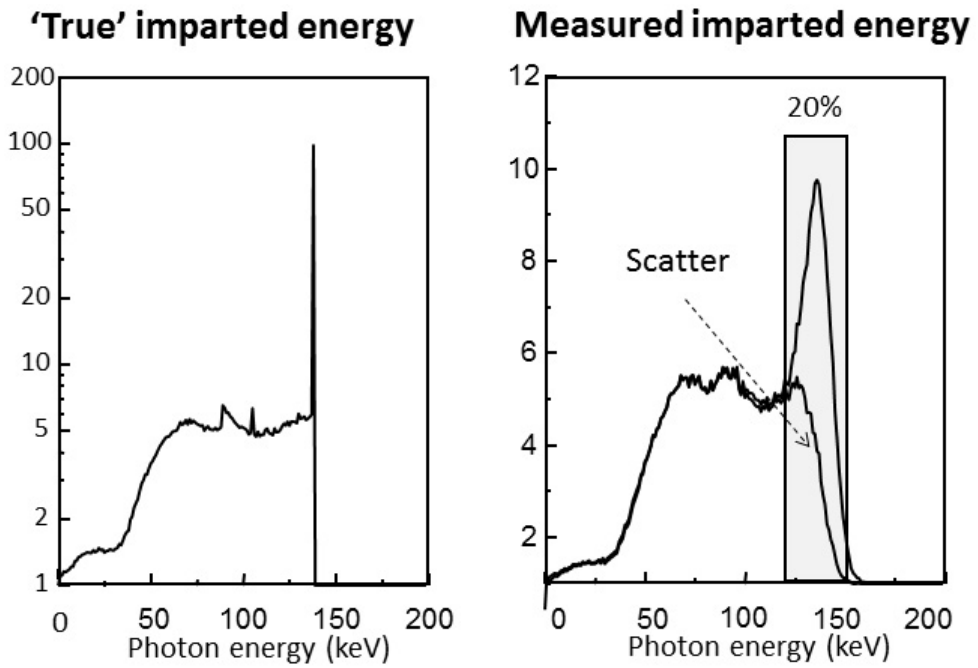

FIG. 4. Energy pulse–height distribution describing the true energy absorbed in a NaI(Tl) crystal (semi-log plot) and the measured distribution from the detection of the related emitted scintillation light (linear plot). Note that the scatter distribution merges into the main photopeak energy window.

2.3.6. Motion

A scintillation camera or tomograph measurement can be likened to taking an ordinary photograph with the shutter of the camera open for a long time period. The acquired images can be degraded by involuntary motions, such as cardiac and respiratory motions, or by voluntary motions. Note that motion affects each modality differently, as will be discussed in the Subsection on motion within the discussion of each modality. In general, motion results either in a loss of spatial resolution or produces image artefacts.

The effects of voluntary motion are best prevented. This can be accomplished by using as short acquisition times as possible to achieve the desired noise levels, instructing the patient to remain as still as possible, positioning the patient to maximize comfort and using straps, pillows or other constraints to restrict motion. Voluntary motion can also be caused by coughing or snoring. Commercial systems often have tools for correcting for some kinds of voluntary motion. There is some active research in the development of motion monitoring systems and these would allow voluntary motion compensation.

Voluntary motions often result in a loss of spatial resolution in images, though respiratory motions can result in artefacts. This loss of resolution may be acceptable for some applications depending on the spatial resolution requirements. In other applications, especially for quantifying activity in small objects such as tumours, quantitative reliability may be improved with the use of respiratory or cardiac gating techniques. In these methods, the image acquisition period is divided into multiple gates representing a number of intervals in the motion cycle; a separate image is produced for each gate representing the average activity distribution during the corresponding gate. For example, in cardiac imaging, the time between R waves is often divided into 8 intervals with counts acquired during each of these intervals binned into one of 8 corresponding gated images. For respiratory gating the signal

may be obtained externally by monitoring the patient's breathing or, when list mode data is acquired, from analysis of the image data. Cardiac gating is routinely available on commercial nuclear medicine imaging systems while respiratory gating is less widely available.

In addition to the intra-acquisition motions described above, inter-acquisition motion is important when quantifying images acquired at multiple time points in order to measure the time/activity curve. For processes that occur rapidly, such as myocardial perfusion or glucose metabolism, the patient can be imaged in a single session while remaining on the bed. However, for processes that occur over a longer timescale, such as the uptake of antibodies, multiple imaging sessions are necessary. In this case, careful repositioning of the patient can help provide better registered images. However, even in this case, some postacquisition registration may be necessary. In some applications, such as organ dosimetry, repositioning and reshaping of organ VOIs may be appropriate. However, even with this there may be inaccuracies and imprecision (e.g. due to inconsistent VOI repositioning and reshaping). For some applications, such as voxel based dosimetry, accurate registration at the voxel level is required. This is easier for regions of the body that can be approximated as rigid, such as the head, than for the chest and abdomen where non-rigid registration is often necessary.

2.3.7. Resolution and partial volume

Spatial resolution refers to a camera's ability to spatially resolve two sources of radioactivity as separate items. Experimentally, this can be made by repetitive measurements using two point sources with decreasing distances until they cannot spatially be resolved. The spatial resolution of scintillation cameras can also be described by the image of a point source, the point spread function (PSF), and is often modelled as a Gaussian function with a particular FWHM. It is advantageous to have an imaging system with as low a FWHM as possible, but this often affects the system sensitivity. The spatial resolution is sometimes described in terms of the modulation transfer function, which is the absolute value of the Fourier transformed PSF. For a scintillation camera collimator, the spatial resolution is distance dependent.

Limited spatial resolution results in the PV effect. PV refers to the fact that a pixel includes a mixture of signals coming from different sources. Two phenomena cause this mixture: the limited spatial resolution of the imaging system and the image sampling.

Owing to the image blur introduced by limited spatial resolution, the signal coming from a point source will be detected not only in one pixel, but also in neighbouring pixels. When considering a functional structure of interest, part of the activity from the structure will thus also be detected outside of a VOI drawn around the structure, an effect that is called spill-out (see Figs 5 and 6). Conversely, activity from structures close to the structure of interest will spill-in to the structure of interest. Therefore, if one considers only the most intense pixel to estimate the source activity, this activity will be underestimated but this underestimation might be partially compensated for by spill-in. Activity in neighbouring pixels will be overestimated. Overall, PV thus introduces quantitative biases.

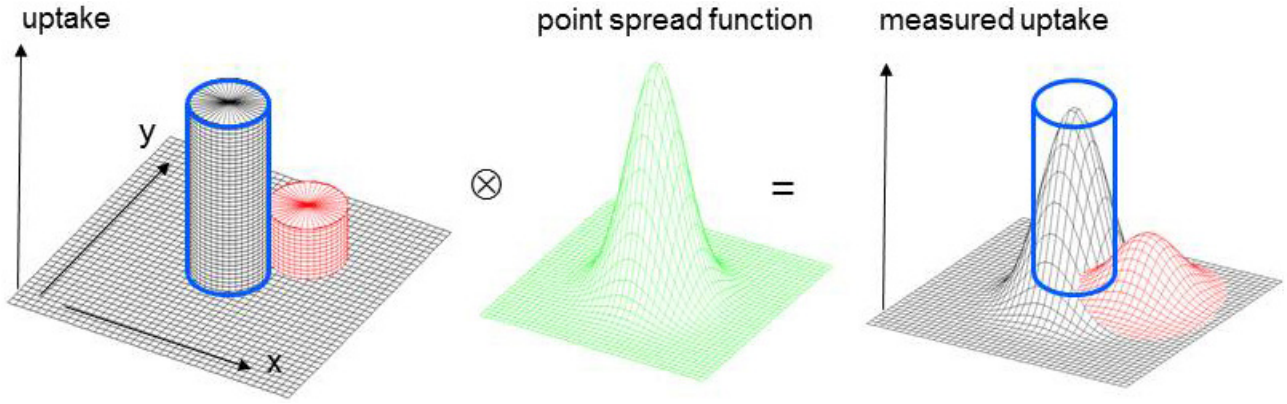

FIG. 5. Partial volume effect due to the spatial resolution of the imaging system.

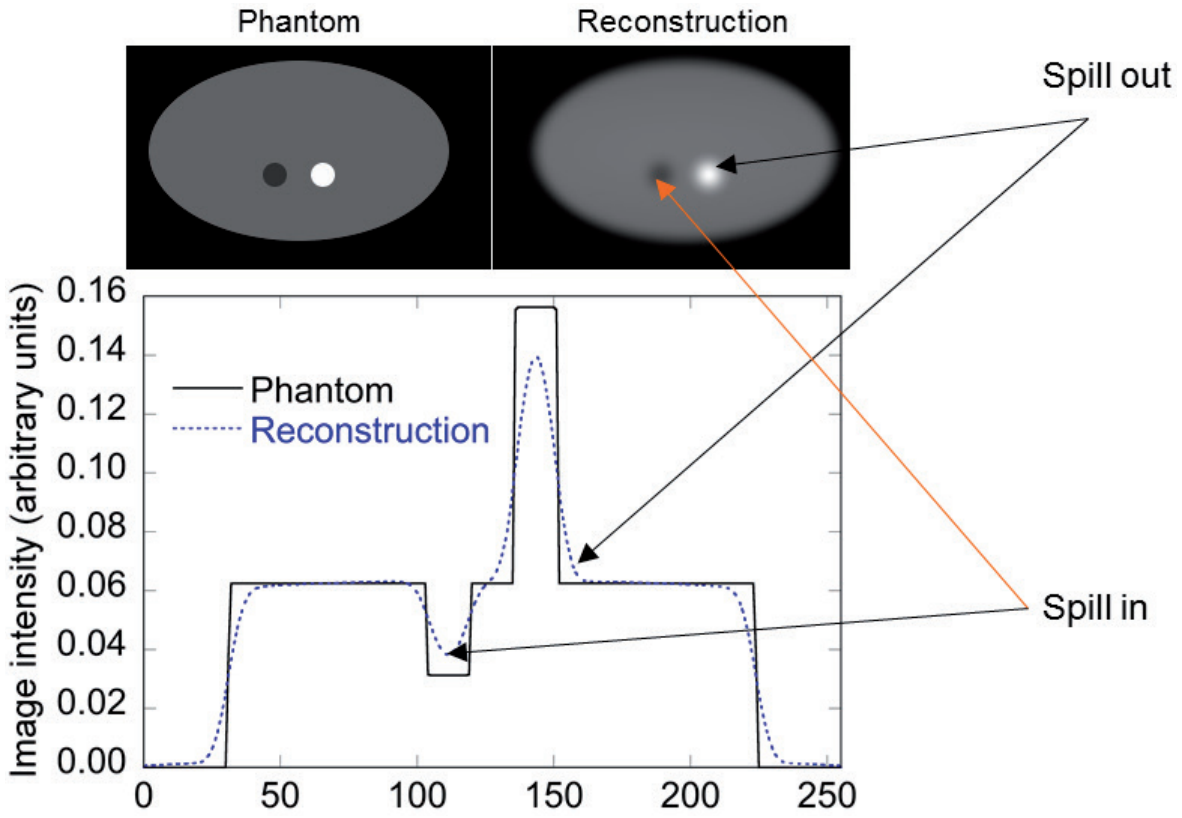

FIG. 6. Illustration of spill-out and spill-in PV effects. Spill-out results in estimating reduced activity in a region that has higher activity than its surroundings; spill-in results in overestimating the activity in a region that has lower activity than its surroundings.

Even if the spatial resolution were ideal, PV effects would still occur owing to image sampling. Indeed, a pixel (or voxel) has a finite size (typically 2–5 mm in SPECT and PET) and most often includes counts from a mixture of tissues with different uptakes. What is seen, even with a perfect spatial resolution, is thus a mixture of the signals coming from different tissues. This is what is called the tissue fraction effect and it affects any imaging modality. For a given spatial resolution in the images, the impact of the tissue fraction effect depends on the image sampling: the larger the voxel, the greater the tissue fraction effect (see Fig. 7).

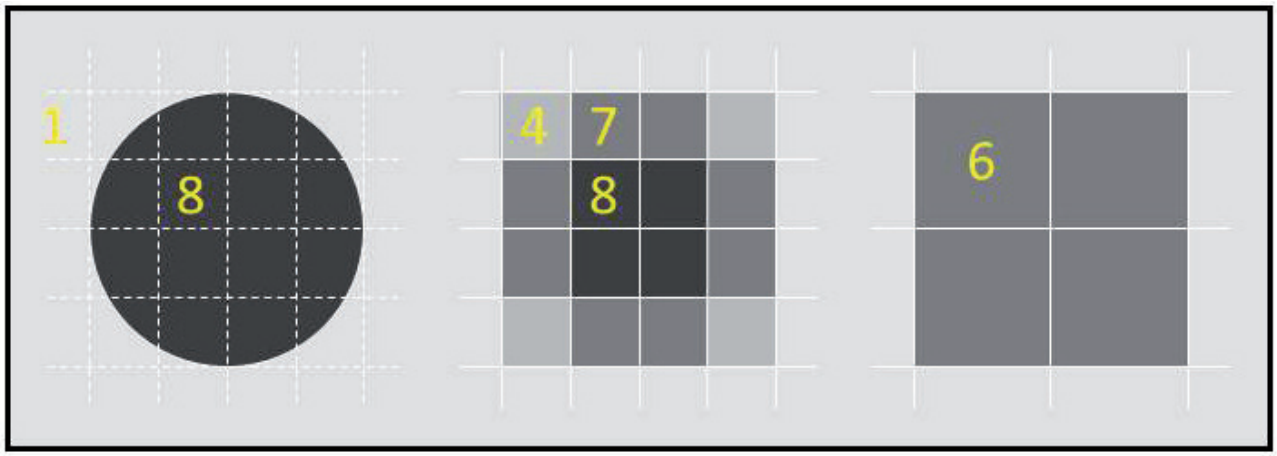

FIG. 7. A demonstration of the PV effect due to the tissue fraction effect. The figure on the left illustrates the true activity distribution with one unit of activity outside the circle and an activity of 8 inside. The figure in the middle illustrates the activities seen in image pixels after discretization. The figure on the right shows the effect of a coarser image matrix.

In a scintillation camera, the image is created by the geometrical collimation of photons, usually using a lead collimator with a large number of parallel hexagonal holes of a particular diameter and length. The detected counts and spatial resolution depend on the design of the collimator and vary inversely: the bigger the holes, the larger the number of detected counts, but the poorer the spatial resolution. It is necessary to have several types of collimators (general purpose, high resolution, high sensitivity, medium energy, etc.) in order to select the most appropriate as a function of whether the application requires high sensitivity or high resolution. A typical spatial resolution is about 9 mm, or more, depending on the collimator and distance from the source to the collimator. This means that, although activity can be measured with high precision, the reliability of the measurement of volume containing the activity determined by a SPECT or PET image is limited by the spatial resolution.

In PET, electronic collimation replaces geometric collimation and spatial resolution is mostly limited by the size of the detectors used in the tomograph, by the mean free path of the positron before annihilation and by the non-colinearity of the two photons resulting from the positron annihilation. As a result, the spatial resolution in the reconstructed images depends on the radionuclide (because the mean free path of the positron depends on the maximum energy of the emitted positrons). The resulting resolution is typically around 5 mm for ^{18}F.

2.3.8. Count rate problems

Radiation detectors used in nuclear medicine involve a series of elements that produce an electrical pulse with a finite temporal width. In other words, an amount of time, often referred to as the dead time, is required to produce and process the signal. If a new event occurs too close in time to the previous event, this signal might be lost or combined with the previous signal, depending on the details of the detector system. This means that the sensitivity (cps per MBq) is a decreasing function of the count rate. In detectors based on scintillators and photodetector arrays, the position of an event is related to the centroid of the light distribution among the photodetectors. Thus, if multiple gamma rays are incident within the system dead time, the centroid of the combined events will be different from the centroid of either event individually, resulting in mispositioning of the event. In addition, the signal, which is proportional to the photon energy, will be greater than the energy of either photon, resulting in errors in estimating the photon's energy. These phenomena are known as pulse pileup. Detection circuits in modern nuclear medicine systems often incorporate elaborate pulse pileup detection and reduction techniques. Nevertheless, for imaging patients with high activities present, corrections for these effects must be made.

In order to make corrections, it is desirable to have a mathematical model for the count rate losses. In general, counting systems can be categorized in two classes: paralysable and non-paralysable. In a paralysable system, events arriving within the dead time of the previous event will not be counted. Further, new events that arrive during the dead time for a previous event extend the time that the system takes to process the event by a time equal to the dead time. In other words, the dead time counter is reset with each new pulse. Paralysable behaviour is typical of the analogue portions of a counting system. In contrast, in a non-paralysable system, events are only counted if they are separated by a time interval greater than the dead time. However, new events do not extend the time the system takes to process the event. This behaviour is typical of digital portions of a counting system. While nuclear medicine counting systems do not behave as purely paralysable systems, they do exhibit many of the important features of such systems, as will be discussed below.

Since photon decay is random, the time between arriving photons will also be random. (Note that this is not true for radiation decay where multiple photons are emitted from a single decay, such as annihilation photons from positron decay or radioactive decay where multiple prompt gamma rays are emitted.) Thus, when the decay rate is high, some pulses will occur within the dead time interval of the preceding pulse. The probability of this occurring can be computed and combined with the counting behaviour of the two counting systems described above to provide expressions for the observed count rate, n, as a function of the true (incident) count rate, N, and the dead time, τ. For a paralysable system, the expression is:

$$n = Ne^{-N\tau} \tag{14}$$

In this case, as the true count rate increases, the observed count rate will rise, reaching a maximum count rate of $n_{max} = (e\tau)^{-1}$ for a true count rate N of τ^{-1}, and then decrease, as illustrated in Fig. 8. For a non-paralysable system, the corresponding expression is:

$$n = \frac{N}{1 + N\tau} \tag{15}$$

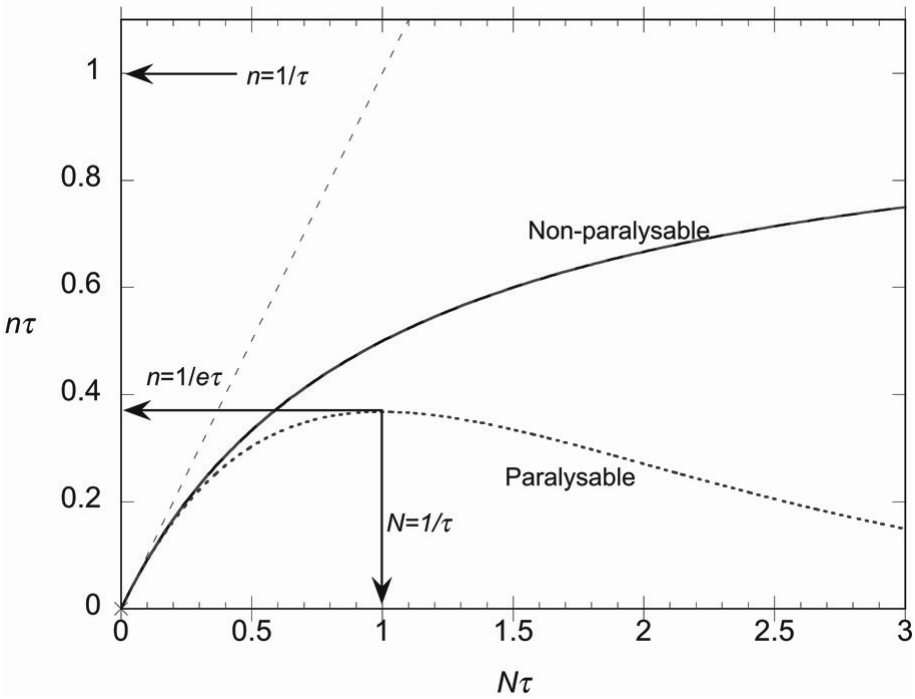

FIG. 8. Plot of observed count rate, n, versus true count rate, N, for paralysable and non-paralysable counting systems compared to an ideal counting system that experiences no count rate losses.

For this, we see that the observed count increases monotonically as a function of the true count rate and asymptotically approaches τ^{-1} as $N \to \infty$. This behaviour is illustrated in Fig. 8. This figure also shows that for low count rates the non-paralysable and paralysable systems behave similarly and can be approximated by:

$$n \approx N(1 - N\tau) \tag{16}$$

Figure 8 also illustrates that for true count rates below $\approx 0.1/\tau$ both systems behave as ideal counting systems and have relatively small count rate losses. Ideally, quantitative imaging should take place in this regime. However, for some applications, such as post-therapy imaging, this might not be possible. In this case, count rate loss (dead time) corrections are needed. These can be performed by measuring the observed versus true count rate curve as a function of true count rate, and inverting the relationship to solve for the true count rate for a given observed rate. The inversion process can be carried out using interpolation methods from the measured curve or by fitting the appropriate count rate model and inverting it numerically. However, as nuclear medicine detection systems are comprised of both paralysable and non-paralysable elements, neither of the ideal count rate equations will be a perfect fit.

The best method for measuring the count rate curve is to use the decaying source method. In this method, a very high activity source is used, giving a count rate as high as the rate expected clinically. The activity of the source should be high enough to provide a count rate slightly greater than the maximum expected clinical count rate. The count rate is measured using the imaging system at a set of times as the source decays. Data should be acquired for long enough at each time to provide a suitable precision (and the measurements decay corrected for the acquisition time, if necessary). Data points should be acquired over a time that is long enough so that the observed count rate

is in the range where count rate losses are small. The true count rate at the other times can then be estimated based on the rates for the lower count rates. One complication is that count rate losses result not only from photons with measured energies in the acquisition energy window, but also with higher and lower energy photons present in the spectrum. As a result, the count rate curve depends on the scatter environment. Thus, the source used should, in principle, be placed in a similar scatter environment as expected for the patient [10].

2.3.9. Recovery of 3-D information

Measuring the activity in a volume inherently requires three dimensional information concerning the conformation of the containing volume (the 'target' volume). Probe counting (see Section 3) carries no spatial information and the target volume will be the patient.

Scintillation cameras acquire images as two dimensional projections of activity (planar scintigraphy). A collimator restricts the photons arriving at the scintillator so that only those travelling in certain directions are recorded. This means that the third dimension (z) cannot be directly resolved from one projection, and the contribution of target and non-target volume activity along the projection line (z) will be more or less superimposed in the acquired image. Section 4 discusses how this is dealt with in planar whole body imaging.

Tomographic imaging aims to resolve this problem by making multiple measurements of the activity distribution within the patient from different projection views. For gamma emitting nuclides, data for SPECT images are acquired by rotating the camera and recording a series of planar projections. From these multiple projection data sets, a set of tomographic images (y, z) for different axial slices through the body (x) can be reconstructed, often under the assumption that the activity distribution remains the same during the SPECT measurement. This method will thus separate over- and underlying activity distributions from the target region. In PET, instead of rotating a planar camera around the patient, the detector actually consists of a ring of detectors, making simultaneous measurements of a set of projections that are then processed using tomographic reconstruction.

The purpose of tomographic reconstruction in emission computed tomography (SPECT and PET) is to estimate the distribution of activity in the object from a set of projections measured at different projection views. There are two basic classes of reconstruction algorithms: analytical and iterative.

2.3.9.1. Analytical reconstruction algorithms

Analytical algorithms approach the tomography problem by trying to analytically solve for the activity distribution from the equations describing the projection image formation process. The most common such algorithm, filtered back projection, is based on a very simple projection model: projections are modelled as line integrals through the object. However, as applied to emission computed tomography, this is not a very accurate model of the imaging process.

In PET, preprocessing can be used so that the line integral model is a good approximation to the real image formation process. In SPECT, analytical algorithms have been derived that handle cases of uniform or non-uniform attenuation [11, 12]. However, noise is not explicitly taken into account in the derivation of the analytical algorithms for either PET or SPECT and thus the noise properties are not as good as those for statistically based iterative reconstruction methods.

2.3.9.2. Iterative reconstruction algorithms

Iterative algorithms can also be used to solve the reconstruction problem. There is extensive literature on iterative reconstruction algorithms for emission computed tomography. An excellent review of this literature and associated concepts is given in Ref. [13]. The following provides a brief summary.

The basic idea is to iteratively modify a current estimate of the activity distribution (usually starting with a uniform estimate) to improve agreement between the projection of the current estimate, modelled using a forward projection algorithm, and the measured projections, as illustrated in Fig. 9. An iterative reconstruction algorithm is based on a cost function measuring the agreement between the measured projections and the estimated ones, and an algorithm for modifying the current activity distribution estimate to optimize the cost (or objective) function.

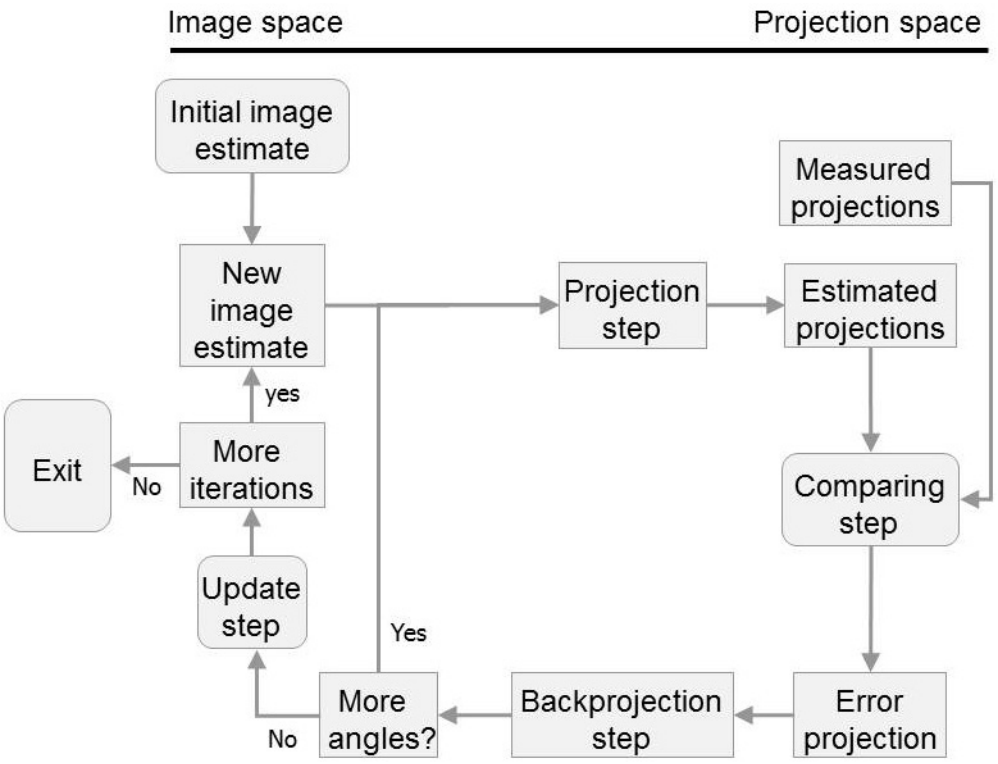

FIG. 9. Flow chart describing the various steps in an iterative reconstruction process.

The cost function is an important determinant of the statistical properties of the reconstructed image. The most commonly used cost function is the maximum likelihood (ML) criterion. Here, the goal is to maximize the statistical likelihood of the measured data given the reconstructed image. In emission computed tomography, in the raw projection data, the noise is Poisson distributed, so the appropriate Poisson likelihood function is maximized. This cost function has properties that are theoretically appealing. Other cost functions, such as maximum a posteriori (MAP), include a term that is an estimate of the probability of the reconstructed image and is used to reduce image noise at the expense of increased bias, for example, by penalizing images where the activity distribution changes very rapidly. More detail on the use of MAP algorithms is provided below. In general, MAP reconstruction algorithms are less common for quantitative applications as they require some tuning of hyperparameters, may produce biased estimates and are not widely commercially available.

The iterative algorithm primarily determines the convergence properties. The iterative algorithm used is often, for reasons of mathematical convenience, related to the mathematical form of the cost function. For example, for maximizing the Poisson likelihood, the first and simplest algorithm was the expectation maximization (EM) algorithm, with the resulting algorithm being referred to as ML-EM (maximum likelihood expectation maximization) [14, 15]. On the other hand, maximizing a Gaussian likelihood function, resulting in a weighted least squares cost function, can be conveniently performed using the conjugate gradient algorithm.

In emission computed tomography, the Poisson likelihood is the most appropriate non-penalized cost function (see below for more discussion of penalties and regularization). While the ML-EM algorithm does monotonically converge to the Poisson ML solution, there are a number of limitations. First, the high frequency features in the image converge very slowly. One reason for this is that the image is updated only once per iteration. As a result, the idea of subsets has been applied to the ML-EM algorithm to improve the convergence rate. The basic idea is to divide the projection views into some number of subsets having an equal number of views in each subset. The grouping of views into subsets and the ordering of subsets is critical to achieving good convergence and avoiding artefacts. The application of this idea to ML-EM is referred to as OS-EM (ordered subset expectation maximization) and has a speedup factor given by approximately the number of subsets [16]. In general, it is a bad idea to have fewer than 4 angles per subset [17]. Also, OS-EM is not a provably convergent algorithm and its noise properties are not as good as ML-EM, especially for large numbers of subsets and very noisy projection data. As a result, for very low count data it is desirable to use a smaller number of subsets. An alternative to OS-EM that

uses the idea of subsets but provably converges to the ML solution is the row action maximum likelihood algorithm (RAMLA) [18]. This algorithm uses a different update equation from the OS-EM algorithm, combined with a set of relaxation parameters. As a result, convergence is dependent on the choice of relaxation parameters and the convergence is generally slower than OS-EM.

A second problem with the Poisson ML cost function is that its noise properties are not ideal, at least for some imaging tasks. When using OS-EM or ML-EM, the resolution tends to improve and noise tends to increase with increasing numbers of iterations. At high numbers of iterations the images become unacceptably noisy for visual interpretation, though they may still be optimal for estimating activity in VOIs. Noise can be reduced by using a smaller number of updates (i.e., the product of the number of subsets and iterations) or by postreconstruction low pass filtering. Alternatively, a modified cost function can be used to help regularize the problem. In this context, regularization refers to the addition of constraint or penalty terms to the cost function that penalize images with features that are viewed as undesirable. These additional terms are often called penalty functions and the resulting combination with statistical likelihood in the cost function results in a penalized likelihood (PL) cost function [19].

One way to look at these penalty functions is to consider them as embodying prior information about the probability of activity distributions [20]. For example, one might expect that a nuclear medicine image would consist of a series of sharp edges, corresponding to the boundaries of anatomical or function features, with relatively modest variations in activity inside these boundaries. Due to this link to the idea of prior information, penalty functions are often referred to as priors. Reconstruction methods that use a cost function that combines a prior with an ML term are often referred to as MAP reconstruction methods. This is because the MAP probability of an activity distribution, **a**, given a set of measured projection data, **p**, $P(\mathbf{a}|\mathbf{p})$ is related to the prior probability of the activity distribution, $P(\mathbf{a})$, and the conditional probability (likelihood) of the projection data given the activity distribution, $P(\mathbf{p}|\mathbf{a})$, by Bayes' Theorem:

$$P(\mathbf{a}|\mathbf{p}) = \frac{P(\mathbf{p}|\mathbf{a})P(\mathbf{a})}{P(\mathbf{p})} \tag{17}$$

Note that the probability of the projection data, $P(\mathbf{p})$, is a constant and does not impact the MAP probability by optimizing the activity distribution, **a**. Because of this connection to MAP estimation, these methods are often referred to as Bayesian reconstruction methods. Partly for mathematical convenience, Gibbs priors are often used in combination with the Poisson Likelihood and are based on the Gibbs distribution:

$$P(\mathbf{p}) = \frac{1}{Z(\beta)} e^{-\beta V(\mathbf{a})} \tag{18}$$

In this equation, $Z(\beta)$ is a normalizing constant that does not affect optimization of the cost function; β is a hyperparameter of the prior that controls the strength of the prior term relative to the ML term (larger values of β result in greater emphasis on the penalty term and are somewhat analogous to the cut-off frequency in a low pass filter); and $V(\mathbf{a})$ is a potential function which is, by analogy to statistical mechanics, the 'potential energy' associated with the activity distribution **a**. A commonly used potential function with many desirable properties is the quadratic potential function, which is a weighted sum of the square difference of each voxel with its neighbouring voxels.

The simplest algorithm for optimizing MAP cost functions using Gibbs priors is the one-step-late algorithm [21]. This algorithm is a straightforward modification of the ML-EM or OS-EM algorithms and is thus very easy to implement. However, it is not provably convergent, so its use is theoretically less well motivated. However, it is often of practical use for the initial exploration of new potential functions. More recently, provably convergent and rapidly converging optimization algorithms have been developed for some forms of potential functions [22–26].

One major advantage of iterative algorithms, in addition to the possibility of modelling the noise in the data, is the ability to model the image formation process more exactly. This is done by modelling physical effects such as attenuation, scatter and system resolution in the forward projection process [27]. For example, the most basic projection model, and the model implicitly used by filtered back projection reconstruction, is to model projections as line integrals through the object in the directions perpendicular to the detector for each projection

view. Attenuation can be modelled in the projector (resulting in attenuation compensation in the reconstruction) by replacing the line integrals with the attenuated line integrals through the object [28]. Similarly, blurring due to the collimator–detector response can be modelled in the projection by convolving the activity distribution in planes parallel to the detector by the collimator–detector response function appropriate for the distance from that plane to the collimator face [29]. For the EM algorithm (and its OS version) and many other iterative algorithms, the update also requires the modelling of the physical effects in transpose of the projection operation, known as back projection. The OS-EM algorithm is the most commonly used and commercially available iterative algorithm for both SPECT and PET.

2.3.10. Region and volume definition

Making a measurement usually involves selecting one or several ROIs (on 2-D images) or VOIs (on 3-D images). Only the pixels belonging to these regions are then used for subsequent calculations. In 3-D imaging (PET and SPECT), 3-D regions should be preferred.

Three approaches can be used to define a region or volume: manual, semi-automatic and automatic. In the manual approach, a user draws a region on the image using an appropriate device (track ball, mouse, etc). In 3-D, the drawing is performed on each slice encompassing the VOI and the set of resulting regions are then combined to form a 3-D volume.

In the semi-automatic approach, an automatic algorithm is used to define the region, but needs operator assistance either for initialization or for fine tuning of the final regions or both. The operator input can be one or several values (such a threshold value, when a region is defined as including all pixels with a value above a certain threshold), clicking on a pixel or any interaction to adjust the contours found by the automatic algorithm. In an automatic approach, the region is entirely defined by the computer using an algorithm without any user interaction.

Manually defined regions are the least reproducible, within and between operators. Automatically defined regions are perfectly reproducible, but the underlying algorithm must be robust enough to be reliable in a large variety of situations. Semi-automatic regions are more reproducible than manual regions and allow the user some control in the resulting regions. The region can be recalculated and tuned by the user if needed.

The quantitative measurements can be strongly dependent on the method used to define the regions. Great care should therefore be taken when defining a region and the regions used for the measurements should be stored to enable the reproduction of the measurement.

Quantification can also be achieved without using any region, based on a voxel by voxel analysis. This is performed in what is called parametric imaging, when the parameter of interest is estimated in each and every voxel.

2.3.11. Calibration

The raw images returned by an imaging system are not in units of activity. As a result, it is necessary to calibrate the system by imaging sources of known activity. Since calibration factors depend on the radionuclide imaged, geometry and imaging system parameters, it is important to acquire calibration images using the same values for these parameters as used for patient studies.

2.4. VALIDATION

Validation of data for quantitative measurements on a regular basis is very important. The validations are usually based on simulations of patients either by physical phantom experiments or by means of mathematical simulations tools, such as Monte Carlo simulation or analytical projector algorithms using anthropomorphic voxel based computer phantoms. Validations can also be made by comparing results to published data. Validation needs to be made of both the methods used to correct for the common issues described above and also for the protocol itself so that an optimal protocol is used.

3. QUANTIFICATION WITH WHOLE BODY PROBES

Hand held or fixed position probes (Geiger and scintillation counters) can be used to follow the time course of radioactivity in a patient. The measurements are easy and quick to perform and do not require that the patient be moved to an imaging room. Measurement can be started immediately following administration when local rules prevent the patient being taken for image based measurements. The simplicity of the measuring process means that non-technical staff can be trained to undertake the measurements. The measurements typically take about one minute and are not burdensome to the patient. This means that frequent measurements can be made even with low compliance patients (e.g. children or those in pain), allowing for good estimation of the patient's overall radiation clearance.

Various groups have reported the use of whole body measurement based dosimetry. The European Association of Nuclear Medicine (EANM) dosimetry committee has recommended the use of a spectroscopic probe, e.g. a sodium iodide detector with a crystal of at least 7.5 cm × 7.5 cm, when using external probes as a possible option for pre-therapeutic determination of the whole body clearance of ^{131}I [30]. Gaze et al. [31] used quantitative probe measurements to ensure accurate radiation absorbed doses in MIBG treatment, while unpublished data from Violet (personal communication) [32] showed correlation between quantitative probe measurement and bone marrow toxicity in ^{131}I radioimmunotherapy. Hindorf et al. [33] compared whole body measurements, conjugate view scintillation camera measurements and three blood sampling methods; none of the methods showed good correlation with platelet toxicity in their study. Based on the EANM recommendations, Verburg et al. [34] reported clinical results in thyroid cancer patients. Based on whole body retention measurements alone, their data indicates that the absorbed dose to the blood is a better predictor of ablation success than the administered ^{131}I activity.

3.1. BACKGROUND

Readings of background activity are taken before and after patient measurement and background correction is applied. Where the measurements are taken in a shielded therapy room the background is measured before the patient is admitted to the room. Care should be taken that no other sources of radioactivity are present during the background measurement or when measuring the patient (e.g. 24 h urine collection containers).

3.2. RADIOACTIVE DECAY

Probe based measurements normally assess the changing body burden of radioactivity so that the radioactive decay which takes place between measurements is correctly included in the measurement. The acquisition time is short compared to the half-life of the nuclides in use and decay during a measurement is negligible.

3.3. NOISE

Noise is a function of accumulated counts and is related to the efficiency of the detection system and the injected activity. Counting takes place over a period long enough that statistical noise is low (typically 1 min).

3.4. ATTENUATION

Absolute attenuation compensation is not generally required for whole body probe measurements. Any difference due to activity at different depths in the body is dealt with by taking anterior and posterior measurements [35] and the geometric mean as described in Section 4.

3.5. SCATTER

Radiation scattered outside the body is reduced by the use of shielding to restrict the acceptance angle of the probe to the region containing the patient. Placing the patient in a low scattering environment has also been used to reduce this problem [36]. Since internal calibration is used (see Section 3.10), the scattering conditions for all measurements in a course of treatment will be similar, further reducing any problem caused by scatter. When using a spectroscopic system, scatter can further be reduced by using adequate peak fitting techniques.

3.6. MOTION

Involuntary motion includes the effect of breathing during a measurement and the change in the distribution of activity within the patient between measurements. Consideration of the inverse square law and the geometry of the measurement system allows the calculation of a suitable distance between the probe and the patient to ensure sufficient uniformity of response so that involuntary motion will have a negligible effect [35]. A distance in the order of 2 m is typical.

3.7. RESOLUTION AND PARTIAL VOLUME

As the whole patient is seen in a single measurement, these effects do not apply.

3.8. RECOVERY OF 3-D INFORMATION

As the whole patient is seen in a single measurement, these effects do not apply.

3.9. COUNT RATE PROBLEMS

In therapeutic monitoring and dosimetry applications a wide range of count rates is typically seen; the patient's burden of radioactivity will decrease by several orders of magnitude during a course of molecular radiotherapy. Chittenden et al. [36] overcome this problem by the use of two probes: a low sensitivity energy compensated Geiger–Müller tube for high count rates and a high sensitivity NaI(Tl) probe for low count rates (see Fig. 10). Care is required in the use of gamma spectroscopy in high count rate situations as the acquisition time is prolonged according to built-in equipment specific dead time correction algorithms. While these algorithms might work well in situations where the dead-time losses are less than a few per cent, the built-in corrections for higher count rates might lead to erroneous data. When applying spectroscopy systems under these circumstances, the dead time characteristics of the system should be checked.

3.10. CALIBRATION

Internal calibration is typically achieved by ensuring the first measurement is taken before the patient voids his or her bladder. This reading is then taken to represent the count rate due to the patient containing the known injected activity.

Probes must be shown to have a sufficiently linear response over the range encountered in practice. Where more than one probe is needed to cover the required range, a sufficient overlap must be allowed.

An exactly reproducible measuring geometry is essential for achieving a reliable activity–time curve of the whole body retention. A set-up with the patient lying under a detector fixed to the ceiling is preferable, although not all patients tolerate several minutes of lying in a prone position [6]. A horizontal spacer could be used to ensure a fixed and reproducible measuring distance if the patients are measured in an upright position (standing).

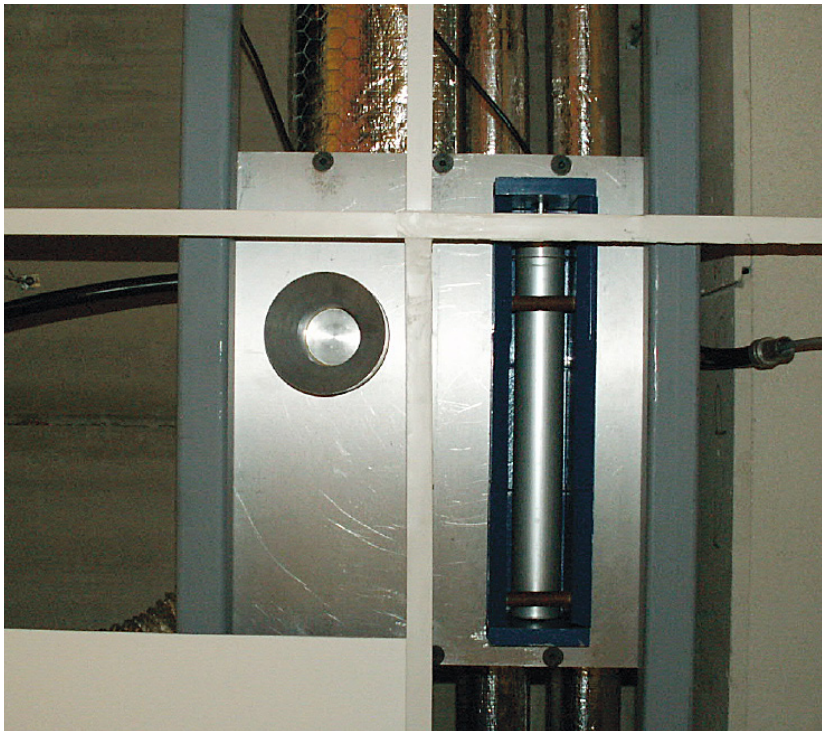

FIG. 10. Shielded monitors installed next to each other in the ceiling space of the patient therapy room. The modular lead construction includes a section that protrudes below the front face of each detector and is shaped to restrict the field of view to an area directly over the patient's bed. (Photograph courtesy of S. Chittenden.)

4. QUANTITATIVE PLANAR IMAGING

Planar scintigraphy creates images in two dimensions by detecting only photons emitted in certain directions that are determined by the collimator with which the camera is equipped. This means that the third dimension (i.e. the depth) cannot be directly resolved from a single projection image.

4.1. COLLIMATOR SELECTION

There are two major issues involved in selecting a collimator appropriate for a given scintillation camera imaging task: the selection of a design appropriate for the energy of the radionuclide and the selection of a collimator with the appropriate resolution–sensitivity trade-off.

Collimators used for a given radionuclide should have been designed to handle the energy of the radionuclide being imaged. For example, a low energy collimator should not be used to image radionuclide emitting energies higher than ≈170 keV. Using an inappropriate collimator can result in the creation of artefacts, degraded spatial resolution and distance dependent sensitivity. All of these tend to decrease quantitative accuracy.

There is a direct relationship between sensitivity (which determines image noise) and spatial resolution. The appropriate trade-off is determined first by the size of the object of interest. For small objects such as tumours, a high or ultrahigh resolution collimator should be used. In cases where injected activities or imaging times are low, a higher sensitivity collimator may be needed. For larger objects of interest, a higher sensitivity collimator may be acceptable, but counting statistics are usually not a major issue for large objects so erring on the side of high resolution is likely to be better.

4.2. ATTENUATION CORRECTION

Correction for attenuation that generally depends on source depth needs special attention. Attenuation correction based on the conjugate view method [37] is by far the most common method in planar imaging and therefore the only method that is described in this text. The method is based on two opposite measurements using the same energy window setting. Assuming a point shaped source located in a uniform medium, the attenuation of the count rate measured in the two projections can be described by the following equations:

$$C_{\mathrm{A}} = C_0 e^{-\mu d} \tag{19}$$

$$C_{\mathrm{P}} = C_0 e^{-\mu(T-d)} \tag{20}$$

where d is the depth to the source in the anterior view and T is the total thickness of the patient. By taking the geometric mean of the opposite projections the attenuation will be reduced to a function of patient thickness T.

$$\sqrt{C_{\mathrm{A}} C_{\mathrm{P}}} = \sqrt{C_0 e^{-\mu d} \cdot C_0 e^{-\mu(T-d)}} = \sqrt{C_0^2 \cdot e^{-\mu T}} = C_0 \cdot e^{-\mu T/2} \tag{21}$$

The activity A is determined from the equation:

$$A = \frac{C_0}{K} = \frac{\sqrt{C_{\mathrm{A}} \cdot C_{\mathrm{P}}}}{K \cdot e^{-\mu T/2}} \tag{22}$$

where K is the system sensitivity (cps per MBq) measured in air. The method becomes useful owing to the fact that it is now only necessary to determine the sum T of the two source depths (i.e. the thickness of the patient for the particular projection bin). The equation above is only valid for a point source. To include the source thickness l, the following correction term has been suggested [38]:

$$A = \frac{\sqrt{C_{\mathrm{A}} \cdot C_{\mathrm{P}}}}{K \cdot e^{-\mu T/2} \cdot \dfrac{\sinh(\mu \cdot l/2)}{\mu \cdot l/2}} \tag{23}$$

It should be noted that this equation is derived assuming that there is no activity in the background, i.e. all activity is in the source and the activity in the object is uniformly distributed. As such, it still represents an approximation for most patient imaging applications.

4.2.1. Patient thickness

To apply attenuation correction, an estimate of the thickness of the patient needs to be obtained. In its simplest form, the thickness can be measured manually at various points of the body. From this, the planar image can be multiplied by an attenuation factor image constructed from a set of boxes with the measured height and where a uniform attenuation has been assigned. Alternatively, the attenuation correction can be applied on the sum of the data within the ROIs.

4.2.2. Transmission measurement

The thickness of the patient, expressed as T in the equations above, can be measured by a separate transmission study if equipment for this is available. By mounting a photon flood source on the opposite side of the camera relative to the patient, the transmission of the photons can be measured. This procedure includes two measurements: one with and one without the patient. The pixel by pixel ratio of the counts with the patient present divided by the counts with the patient absent gives the attenuation factor. This factor needs to be adjusted to account for differences in energy if a flood source of different energy has been used (e.g. ^{57}Co). On SPECT/CT

systems, a scout measurement can be performed to obtain a transmission measurement with high resolution and low noise compared to a radionuclide source [39] (see Fig. 11).

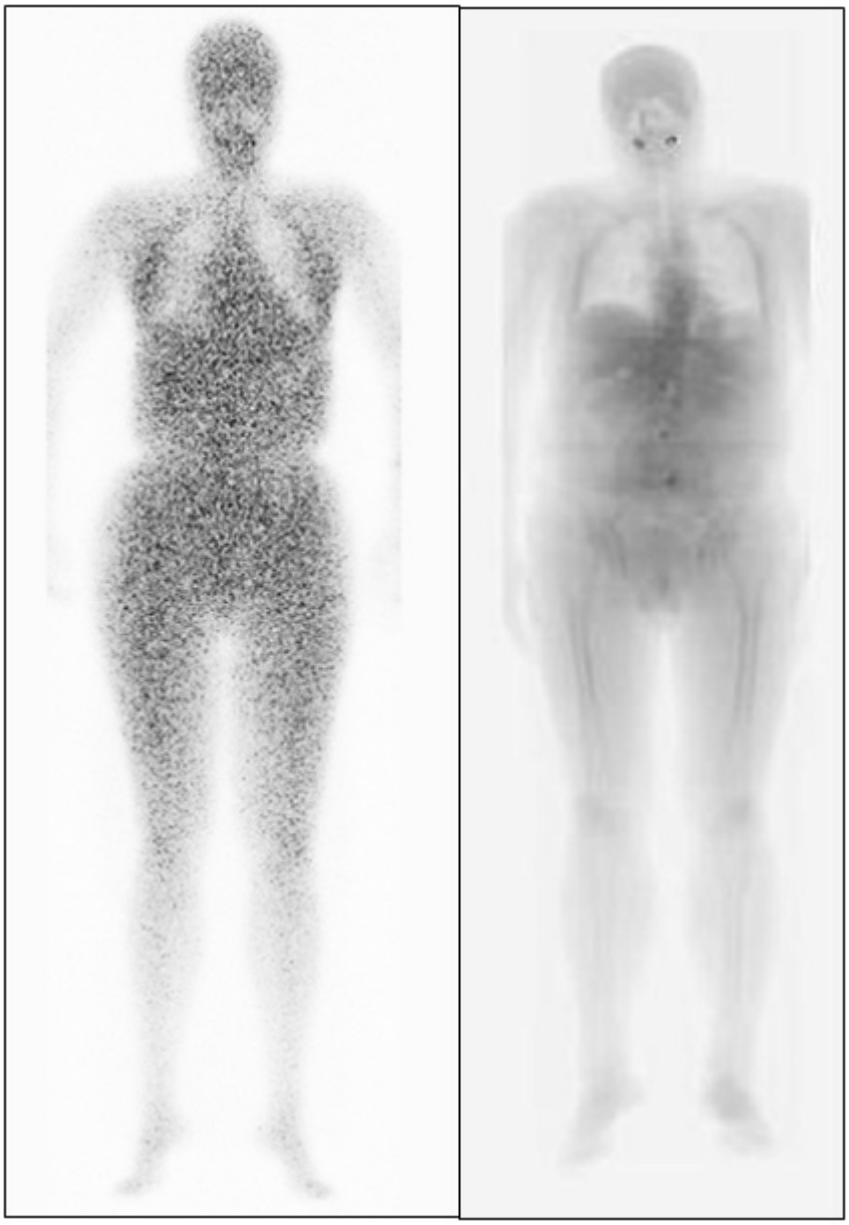

FIG. 11. The image on the left shows a transmission scan in inverse greyscale using a standard ^{57}Co flood source mounted on the scintillation camera system. The image on the right shows a transmission image obtained from a scout measurement using the X ray unit on the SPECT/CT system.

It is important that the patient remain in the same position for the transmission scan since the correction is usually made on a pixel by pixel basis. If not, the transmission scan needs to be registered to the whole body measurement by appropriate software.

Often, the energy for the emission radionuclide is higher than the energy from the transmission radionuclide in order to avoid contamination in the emission image. However, when measuring transmission data with a radionuclide flood source, scatter both from photons emitted by the transmission source and by the administered emission source can affect the accuracy of the transmission data. This may lead to an undercorrection of the attenuation. Thus, it is important to correct for this effect in order to avoid problems when applying the transmission data for attenuation correction. Energy window based methods can be used here (see Section 4.3.2). Due to the

high photon fluence from an X ray tube, this problem is negligible when a scout measurement from a SPECT/CT system is used.

4.3. SCATTER

Scatter results in a spatially varying low frequency blurring, loss of contrast and, in attenuation compensated images, a spurious and spatially varying increase in image intensity. The quantitative effects of scatter are greater for low energy photons, larger objects, and wider energy windows and poorer energy resolutions. Scattered photons can result in spatially varying quantitative errors.

4.3.1. Effective attenuation coefficient

A simple method to compensate for the additional counts in the projections from scattered photons is to reduce the magnitude of the attenuation correction by using an 'effective' attenuation coefficient that is lower in magnitude than the tabulated linear attenuation coefficient based on a narrow-beam geometry. This type of correction does not improve contrast since it does not remove the scatter radiations. An effective attenuation coefficient also depends on the source distribution and surrounding attenuating tissue and in theory needs to be determined for each imaging situation.

4.3.2. Energy window based scatter correction methods

Energy window based methods are simple and effective methods for scatter compensation. In these methods, the scatter component in the photopeak is estimated, based on measurements in one or more additional scatter windows. A commonly used method that is simple to implement is the triple energy window (TEW) method [40]. In this method, scatter energy windows are placed just above and just below the photopeak energy windows. The scatter in the photopeak energy window is then estimated using a trapezoidal approximation. Careful selection of the position and width of the energy windows is required. Wider energy windows reduce noise in the scatter estimate, but result in more biased estimates. Low pass filtering of scatter estimates is necessary to reduce noise, but can increase bias.

Implementation of the TEW method requires a scintillation camera that can separately acquire images using several energy windows. By defining two adjacent narrow energy windows on each side of the main photopeak and taking into account the different energy window sizes, an estimate of the scatter in the photo peak window can be calculated from the average of the two images on a pixel by pixel basis. The estimation process is illustrated in Fig. 12 and the equation for the scatter estimate image is:

$$I_{\text{scatt}}^{\text{TEW}}(x,y)=\left[\frac{I_{\text{lower}}(x,y)}{W_{\text{lower}}}+\frac{I_{\text{upper}}(x,y)}{W_{\text{upper}}}\right]\cdot\frac{W_{\text{peak}}}{2}. \tag{24}$$

where x and y are the pixel indices, $I_{\text{Scatt}}^{\text{TEW}}$ is the scatter estimate image, I_{lower} and I_{upper} are the scatter images from the lower and upper energy windows, respectively, and W_{lower}, $W_{\text{upper,}}$ and W_{peak} are the windows of the lower scatter, upper scatter and photopeak energy windows, respectively. This equation represents a trapezoidal approximation to the scatter in the energy window, where W_{peak} represents the width of the trapezoid and half the term in square brackets represents the average of the heights. Note that the trapezoidal approximation will not be a good one when the energy spectrum in the photopeak energy window changes in a way not well described by a straight line, for example, due to the presence of characteristic X rays (such as Pb X rays in the collimator for ^{201}Tl) or backscatter edges from high energy photopeaks. Since the energy windows are usually narrow in width, additional low pass filtering may be necessary to reduce image noise. The scatter estimate is subtracted from the photopeak image. The upper energy window is useful to take into account downscatter from high energy photons. This is important when imaging radionuclides such as ^{111}In, ^{123}I and ^{131}I.

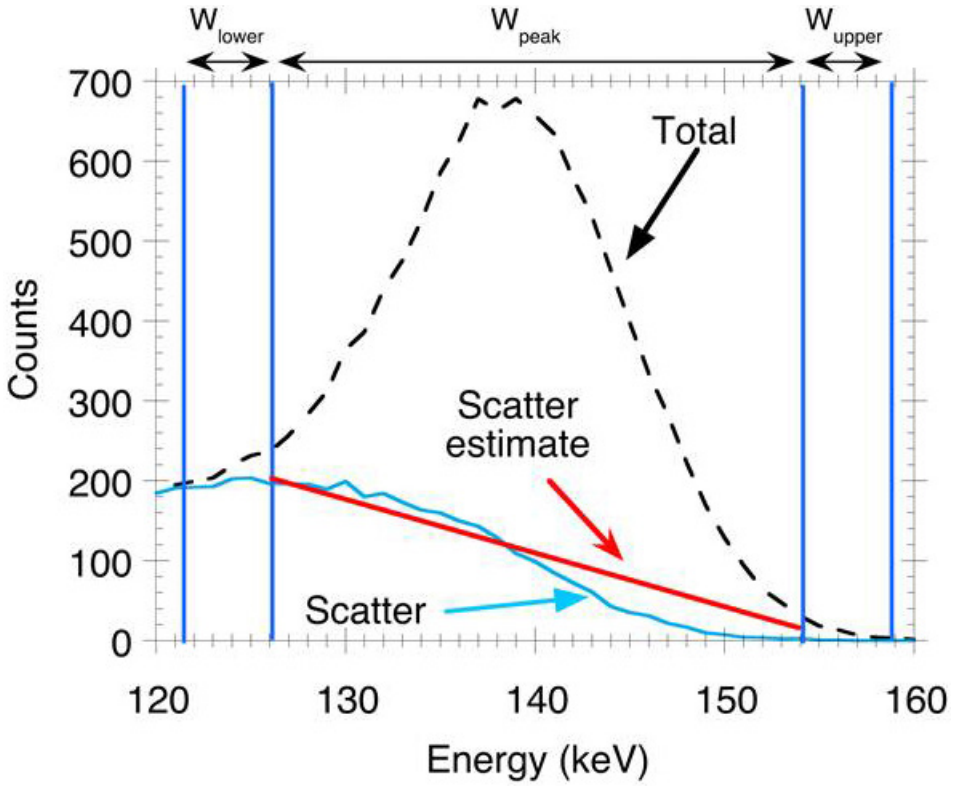

FIG. 12. Illustration of the use of a trapezoidal approximation to estimate the scatter in the photopeak energy window in TEW scatter compensation for ^{99m}Tc. Note that in this example the windows are not necessarily optimally placed. In particular, the scatter windows are positioned so that there is a non-zero contribution from unscattered photons in the scatter energy windows. This is especially evident for the upper energy window. In the case of ^{99m}Tc, the counts in the upper window are often assumed to be zero.

One major limitation to this method is the need for two additional energy windows for each photopeak. For radionuclides with multiple photopeaks, and when using older scintillation cameras, sufficient energy windows may not be available. In cases where the scatter component of the upper scatter window is expected to be zero (e.g. for ^{99m}Tc or the 245 keV photopeak of ^{111}In), a single scatter window may be used. In other cases, it may be possible to combine energy windows to meet camera limitations. These methods can generally be implemented on modern scintillation cameras with relative ease, but some care is needed to select optimal energy windows and filtering.

4.3.3. The buildup function method

Scatter is sometimes described in terms of buildup functions (i.e. total to primary ratios). A suggested scatter compensation method [41] is based on the conjugate view method combined with a depth dependent buildup function. The method is an iterative method that starts by assuming the activity in the middle of the volume, that is $d = T/2$. The count rate in air, C_0, and the depth from the anterior view, d, is calculated from the two equations:

$$C_A = C_0 \cdot B(\mu d) \cdot e^{-\mu d} \tag{25}$$

$$C_P = C_0 \cdot B(\mu(T-d)) \cdot e^{-\mu(T-d)} \tag{26}$$

where C_A and C_P are the measured count rates in the anterior and the posterior views, respectively. New values of d are calculated until the C_0 is equal for both equations. The method assumes buildup functions for current camera characteristics (energy window and energy resolution).

4.4. RESOLUTION AND PARTIAL VOLUME

The images obtained by planar imaging are affected by depth dependent spatial resolution due to the design of the collimator. Methods to improve resolution can be based on hardware solutions (e.g. contour based motion of the camera) or postprocessing restoration filtering (Wiener or Metz filters) where a description of PSF is used to restore the images. Methods that also include scatter and collimator penetration effects in the PSF have been reported [42]. For activity quantification of small targets such as tumours, recovery coefficients can be used. These coefficients are usually determined from phantom experiments with spherical sources of known sizes and activity contents and similar acquisition conditions.

4.5. RECOVERY OF 3-D INFORMATION

Non-target activity can be defined as both over- and underlying activity from other organs and tissues but also the blood activity within the organ itself. A proper ROI location correcting for the non-target activity is therefore of great importance. A method that compensates for over- and underlapping activities has been proposed by Sjögreen et al. [42]. In this method, ROIs are drawn over the whole organs despite overlap and the area of overlap is determined. The contribution from activity in the overlap region is determined from the data in the non-overlapped regions. The background activity is determined from the activity per pixel in a representative ROI and the fraction of patient thickness occupied by the particular organ. This fraction has been estimated for some organs using two phantoms.

As mentioned above, recovering information about organ activity in 3-D requires compensation for overlap in the planar image of the organ of interest and other organs or the background. Accurately compensating for these effects requires some 3-D information about the organ shape and its relationship to the background and other organs, e.g. the fraction of the thickness of each voxel that is the target organ or background and the overlapping volume fractions of overlapping organs. In addition, geometric mean attenuation compensation requires 3-D information about the object, such as the source thickness, to accurately correct for attenuation. Even with this information, these compensation methods are not fully theoretically rigorous. An alternative to this is to use concepts from 3-D tomography to, in some sense, reconstruct the organ activities [43, 44]. The general idea of these approaches is to use a registered 3-D CT image combined with a set of 3-D VOIs, obtained either by segmenting the CT image or from a registered SPECT image. The activity in the VOIs is assumed to be uniform and each of the VOIs is projected including modelling of the image formation process just as in iterative reconstruction. The set of 3-D VOI projections forms an $n \times m$ matrix, where n is equal to the number of pixels in all the projections and m is equal to the number of VOIs. The $m \times 1$ matrix of organ activities can be estimated by inverting the matrix and multiplying the inverse by the $n \times 1$ vector of voxel values [43]. Alternatively, the iterative ML-EM algorithm can be used to estimate (in a sense, to reconstruct) the vector of organ activities [44]. The latter approach has the advantage that the estimate takes into account the statistical properties while the former implicitly uses a least squares solution. In addition, Ref. [44] models scatter using a scatter model as opposed to a buildup function method and models the full collimator–detector response (CDR), including collimator scatter and penetration. The principal difficulty in applying these methods is the requirement for a registered CT image and 3-D VOIs.

4.6. COUNT RATE PROBLEM

The magnitude of count rate losses is determined by the characteristics of the particular scintillation camera system. The effects on activity quantification result from changes in the detected count rate relative to expected count rate and mispositioning of events due to the Anger positioning logic. Count rate losses can be compensated for using the general methods discussed in Section 2.3.8. There has been some work in the literature on these correction methods [4, 45, 46], though they have not been implemented in commercial systems. For whole body scans acquired in continuous acquisition mode the problem can be especially difficult since the count rate for each row of pixels in the image changes as the gamma camera scans over the patient [46].

4.7. NOISE

Unprocessed planar images generally follow Poisson statistics and the precision can be determined from well known statistical relations. The noise levels in planar imaging is a function of administered activity, duration of the acquisition (scanning speed) and camera specific parameters such as choice of collimator, energy window setting and crystal thickness.

4.8. REGION AND VOLUME DEFINITION

ROIs are often defined for whole organs from either anterior or posterior views. If methods for correction of the contribution from over- or underlying tissues are available, regions containing the whole organ can be defined. Care should be taken in regions where spill-in or spill-out due to the spatial resolution is important.

4.9. MOTION

Patient motion affects the spatial resolution and therefore devices that aid the patient in remaining still should be used. This can include straps and comfortable pillows. When performing dosimetry calculations, misalignment due to patient repositioning on the couch for the different imaging sessions will occur even with careful repositioning. This can be compensated for by image registration or alternatively by drawing separate ROIs for each of the time point measurements.

If only one transmission study is performed then it is important that the patient remains in the same position for the transmission scan since the correction is usually made on a pixel by pixel basis. If not, the transmission scan needs to be registered to the whole body measurement by appropriate software. Alternatively, a transmission study for each time point can be performed; this will, however, increase the absorbed dose to the patient.

4.10. CALIBRATION

A calibration of the system sensitivity in units of cps per MBq needs to be performed for each type of collimator and for each energy window setting. The source should be located at a distance that as closely as possible matches the centre of the patient. Depending on the type of acquisition (single planar image or whole body scanning), calibration factors need to be measured for corresponding acquisition protocols. It is also advantageous to acquire an image before voiding in order to compare measured total body activity versus administered activity.

5. QUANTITATIVE SPECT OR SPECT/CT IMAGING

This section discusses the current state of the practice and state of the art in quantitative SPECT at the time of publication. A focus committee of the Society of Nuclear Medicine gave a complete review of various factors affecting quantitative SPECT in 1995 [47]. As there have been significant advances since then, this section will build on that work by providing an update on compensation methods for the factors discussed in Ref. [47].

5.1. TOMOGRAPHIC RECONSTRUCTION

Filtered back projection is widely used for SPECT reconstruction, sometimes in combination with Chang attenuation compensation. Absolute quantification is generally not possible using this approach, though it may be attempted using careful phantom based calibration. Although relative quantification is possible, absolute and better relative quantification can be obtained with iterative reconstruction using compensation for the image degrading

effects discussed below. Filtered back projection has the advantage that it has universal commercial availability, as well as availability in many general purpose image processing packages.

The most widely used and available iterative algorithms for SPECT reconstruction are OS-EM and ML-EM. While ML-EM is not often listed as available on commercial systems, it is equivalent to OS-EM using a single subset per iteration. While the ML-EM algorithm is theoretically appealing, it requires a relatively large number of iterations, especially when using CDR modelling, to produce quantitatively accurate images. As a result, OS-EM using as few as four views per subset is often used. OS-EM is available on recent commercial SPECT systems. It is considered state of the art and the current clinical standard for obtaining quantitative SPECT images. It is particularly advantageous when combined with compensation for attenuation, CDR or scatter, or all three.

5.2. PHOTON ATTENUATION

Attenuation is the single biggest factor degrading quantification in SPECT. Without attenuation compensation, absolute estimates of activity will be underestimated by factors of 5–20, though relative errors will generally be smaller. The magnitude of this effect is greater for low energy photons and for larger and denser regions of the body. Non-uniform attenuation in the chest and head can cause undesirable artefacts that impede both quantification and visual interpretation. Figure 13 shows an example of a simulated uniformly attenuating elliptical cylinder filled with water reconstructed without attenuation compensation. Note the reduced voxel values in the background at the centre of the phantom compared to the edge. Similarly, despite the equal total activity in the two disks, the sum of the reconstructed voxel values for the central disk are substantially lower than for the disk at the edge of the phantom. This demonstrates the spatially varying effects of attenuation on image quantitative accuracy and illustrates that performing relative quantification of objects at different positions in the object is likely to give poor results.

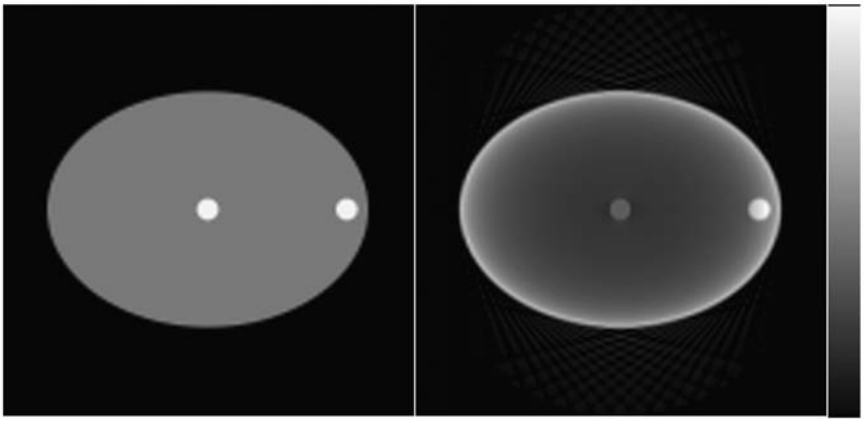

FIG. 13. Water filled cylindrical phantom (left) containing two disks with a higher activity than the background and (right) the image reconstructed from attenuated projections without attenuation compensation.

Both analytical [11, 12, 46–49] and statistical iterative reconstruction [28] attenuation compensation methods have been developed. It should be noted that these methods only compensate for the impact of attenuation on accuracy; the loss of photons due to attenuation results in a non-recoverable loss of precision.

Analytical methods include exact methods [11, 12, 47–51] and approximate methods, such as the Chang attenuation compensation method [46].

The exact analytical methods generally have poor noise properties, are not widely commercially available and are not considered state of the art. Their principal advantage is short reconstruction times, but the development of fast iterative algorithms and the wide availability of powerful computers have resulted in reduced interest in these methods.

The Chang attenuation compensation method is often available commercially and is sometimes used in cases where the attenuation distribution in the area of interest is uniform (e.g. outside the thorax). Often an ellipse is

fit to the data and uniform attenuation inside the ellipse is assumed. The Chang method (sometimes called zero order Chang) performs voxel by voxel attenuation compensation of an image reconstructed without attenuation compensation, typically using filtered back projection. In each voxel the distance from the source to the surface of the object in each projection direction is computed and the average attenuation factor for voxel i, $\overline{f}_i$, is then calculated using:

$$\overline{f}_i = \frac{1}{N}\sum_j e^{-\mu d_{ij}} \tag{27}$$

where N is the number of projections, μ is the attenuation coefficient in the object (often assumed to be water), d_{ij} is the distance from to the ith voxel to the surface in the direction of the jth projection, as illustrated in Fig. 14. Next, to form higher order corrections, the reconstructed image is forward projected, included modelling for attenuation. This forward projection can be done analytically if a uniform attenuation distribution is used and is represented by a geometric shape such as an ellipse for each slice. This projection image is subtracted from the measured projection image, giving error projections. The error projections are reconstructed using filtered back projection. The resulting error image is approximately corrected for attenuation using the attenuation factors above and added to the original reconstructed image. This is the first order Chang estimate and the procedure can be repeated, in which case the method becomes a class of iterative filtered back projection. However, it results in imperfect attenuation compensation and has inferior noise and convergence properties [52]. Typically, commercial systems use the zero order Chang estimate.

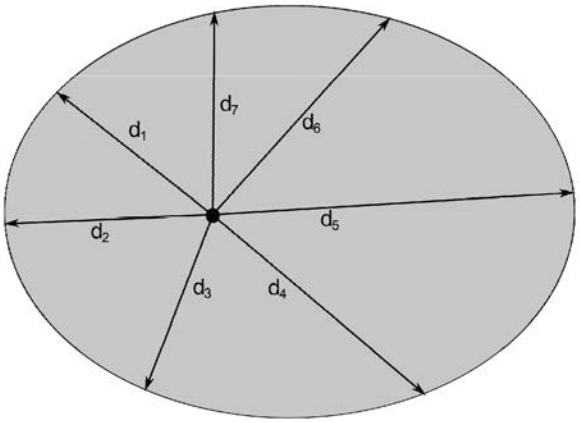

FIG. 14. Illustration of distances from the point to the edge of the attenuator used in the Chang attenuation compensation method.

As a result of the poor noise properties of exact analytical algorithms and the inferior performance of approximate algorithms, the use of statistical iterative reconstruction algorithms such as ML-EM or OS-EM is greatly preferred and considered state of the art. These algorithms are commercially available on all commercial systems that include the ability to measure the requisite attenuation maps.

Attenuation compensation methods require as an input an attenuation map giving the attenuation coefficient in each image pixel. These can either be estimated from the emission data or measured. Estimated attenuation maps are often used in conjunction with the Chang method and are often obtained by fitting an ellipse to the boundaries of the object in the emission projection data. Measured maps can be obtained using a radionuclide source [53–57] or based on a registered CT image [58]. Commercial systems based on radioactive radionuclides have been produced, but are no longer in widespread production. They had the advantage of lower cost and complexity, but required the handling and replacing of high activity (400–2000 MBq) radionuclide sources and the handling of crosstalk between the emission and transmission radionuclides. The attenuation maps produced are generally noisy and have poor resolution, too poor to provide anatomical information. However, as long as the resolution is approximately matched to that of the SPECT image, the poor resolution does not degrade attenuation compensation [59]. Similarly, attenuation compensation in SPECT is not degraded substantially by noise in the attenuation maps [57]. More

important than noise and resolution is having a high enough source strength so that sufficient photons pass through the thickest portion of the patient and compensating for crosstalk in the emission image to avoid biased attenuation maps. With careful attention to these issues and regular source replacement, attenuation maps from radioactive sources can be quite effective for attenuation compensation.

Attenuation maps can also be obtained from CT images. This requires scaling the map to take into account the difference in the energy of the CT X rays compared to the emission radionuclide. As long as a contrast agent was not used during the CT imaging, this translation can be handled by a piecewise linear scaling [60–62], similar to PET. Some additional care is required in translating the attenuation map when reconstructing projection data obtained by summing photopeaks with significantly different energies (e.g. for ^{111}In [63]). The major issue with using CT attenuation maps is that they must be well registered with the emission image. Registration of more than one emission image pixel is required to avoid artefacts. Using CT images obtained from a diagnostic CT scan performed on an independent CT scanner is difficult due to differences in patient position during the scans and generally requires non-rigid registration. The state of the art method for obtaining registered CT images, and the most widespread method used in clinical practice, is the use of SPECT/CT scanners. Even with these scanners, artefacts due to patient breathing motion or misregistration due to imaging table sag, system miscalibration or patient movement between the emission and CT scan can cause artefacts in attenuation compensated images [64, 65]. As a result, careful QC, via inspection of the registration of the CT and non-attenuation compensated image, is advised prior to attenuation compensation.

Sometimes, particularly with the Chang attenuation compensation method assuming uniform attenuation, broadbeam (effective) attenuation coefficients are used to offset the quantitative effects of scatter. While these can be partially effective, the appropriate widebeam attenuation coefficient is both object and activity distribution dependent. As a result, this is not recommended unless no better scatter compensation methods are available, and, if used, careful calibration is required using objects similar in size to the object of interest.

Properly implemented attenuation compensation using a well scaled and registered map can achieve almost perfect compensation for the effects of attenuation on bias.

5.3. SCATTER

In SPECT, scatter fractions are in the order of 20% in the brain and 40% or more in the thorax and abdomen. This can result in spatially varying quantitative errors of a similar magnitude. The scatter to primary ratio increases approximately linearly with source depth, so the quantitative effects of scatter are larger for source positions near the centre of the object. When attenuation compensation is performed using the narrow beam attenuation coefficient, scattered photons affect the image as a spatially varying increase in voxel values, as illustrated in Fig. 15. Note that without scatter, attenuation compensation using an ideal attenuation map almost perfectly recovers the activity concentration in the phantom. However, when scattered photons are present in the projection data, the reconstructed image exhibits spatially varying overestimation of activity in the order of 20–50% depending on the position, even for this relatively small object. Note also that the effects of scatter are greatest in the low activity regions of the phantom.

Scatter compensation requires a scatter estimate and a compensation method. Scatter estimates can be obtained either spatially or based on measurements in additional non-photopeak energy windows (see Section 4.3 for further details). Spatial estimates of the scatter can either be based on stationary approximation of the scatter response function, scatter models or fast Monte Carlo simulations.

A fundamental limitation of all spatially based methods for scatter estimation is difficulty in compensating for scatter from activity outside the field of view. For these methods to be successful, the region reconstructed should extend at least 5 cm above and below the ROI [66], and an attenuation map (or at least an approximate one) must be available in this region.

Methods such as convolution subtraction [67] or scatter deconvolution [68, 69] that assume a spatially invariant scatter response result in poorer scatter estimates than other methods discussed. These methods should only be used when other methods are not possible (i.e. model based methods or additional energy windows are not available), after careful calibration and when reduced quantitative accuracy is acceptable. Transmission based modification of the scatter estimate from convolution subtraction is a significant improvement over standard convolution subtraction and is a superior alternative [70]. These methods are generally not available on commercial systems.

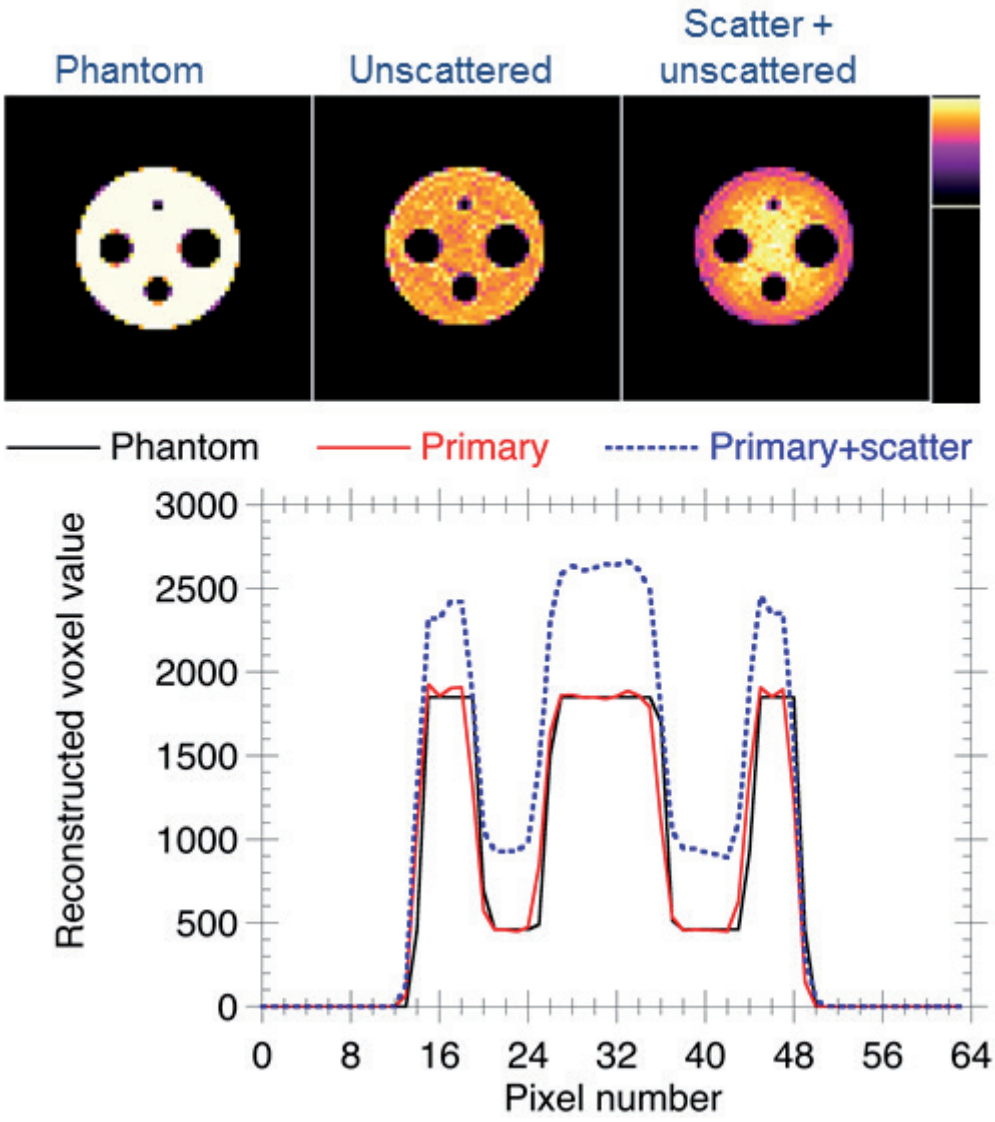

FIG. 15. Images (top) and profiles through images (bottom) at the position indicated at the image on the top right from a simulation of a 22 cm diameter cylindrical water phantom filled with ^{99m}Tc. The phantom contains four cold compartments of varying sizes. The top centre and right images were reconstructed with attenuation compensation from Monte Carlo simulated projections with and without scattered photons.

Model based methods provide rapid estimation of the spatially varying scatter response function [71–75]. While approximate, they are based, to varying degrees, on the physics of the scattering process and use calibrations based on Monte Carlo simulations or experimental measurements of the scatter response function. In model based methods, the scatter in the projection data is estimated from an assumed activity distribution and an input attenuation map. These methods model the spatial variance of the scatter response and give very good agreement for regions with uniform attenuation distributions. Even in regions where the attenuation distribution is non-uniform, such as the chest, these methods have been shown to give good scatter estimates for radionuclides such as ^{201}Tl [76], ^{99m}Tc [70–73, 77], ^{123}I [78], ^{111}In [79, 80], ^{131}I [81] and ^{90}Y bremsstrahlung [82]. Scatter models require significant computational time, but optimized versions can produce scatter estimates in times that are clinically acceptable, adding on the order of a few seconds per iteration for a 64^3 reconstruction volume. These methods are considered close to state of the art for photopeak energy windows and have some commercial availability. Implementing these methods has a moderately high level of difficulty and is not recommended for non-experts.

For cases where downscatter is important and for the highest level of accuracy in areas with non-uniform attenuation distributions, fast Monte Carlo simulation estimation of scatter estimates are the methods of choice [83, 84]. The principal disadvantages of these methods are the longer computation time compared to model based

methods (10 s or more per iteration for a 64^3 reconstruction volume) and the lack of commercial availability. Implementing these methods has a high level of difficulty and is not recommended for non-experts.

Scatter compensation using one of the scatter estimation methods above can be accomplished either using pre-reconstruction subtraction or by including the scatter estimate in the reconstruction process. Especially when used in conjunction with an iterative reconstruction method, pre-reconstruction subtraction is not desirable: it can result in negative projection pixel values that must be handled carefully and results in undesirable increases in reconstructed image noise. Incorporating the scatter estimate into the reconstruction is thus highly desirable for iterative reconstruction methods [85]. This is used in some, but not all, commercial implementations. For model and Monte Carlo based scatter estimates, the scatter estimate can be updated during each iteration via the forward projection process, but, since the scatter estimate converges slowly, updating for only the first two iterations is often sufficient [86]. Additional reductions of computation time can be realized by modelling scatter in the forward projection process only [87, 88].

Well implemented and calibrated TEW (see Section 4.3.2), model or Monte Carlo based methods are capable of reducing the effects of scatter on accuracy to less than 5%.

5.4. RESOLUTION AND PARTIAL VOLUME

In SPECT, the spatially variant CDR significantly degrades spatial resolution and creates significant partial volume effects (PVEs) for small objects. The FWHM of the CDR function increases approximately in proportion to the distance from the collimator. As a result, SPECT images have spatially varying resolution. This means that PVEs will be spatially varying and accuracy of quantifying small objects will thus be position dependent. This is illustrated in Fig. 16. Note the spatially varying resolution with the point source phantom. In general, the tangential resolution improves away from the centre of rotation, while the radial resolution is almost constant. Also note that the spatially varying resolution reduces the contrast of the objects near the centre of rotation as a result of increased PVEs. Thus, the accuracy of estimated activity for small objects near the centre of rotation is worse than for objects closer to the edge of the phantom. For the ^{131}I object note the artefacts due to the septal penetration and scatter in the projections. In an extended source these artefacts would largely result in reduced contrast.

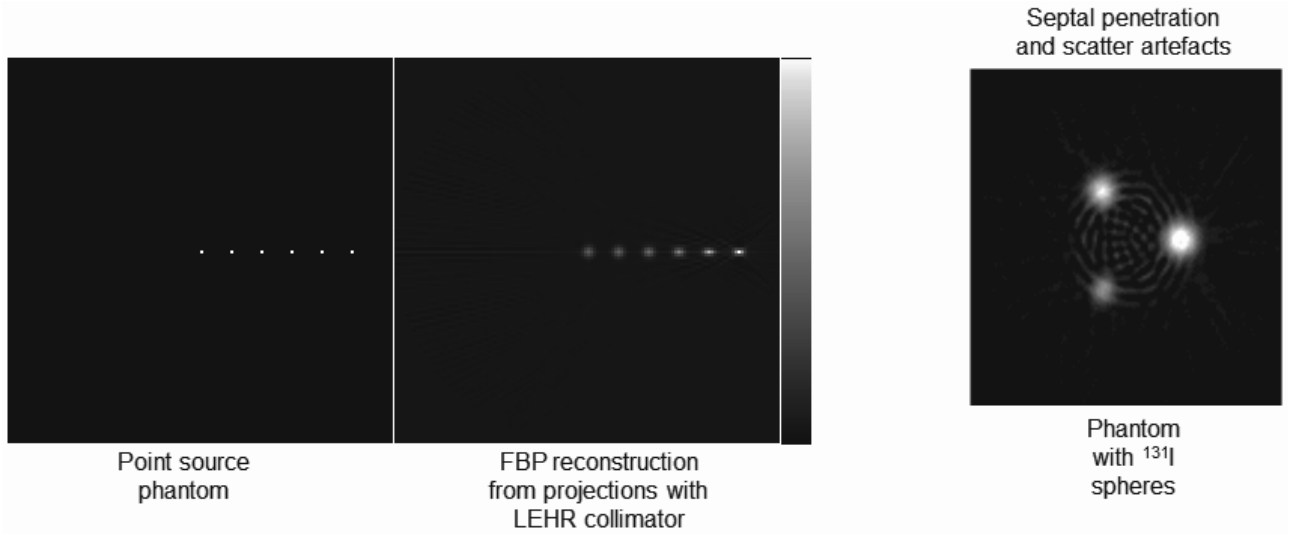

FIG. 16. The image on the left shows the reconstruction of a phantom consisting of a series of ^{99m}Tc point sources imaged in air using a low energy high resolution (LEHR) collimator. The image on the right shows a reconstructed image obtained from a phantom consisting of three ^{131}I spheres. In both cases, the images were reconstructed using filtered back projection without CDR compensation.

Quantification errors due to these resolution effects primarily impact objects with sizes in any direction less than 3 times the FWHM of the CDR. For small objects, the magnitude can be 50% or more with larger effects for small objects and high object to background ratios.

The effects of CDR blurring on quantification are best handled by a combination of appropriate collimator selection, CDR compensation and PVC. Collimator selection has been addressed in the context of planar imaging (Section 4.1) and similar considerations apply to SPECT. Even with appropriate collimator selection there will be some CDR blurring of the projections.

5.5. RESOLUTION COMPENSATION

In SPECT, resolution compensation is accomplished by compensating for the effects of the CDR. This results in improved resolution in the reconstructed images and improved quantitative accuracy (via reduced PVEs) for small objects. There are two basic classes of methods: iterative and non-iterative methods.

The non-iterative methods include inverse filters, such as Wiener or Metz filters, which assume the CDR is spatially invariant [89–93]. These methods are sometimes available on commercial systems, but the choice of CDR functions may be limited and not physically realistic. Implementation of these methods is relatively easy using general purpose image processing software. They will not be as effective at reducing spatially varying effects as iterative methods. While inverse filtering methods that model the spatially varying CDR have been developed, they tend to make approximations of the shape of the CDR [94–97]. In addition, they tend to have poor noise properties. As a result, they have not been implemented commercially and are not considered state of the art.

Iterative reconstruction based methods perform CDR compensation by modelling the CDR in the forward and backward projection processes of an iterative reconstruction algorithm [29, 98–100]. Inclusion of CDR compensation generally requires more iterations to achieve optimal images than when only attenuation modelling is used. It should be noted that iterative CDR compensation does not fully remove the blurring due to the CDR: some information on high spatial frequencies is permanently lost. In addition, the resolution, while improved throughout the image, remains spatially varying. This is illustrated in Fig. 17. More uniform spatial resolution may be obtained by low pass filtering, but this is likely to be undesirable for quantitative applications. Also, iterative reconstruction CDR compensation tends to produce a very different noise texture than either filtered back projection or iterative reconstruction without CDR compensation. In general, there are significant increases in the noise power at middle frequencies, which can result in a blobby texture in the reconstructed image. This is illustrated in Fig. 18. Note the differences in the noise texture as a function of position, compensation method and number of updates.

The heart of iterative reconstruction CDR compensation is the model of the CDR. Often, the model of the CDR is limited to modelling the geometric component of the CDR (i.e. the component due to photons passing through the collimator holes). The advantage of this is that the geometric CDR can be described either by exact [101] or approximate analytical expressions (such as a Gaussian function). For radionuclides and collimators where septal penetration and scatter are important, CDR modelling can be implemented to include these effects. These CDRs must either be measured or estimated with Monte Carlo simulations that include full collimator–detector modelling [80]. When radionuclide appropriate collimators are used, with the possible exception of radionuclides emitting high energy photons such as ^{131}I, much of the benefit of CDR compensation can be obtained by modelling only the geometric component.

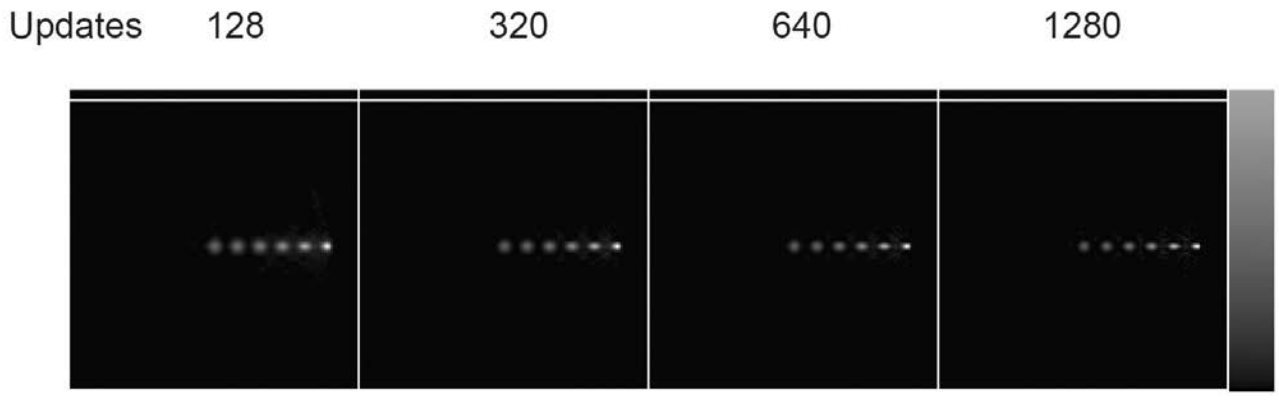

FIG. 17. Reconstruction of projections of the point source phantom in Fig. 16, obtained using OS-EM with compensation for the geometric CDR. The number of updates is shown above each image.

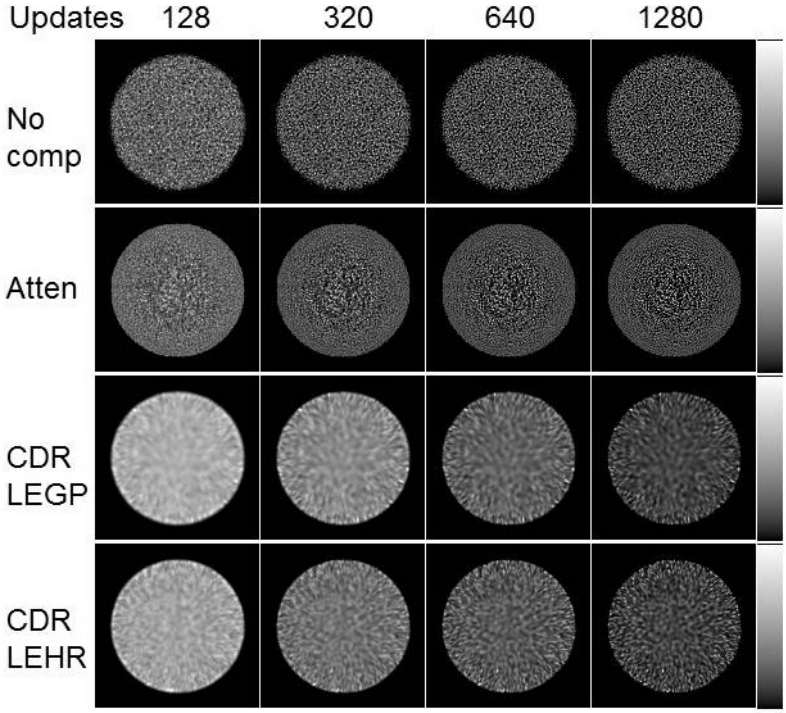

FIG. 18. Reconstruction of noisy projections from a uniformly emitting and attenuating cylindrical phantom. The images were obtained using OS-EM with the indicated number of updates. The reconstructions include various combinations of compensations. The effects included in the projection data match those compensated for in the reconstruction.

The CDR is a function of the distance from the face of the collimator. As a result, CDR modelling requires knowledge of the distance from the centre of rotation to the collimator face for every projection view. For acquisition using circular orbits, one needs to know only the radius of rotation. For non-circular orbits, a table giving the distance from the collimator face to the centre of rotation for each view is required. This information is not always available on commercial scintillation cameras and, if available, is typically stored in vendor specific fields in image files and thus may be difficult to access in a general way.

Recent software from commercial vendors provides the capability to perform iterative reconstruction based geometric CDR compensation, though this capability may be available only for certain imaging protocols. Iterative reconstruction based CDR compensation is considered state of the art but has limited use in current clinical practice, partly due to its relatively recent availability. It is often used to reduce scan time by providing an improved resolution–noise trade off compared to conventional low pass filtering [102]. It should also be emphasized that CDR compensation is not complete and residual PV effects remain.

5.6. PARTIAL VOLUME CORRECTION

With or without CDR compensation, SPECT images tend to be degraded by the effects of the CDR. This can result in significant PVEs. As a result, when quantifying activity in volumes that are neighbouring objects with very high activity, spill-in effects can be significant. Similarly, when quantifying objects smaller than three times the width of the CDR, quantification can be severely degraded by spill-out. Achieving the highest level of quantitative accuracy requires the addition of PVC. The basic idea of all PVC methods is to make the assumption that the activity distribution inside a VOI is uniform and to use this information to try to compensate for the effects of spill-out or spill-in. PVC methods can be divided into those based on calibration methods, postprocessing methods or reconstruction based methods.

Calibration methods involve the use of phantom experiments to estimate recovery coefficients, defined as the ratio of the true activity divided by the measured activity [103–108]. The recovery coefficient is a function of the object shape, size, activity relative to the background and, due to the spatially varying resolution in SPECT images, the position in the image. Due to the number of variables, recovery coefficients are typically tabulated only as a

function of object size. Since they are applied to the quantification of small objects, the shape is assumed to be spherical, spatial variations are ignored and the background activity is often assumed to be zero. As a result, these methods have limited accuracy [108]. On the other hand, while they do require the performance of a set of careful phantom experiments, they can be implemented on any camera system and do not require any special software.

The idea of post-reconstruction methods is to measure spill-in and spill-out effects for each VOI or voxel for each patient. This allows the taking into account of the effects of activity in neighbouring VOIs or voxels, the shapes of the VOIs and the spatial variation of resolution. There are two classes of these methods: those that perform PVC for each voxel [109–112] and produce a PV compensated image and those that compensate for the PVEs of the activity estimates of each VOI [113, 114]. The voxel based techniques tend to be less theoretically sound and are perhaps less appropriate for quantitative imaging tasks; they will not be discussed in this publication. They do, however, have the advantage of providing a PV corrected image.

Post-reconstruction VOI based PVC is done by modelling the blurring that occurs during the image formation process for each VOI and measuring the fraction of activity that spills-out of the VOI and spills-in to each of the other VOIs. The set of these is used to form a geometric transfer matrix (GTM), which can then be inverted and applied to the set of measured activities [113]. When applied to images obtained using iterative reconstruction CDR compensation, the non-linearity of the reconstruction process must be taken into account and the GTM can be determined using perturbation techniques [114]. As a simplification, the blurring can be modelled as spatially variant. While still an improvement over calibration methods, this will limit the accuracy of PVC. When carefully implemented, these methods can give significant improvements in accuracy, but result in degraded precision for the activity estimates. These methods are not currently commercially available. Implementation of GTM based methods can be done with general purpose image processing software when spatially invariant resolution is assumed. Implementing the GTM method for spatially varying resolution requires the ability to perform forward projection of images of the VOIs and reconstruct the resulting projection data and thus requires significant expertise to develop.

PVC is not used or available in current clinical practice. It is considered state of the art and important for quantifying activity in small objects such as tumours.

5.7. RECOVERY OF 3-D INFORMATION

In SPECT, 3-D information is recovered by tomographic reconstruction (see Sections 2.3.9 and 5.1). The 3-D nature of SPECT images eliminates the issue of overlap of target and non-target activity except for PVEs discussed above.

5.8. COUNT RATE PROBLEMS

The issues are similar to those for planar imaging. Significant count rate losses are only an issue for very high count rates, usually well above count rates obtained in the imaging of diagnostic or treatment planning injected activities. For imaging patients after administration of therapeutic doses, the effects may be significant and are dependent on the camera manufacturer and model. The effects on quantification are not well studied and there has been limited work on developing compensation methods.

5.9. NOISE

Noise in SPECT images originates from the Poisson noise in the projection data. It is correlated by the tomographic reconstruction algorithm and compensation methods in a way that is specific to each method. It results in a loss of precision for quantitative estimates. For quantitative tasks, regularization of image reconstruction by post reconstruction filtering or the use of MAP reconstruction methods will reduce variance (improve precision) at the expense of increased bias. The effects of noise can be reduced by using longer acquisition times or larger injected tracer activities. Higher sensitivity collimators can also reduce noise in the projection data, but when combined with CDR or PVC compensation, the benefits in terms of precision of quantitative estimates are unclear.

In general, for large VOIs such as the liver, kidneys or lungs, the effects of noise on precision for typical acquisition times and injected activities is relatively modest (less than 1%) [44, 80, 115, 116]. The effects on precision due to variations in patient anatomy and uptake will generally be larger (in the order of several per cent) [117].

5.10. REGION AND VOLUME DEFINITION

Quantifying activity in an organ or VOI requires defining VOIs in the SPECT images. Because the noise in SPECT images is relatively high and resolution is relatively poor, VOIs defined in SPECT can be both inaccurate, operator dependent and imprecise. Automatic or semi-automatic segmentation of SPECT images is difficult. Use of well registered, high resolution anatomical images for VOI definition can enable improved manual or automated definition of VOIs. The use of SPECT/CT systems thus has the potential to provide significant improvement in definition of VOIs, but there can be mismatch between functional and anatomical volumes. In one study using a physical phantom, compartment volumes were estimated very accurately using CT images [118]. However, misregistration between SPECT and CT images can result in significant errors. Registration should be accurate to more than one SPECT voxel in order to obtain good accuracy [119]. Variation in the definition of organ boundaries and the degree of misregistration can introduce uncertainties in organ activities in the order of those due to noise [119, 120].

5.11. MOTION

Motion is a significant problem degrading SPECT images. There has been little study of the effects of motion on quantitative accuracy in SPECT. In general, the effects are likely to be large for small objects such as tumours but less important for large objects such as the liver.

Blurring due to the beating of the heart is generally smaller or similar in size to CDR blurring and is thus not a major effect. Cardiac gating is generally available to reduce these effects, but gated images will generally have higher noise, and methods of non-rigidly transforming images obtained in different gates are not mature. Respiratory motion can cause artefacts and blurring, especially of objects inside the lungs, mediastinum or close to the diaphragm. Respiratory gating is generally not available on SPECT systems and respiratory motion compensation is still an area needing research attention. Voluntary motion is a significant source of artefacts in SPECT images due to the relatively long acquisition times. The use of patient restraints is recommended to reduce these effects. Limited post-acquisition compensation for patient motion is commercially available.

Voluntary patient motion compensation is commercially available [121–126]. However, these methods have not been validated for quantitative applications. They tend to be unreliable and should be used with caution. Compensation for cardiac and respiratory motions is not commercially available and no well validated and established methods are currently available.

5.12. CALIBRATION

The units of reconstructed SPECT images are typically not activity per voxel. Instead they are (or at least should be) proportional to the number of decays that occur in a voxel during the acquisition, where the proportionality constant is unknown. Thus, the activity, A_a, in some VOI (which could be a single voxel in size) is equal to the sum of the SPECT voxel values in the VOI, D_a, obtained for SPECT acquisition a multiplied by a calibration factor, k. That is:

$$A_a = k\frac{D_a}{t_a} \tag{28}$$

where t_a is the total acquisition duration for the SPECT, i.e. the number of views multiplied by the acquisition time per view. The units of k are activity multiplied by time per SPECT voxel value. This calibration factor depends, in principle, on the imaging system, acquisition parameters and patient, and on the reconstruction and compensation

methods used to obtain the image. The use of appropriate attenuation and scatter compensation should largely remove the effect of patient dependent factors and this will be assumed in the following discussion. However, quantifying SPECT images requires measuring a calibration factor that accounts for the effects of the remaining factors.

For convenience, the calibration factor, k, can be divided into two components: (1) the sensitivity of the collimator and detector for the specific collimator, system and radionuclide used for the imaging and (2) protocol specific factors including residual errors resulting from the image processing and compensation methods and scaling factors sometimes used when images are stored. The sensitivity, S, is often expressed in units of counts per unit activity per unit time and tends to vary over time due to changes in the gain of the detector system resulting in shifts in the energy gain. Fortunately, the sensitivity is relatively easy to measure and so can be calibrated frequently. As described below, the protocol specific factor, referred to hereafter as the reconstruction factor, R, is more difficult to measure, but tends to be less dependent on time. The unit of R is counts per SPECT voxel value. The calibration factor can be expressed in terms of S and R:

$$k = \frac{R}{S} \tag{29}$$

In the following, we discuss measurement of both factors and combining them into a single factor for use with each patient.

The sensitivity of the collimator detector system can be measured using a calibration source. The calibration source should be small enough so that attenuation is not a major issue and have an activity small enough not to cause count rate loss problems but large enough to produce a count rate significantly higher than the natural background. Typically, activities of 10–40 MBq and volumes of 5–10 mL are appropriate. The acquisition time for the sensitivity measurement should be such that a total of 10^5–10^6 counts are obtained, ensuring that the precision of the sensitivity measurement is better than 0.5%. Since the sensitivity depends on the collimator, radionuclide and energy window settings, the sensitivity must be measured for the same values of these parameters as used for the study to be quantified. In addition, since the energy calibration can vary with time, the sensitivity should be measured at least daily and, ideally, for each patient study to be quantified, using the same energy window settings used in the patient study. In addition, when septal penetration and sensitivity are non-negligible, the sensitivity depends on the distance from the collimator. Thus, the distance from the collimator to the detector calibration source should be standardized. To reduce the effects of attenuation the source should be suspended between the collimators. It is wise to acquire an image of the natural background (with the calibration source well shielded or out of the room). Good practice is to suspend the source at a distance from the collimator approximately equal to the average radius of rotation for a typical patient study. The natural background image should be acquired for the same acquisition time and then subtracted from the acquired image. An ROI is drawn over the source. It should be large enough to include all the geometrically collimated photons but as small as possible to exclude as many photons undergoing septal penetration and scatter as possible. The size of this ROI should be standardized for all measurements for the same collimator and radionuclide combination. From this measurement, sensitivity is calculated as the counts in the ROI in the background corrected calibration source image divided by the acquisition time and the activity in the source. Mathematically, we have:

$$S = \frac{C - B}{t} \tag{30}$$

where t is the acquisition duration, C is the counts in the ROI in the image of the standard source and B is the counts in the ROI in the background image.

The reconstruction factor should be measured using a phantom with known activity or activity concentration. Ideally, the phantom used should mimic, at least to some extent, the patient images to which the protocol will be applied. A set of SPECT projections are then acquired using the same protocol (including energy window settings, acquisition time, collimator and camera) as for the patients. The data are reconstructed using the same algorithm,

compensations and post processing. The reconstructed image is then quantified in a way relevant to the imaging task. For the following discussion we will assume that the task is to estimate the total activity in some volume in the object. Let the total activity in the portion of the phantom used in the calibration procedure be A_{phan} and D_{phan} be the sum of the SPECT voxel values in that volume. Combining Eqs (28) and (29) above, we have:

$$R = S_{\text{phan}} k = S_{\text{phan}} \frac{A_{\text{phan}} t_{\text{phan}}}{D_{\text{phan}}} \tag{31}$$

(Note that the above equation can be used for a phantom with known activity concentration by replacing A_{phan} with the value of the known activity concentration and D_{phan} with the sum of the SPECT voxel value in the desired VOI divided by the volume of the VOI.)

To find the activity in a VOI from a patient image, A_{pat}, first the sum of the SPECT voxel values in the VOI, D_{pat}, is computed. Using Eqs (28), (29) and (31), above, we have:

$$A_{\text{pat}} = \frac{R}{S_{\text{pat}}} \frac{D_{\text{pat}}}{t_{\text{pat}}} = \left[S_{\text{phan}} \frac{A_{\text{phan}}\, t_{\text{phan}}}{D_{\text{phan}}} \right] \frac{1}{S_{\text{pat}}} \frac{D_{\text{pat}}}{t_{\text{pat}}} = \frac{S_{\text{phan}}}{S_{\text{pat}}} \left[\frac{A_{\text{phan}}\, t_{\text{phan}}}{D_{\text{phan}}} \right] \frac{D_{\text{pat}}}{t_{\text{pat}}} \tag{32}$$

where t_{pat} is the duration for the patient study and S_{pat} is the sensitivity for the patient scan.

As an example of the above procedure, consider the task of quantifying the activity in the liver for a targeted radiotherapy treatment planning application. A phantom having a compartment similar in size to a liver embedded in a phantom with a cross-section similar to a patient should ideally be used. The liver compartment would be filled with a total activity proportional to that expected in the patient and the background filled to give the expected target to background ratio. SPECT projections would then be acquired using the same energy window, collimators and other protocol settings that would be used for patient imaging. Note that the acquisition time might be extended in order to increase the precision of the calibration factor. A standard source would then be imaged to measure the system sensitivity. A reconstructed image would be obtained using appropriate compensations for degrading factors. The counts in the liver VOI are obtained and used in Eq. (31) to calculate the reconstruction factor. This factor is then used in Eq. (32) to compute the activity in the patient's liver.

6. QUANTITATIVE PET OR PET/CT IMAGING

PET has always been considered a quantitative imaging modality since it has the potential to precisely estimate local concentration of the radiotracer and since meaningful physiological parameters can be derived from these local concentration values. However, obtaining quantitative PET images requires careful attention to a number of details, some of which are typically hidden from the operator. These details will be discussed below. The quantitative interpretation of PET images was first widely used in brain studies, for instance to characterize neurotransmission and brain processes altered by neurodegenerative diseases. This application has been recently superseded by oncology studies, in which both the detection and the quantification of abnormal uptake are relevant. In that specific application, the uptake is most often characterized by the SUV (see Section 2.1.7). SUV is especially used for patient monitoring, i.e. as a way to determine whether tumours respond to therapy by performing PET/CT scans over the course of therapy or at the end of the treatment. Also, accurate SUV maps are considered to be a potentially useful adjunct to CT for designing treatment plans in radiotherapy. In all these applications, accurate quantification of the PET images is a prerequisite. The following is an overview of the major issues; additional detail can be found in Refs [127–129].

6.1. TOMOGRAPHIC RECONSTRUCTION

Tomographic reconstruction affects the quantitative reliability of PET images indirectly through the spatial resolution and the noise properties of the reconstructed images. However, from a practical point of view, because various reconstruction approaches lead to different trade-offs between spatial resolution and noise level, the reconstruction algorithm impacts the quantitative accuracy and differences of up to 40% in metabolic parameters can be observed depending on the reconstruction approach that is used [130].

Reconstruction algorithms used can be classified based on whether they are applied to list mode or sinogram data. For sinogram data, iterative or analytical algorithms are available. For list mode data, only iterative reconstruction algorithms are available. An additional classification of algorithms is whether they come from 2-D or 3-D acquisition modes. Data acquired in 2-D acquisition mode is reconstructed using 2-D reconstruction algorithms applied to sinogram data from each 2-D slice. Data acquired in 3-D mode can be reconstructed either by first rebinning into 2-D sinograms and then using 2-D reconstruction or by using fully 3-D reconstruction algorithms. This section first briefly reviews sinogram and list mode data formats, followed by 2-D and 3-D acquisition modes and then analytical and iterative reconstruction methods.

In PET, each detected event defines a line of response (LOR), which is defined as a line joining the centres of two detectors along which the associated radioactive decay is assumed to have occurred. The detected event can be recorded in either sinogram or list mode format. A sinogram is an array of all geometrically valid lines of response; the event is recorded in the sinogram by incrementing the count in the appropriate bin of the sinogram. In list mode format, detected events are recorded in a sequential list that includes the coincident detectors, detected photon energies and detection time stored for each detected coincidence in the order they were detected. Given the very high number of possible LORs, the list mode format can actually be more compact than sinogram format. Iterative reconstruction techniques can take advantage of the fine sampling of the list mode data using list mode reconstruction methods. In these methods, unlike the sinogram format, no a priori sampling needs to be defined [131, 132]. This can help improve the spatial resolution of the reconstructed image. List mode reconstruction is primarily applied to data acquired in 3-D acquisition mode.

PET data can be acquired in either 2-D or 3-D acquisition modes. In understanding the difference, it is helpful to consider the individual detector elements as being organized into rings, where rings of detector elements have centres lying in planes perpendicular to the axis of the tomograph. A LOR can be characterized by its ring difference: the difference in the ring number for the two coincident detectors when rings are numbered sequentially along the axis of the tomograph. In 2-D acquisition mode, septa physically restrict the possible lines of response to ones that are near-perpendicular to the axis of the tomograph and LOR data are only saved for ring differences of 0 or 1. Data for ring differences of 1 are treated as if they came from a virtual ring halfway between the neighbouring rings and are referred to as cross-plan slices. As a result, data from each direct or cross-plan slice can be treated as data acquired from a single 2-D slice through the patient and thus be reconstructed using 2-D reconstruction methods. In 3-D acquisition mode, septa are not present and data can be acquired from LORs with every possible ring difference. Data acquired in 3-D mode cannot be treated as data from a set of independent slices and 3-D reconstruction methods must be used. These methods can include both fully 3-D reconstruction algorithms or rebinning the 3-D data into 2-D data followed by reconstruction using a 2-D algorithm. 2-D acquisition mode has reduced sensitivity, resulting in fewer detected events and thus noisier images. However, 2-D mode also results in substantial reduction in scatter and random coincidences. Imperfect scatter and random corrections can introduce bias into PET images and reduce quantitative accuracy. Thus, 2-D mode is sometimes preferred for the highest quantitative accuracy, assuming it provides sufficient count levels for adequate precision. 2-D acquisition mode is not available with all current commercial scanners.

Both analytical (filtered back projection) and iterative reconstruction approaches are used in 2-D and 3-D PET. The use of iterative reconstruction allows for more accurate compensation of the physical factors affecting the measured data, especially the limited spatial resolution of the detector. Note that, while attenuation can accurately be precorrected in the sinograms in PET (see Section 6.2 for a more detailed discussion), there are also some approximate precorrections of scatter available for PET (see Section 6.3 for a discussion of the limitations of these pre-correction methods). In addition, statistical iterative reconstruction algorithms have the advantage of explicitly taking into account the noise properties of the projection data in the reconstruction process.

As described above, analytical algorithms for data acquired in 2-D mode are relatively straightforward: the 3-D activity distribution is reconstructed slice by slice using standard 2-D filtered back projection reconstruction applied to the sinogram data for each slice. Analytical reconstruction for 3-D data is somewhat more difficult because the 3-D data from a PET scanner are axially truncated. In other words, full projections of the field of view are not acquired for projection directions making oblique angles to the axis of the tomograph. Analytical fully 3-D reconstruction algorithms have been derived for the case where sinogram data are available for LORs making a range of oblique angles with the axis of the tomogram [133, 134]. However, these data require that full untruncated projections of the object be available for each oblique angle. In 3-D PET systems, full data is only available for the direct planes and thus these fully 3-D algorithms are not directly applicable. To solve this problem, the 3-D reprojection algorithm (3-D-RP) is most often used to reconstruct 3-D data [135]. In 3-D-RP the object is initially reconstructed from the direct plane data using 2-D reconstruction. It is then reprojected to estimate the missing data. The resulting 3-D data can then be reconstructed using a 3-D analytical reconstruction algorithm.

The most common iterative reconstruction algorithms used in PET are ML-EM and its accelerated versions, OS-EM and RAMLA [27]. Unlike OS-EM, RAMLA includes an explicit regularization parameter to control noise (while noise is only controlled through the number of iterations, or post-filtering, when using ML-EM and OS-EM). All these iterative algorithms come in 2-D versions, appropriate for 2-D PET data and in a 3-D version, appropriate for 3-D PET data. The 2-D versions can also be used to reconstruct 3-D PET data after what is called rebinning. The rebinning approaches consist in taking 3-D PET data and re-sorting the detected coincidences so as to assign each of them to sinograms corresponding to slices perpendicular to the patient axis, as acquired in a 2-D PET configuration. These rebinning approaches were initially proposed to handle the 3-D data with conventional 2-D reconstruction algorithms at a time when fully 3-D reconstruction algorithms were not practical. Different approaches for rebinning have been proposed including single slice rebinning [136], multislice rebinning [137] and Fourier rebinning [138]. The latter has gained wide acceptance, offering a good compromise between computational efficiency and accuracy. All these rebinning approaches include approximations and typically result in a loss of axial resolution. For this reason, 3-D PET data should ideally be reconstructed with fully 3-D reconstruction approaches instead of 2-D methods after rebinning. All PET system vendors now offer 3-D reconstruction.

When using iterative reconstruction, fully 3-D reconstructions provide the opportunity to fully model physical effects such as scatter, geometric effects or detector response. However, accurate modelling of the 3-D effects such as scatter and detector response requires accurate simulation, such as Monte Carlo simulations or other precise characterization of the non-stationary detector and scatter response, which are not easy to achieve in practice. In addition, the system matrix modelling the relationship between the actual activity distribution in the patient and the detected signal becomes highly non-sparse when modelling these effects, while it contains a lot of zeros when the 3-D effects of scatter and the detector response are ignored. Despite these practical difficulties, fully 3-D reconstruction with full modelling of physical effects is the solution that will likely become the standard in the near future, even if it is based on approximate models of scatter and non-stationary detector response.

6.2. PHOTON ATTENUATION

Attenuation is a major source of bias in PET and PET/CT imaging: without attenuation compensation, activity values can be underestimated by 70% or more, depending on the actual patient body size and on the location of the organ (or tumour) of interest. In addition, attenuation introduces strong distortions in the apparent activity distribution (see Fig. 19), making relative quantification unreliable [139].

Accurate attenuation correction can be performed in PET, based on a transmission measurement [140]. The transmission measurement leads to an estimate of an attenuation coefficient map, μ, (the attenuation coefficients in the map are expressed in cm^{-1}), which characterizes the attenuation properties of the tissues. Such a map is typically estimated in one of two ways:

(1) By using a transmission device consisting of a gamma ray (such as ^{137}Cs) or positron emitting source (such as ^{68}Ge) that rotates around the patient and acquires transmission data;
(2) By using a CT scan, taken either independently in the radiology department or during the same imaging session as the PET scan when using a PET/CT scanner, which leads to HU units that can be converted into μ maps at 511 keV.

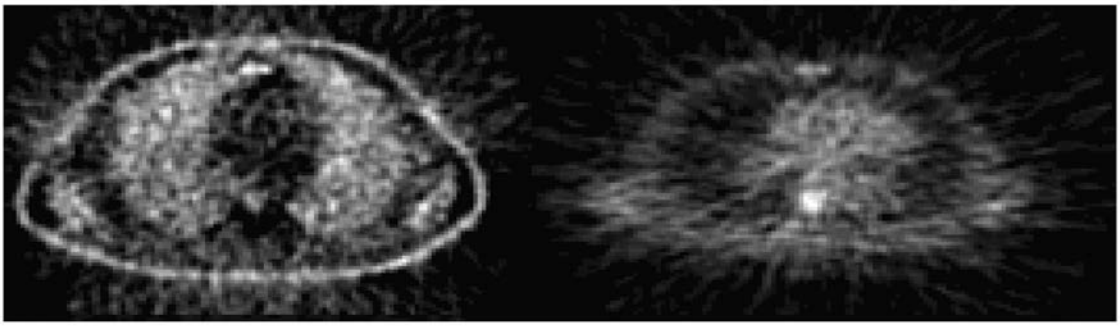

FIG. 19. Thorax PET images without attenuation correction (left) and with attenuation correction (right).

All commercial scanners now have CT as standard, so that attenuation correction is almost always based on CT images.

Using a CT for attenuation correction has become a standard as it has several benefits over maps derived from a gamma or positron based transmission device (so-called conventional transmission devices). First, the duration of the transmission scan is much shorter with a CT than with a conventional transmission device. Second, the attenuation maps resulting from the CT data are almost noise free, unlike the maps resulting from the conventional transmission device. The CT attenuation maps also have better spatial resolution than those obtained from the conventional transmission device, but this does not necessarily provide an advantage in terms of attenuation correction. Indeed, the mismatch in spatial resolution between the CT based attenuation map and the PET data can create artefacts at the interface between tissues of different densities (soft tissue and lungs for instance) and the CT attenuation map should actually be blurred to match the spatial resolution of the PET data to avoid such artefacts. The most important drawback of using CT to derive the attenuation map for attenuation correction is the mismatch due to the differences in respiration during CT and PET acquisitions. CT data typically correspond to a specific phase of the respiratory motion, while PET data includes averaged respiratory blur. This creates well known artefacts, especially at the interface between the lung and liver [141, 142], which must be carefully recognized to avoid misinterpretation. These artefacts can also cause quantitative errors in this region. Respiratory gated PET associated with respiratory gated CT could offer a solution to this problem, but the radiation dose from the 4-D CT scans is potentially high and must be reduced before this can be used routinely. The dose increase associated with the systematic use of the CT to compensate the PET data for attenuation is carefully considered by the vendors, who have proposed low dose CT scans to avoid a significant dose increase to patients undergoing repeated PET/CT scans.

In PET, noise from transmission images propagates directly into the PET images and thus must be treated carefully. This is a very minor issue for CT attenuation correction. However, the noise for conventional transmission devices can be significant. Reduced noise can be achieved by smoothing the attenuation map reconstructed from the transmission data before reprojection in order to reduce the propagation of the noise present in the attenuation map to the attenuation corrected PET images [143]. Additional details and references for this are provided in Ref. [139].

In both cases, the accuracy of the registration of the attenuation map with the emission data should be carefully checked to avoid attenuation compensation induced artefacts.

One important issue with measured attenuation maps is rescaling if the energy of the transmission source is different from 511 keV (which is the case for gamma ray emitting sources and CT sources). In these cases, the attenuation coefficient values need to be translated so they describe the attenuation coefficients at 511 keV. One difficulty is that the attenuation coefficients for soft tissue, bone and contrast agents scale differently with energy. Thus, no single scale factor can be applied to the attenuation map. Bilinear rescaling is usually recommended when no contrast material is used [144]. However, when iodinated contrast is used in CT to enhance attenuation in the vessels (intravenous (IV) administration) or gastrointestinal tract (oral administration), HU units in contrast enhanced pixels scaled using this bilinear approach will be too high and yield overcorrection of the PET data. It has been shown that IV contrast at normal concentrations does not introduce significant biases in the PET images corrected for attenuation using the CT and bilinear scaling [145], but oral contrast does. To account for oral contrast in the attenuation map scaling, one solution is to first separate contrast enhanced regions corresponding to oral contrast from those corresponding to bone attenuation [146] and then set the voxels identified as including oral

contrast to a tissue equivalent attenuation coefficient value, to ensure accurate attenuation correction in the presence of oral contrast medium. Another option is to administer dilute IV or oral contrast material so that the impact of these agents on the scaled attenuation map is small.

Given the rescaled attenuation map, there are two mechanisms for attenuation correction:

(1) Multiplication of each LOR signal by the appropriate attenuation coefficient factors derived from the transmission measurement;
(2) Modelling of the attenuation in the transfer matrix used for image reconstruction, based on the estimated attenuation map.

Both approaches are theoretically accurate, but the latter provides improved noise properties compared to the former.

Attenuation correction is available on all PET scanners, although the transmission map measurements and the actual correction method may differ from one scanner to another. Attenuation correction should be routinely used to obtain quantitative estimates of the activity distribution in PET.

6.3. SCATTER

Because of the limited energy resolution of the PET or PET/CT scanners, coincidences including one or two scattered photons are frequently detected. In 3-D PET, the fraction of scattered events can exceed 50%, while smaller fractions of scattered events are detected in 2-D PET [147]. The detection of scattered events leads to incorrectly located events in the reconstructed PET image. The point response due to scattered events is very broad in PET and extends beyond the boundary of the object. As a result, activity can be detected in activity free regions and overall, contrast and quantitative accuracy are reduced by the presence of scatter. For accurate quantification, scatter must be compensated for, especially in 3-D PET.

Three strategies are commonly used for scatter compensation [147]:

(1) *Energy window based methods, requiring the acquisition of the coincidences detected in several energy windows.* The scatter distribution is estimated by combining the data from different energy windows. These approaches are most appropriate for scanners with high energy resolution. The estimated scatter distribution can be either subtracted from the projection data or, preferably, modelled during the reconstruction. The main advantage of this approach is that, unlike most other scatter correction methods, it can account for scatter coming from out of the field of view activity.
(2) *Fitting of activity measured outside the patient boundaries to estimate the scatter distribution inside the patient boundaries.* This approach is justified by the fact that in PET, coincidences involving scattered photons (unlike coincidences involving only unscattered photons) are detected outside the patient boundaries and can thus be easily identified as resulting from scatter. Because the scatter distribution is most often low frequency, extrapolation of the scatter spatial distribution within the patient boundaries based on the scattered coincidences measured outside can be performed using smooth functions.
(3) *Estimating the distribution of scattered coincidences using only scatter models.* In this method, the scatter distribution is estimated based on the attenuation map, which describes the scattering medium, and on a preliminary estimate of the true activity distribution. The latter is usually obtained using a first reconstruction without any scatter compensation. The image of scattered photons is then estimated, most often using a single scatter simulation model, meaning that only contributions from photons that scatter once are modelled. For single scatter simulation methods, the contribution from higher order scatter is often estimated, for example, by rescaling the scatter distribution so that it matches the portion of the sinogram outside the patient boundaries. The sinograms of this scatter image are calculated and then subtracted from the sinograms that are actually measured. Reconstruction of this supposedly scatter free sinogram leads to a scatter corrected PET image. More sophisticated models for estimating the contribution of the scattered coincidences to the sinograms can also be used. Alternatively, the scatter response function can be incorporated into the forward model used in tomographic reconstruction. The disadvantage of this approach is that it does not compensate

for scatter due to out of the field of view activity, as it is based on a preliminary reconstruction of field of view activity only.

Scatter correction methods are available on all PET or PET/CT scanners (although the actual correction method varies from one vendor to another) and should be systematically used, especially in 3-D PET.

6.4. RESOLUTION AND PV

Effects of resolution and PV problems are quite similar to those encountered in SPECT imaging (see Section 5.6). The imperfect spatial response function of the PET scanner can be accounted for by modelling the spatial blurring introduced by this response function into the system matrix model used in tomographic reconstruction. This correction has been shown to significantly improve quantification in small structures [148].

PVE can introduce significant biases (greater than 50%) when assessing the tumour uptake (or SUV) in small tumours or in small brain structures. Compensation methods exist [149].

The simplest approach consists of multiplying the measured activity (or estimated count level) value in an ROI or VOI by a recovery coefficient. This coefficient is measured as a function of the object size (often considered as a sphere, but any shape could actually be considered when calculating the recovery coefficient), the surrounding activity, the spatial resolution in the reconstructed images and ideally, the image sampling. A limitation of this approach is the need to first estimate the volume of the object of interest, which is often obtained using the CT when using a combined PET/CT scanner. Ideally, the recovery coefficient should be calculated for each object to account for the object shape and contrast, which is feasible in practice [150].

A more sophisticated approach consists of segmenting the images into N non-overlapping regions with assumed uniform activity in each and calculating the spill-out and spill-in between these regions, assuming that the spatial resolution in the reconstructed images is known. This leads to an $N \times N$ matrix, in which each entry (i, j) corresponds to the fraction of activity emitted from region i that is actually measured in region j. By inverting this matrix, the GTM, the activity values in each compartment can be estimated given the activity value measured in the reconstructed image. Similar to the recovery coefficient approach, this correction first requires a segmentation of the VOI. In addition, it requires a segmentation of the other compartments of the images characterized by different activity values and makes the assumption that the activities in these compartments are uniform.

The GTM approach can also be applied at the voxel level, so as to lead to a PVE corrected image instead of only PVE corrected uptake values for specific regions [109, 151]. Other methods yielding PVE corrected images include using a multiresolution approach to extract high resolution details from the CT data and transform and incorporate them in the low resolution PET image [152]. Discrete wavelet transforms of both the high and low resolution images are performed to identify a level of spatial resolution common to both types of images. However, this 2-D method assumes a positive correlation between the grey levels in the anatomical and PET images, which is not a realistic assumption in whole body images.

Other more sophisticated PVCs have been developed for PET and have been extensively described in Ref. [149]. Most of these have been demonstrated to improve quantitative accuracy, without substantial increase in variability compared to not using any PVC.

6.5. RECOVERY OF 3-D INFORMATION

The issue of background activity is solved through tomographic reconstruction and is thus not relevant here.

6.6. COUNT RATE PROBLEMS

Dead time issues (especially in 3-D PET) are dealt with by calculating a calibration factor for a count rate similar to that used in a clinical setting. PET scanners are calibrated using a calibration curve that depends on the count rate and implicitly corrects for dead time effects.

Random coincidences are systematically compensated for by the manufacturer, either based on recording the single events or using a delayed time window to estimate the random fraction in each LOR and subtract it accordingly [153]. Random coincidences can be pre-subtracted or corrected by incorporation into an iterative reconstruction algorithm.

6.7. NOISE

Noise can bias quantitative measurements in PET, especially the SUV when calculated from the maximum pixel value in a tumour region [130]. It can also complicate the fitting of curves when using kinetic analysis. Noise can be reduced by reducing the number of updates (iterations multiplied by subsets for OS-EM), low pass post-reconstruction filtering of the reconstructed images, regularization of the reconstruction (e.g. in RAMLA) or by increasing the smoothing in the reconstruction filter for filtered back projection methods.

Application of the above noise reduction methods is usually associated with a reduction in the spatial resolution of the reconstructed activity distribution. Any action reduces noise at the expense of spatial resolution, increases PVEs and thus introduces potential biases when quantifying activity concentrations in small structures. Thus, reduced noise (or increased precision) is typically traded for increased bias. It should be emphasized that low noise images obtained through one of the above methods do not guarantee low error quantities estimated from the images. Most often, the opposite is actually true: the greater the noise control, the greater the bias in the images, because the noise reduction indirectly increases the PVEs by worsening the spatial resolution in the images (Fig. 20). Note that this does not apply to noise reduction through the use of increased acquisition times or administered activities.

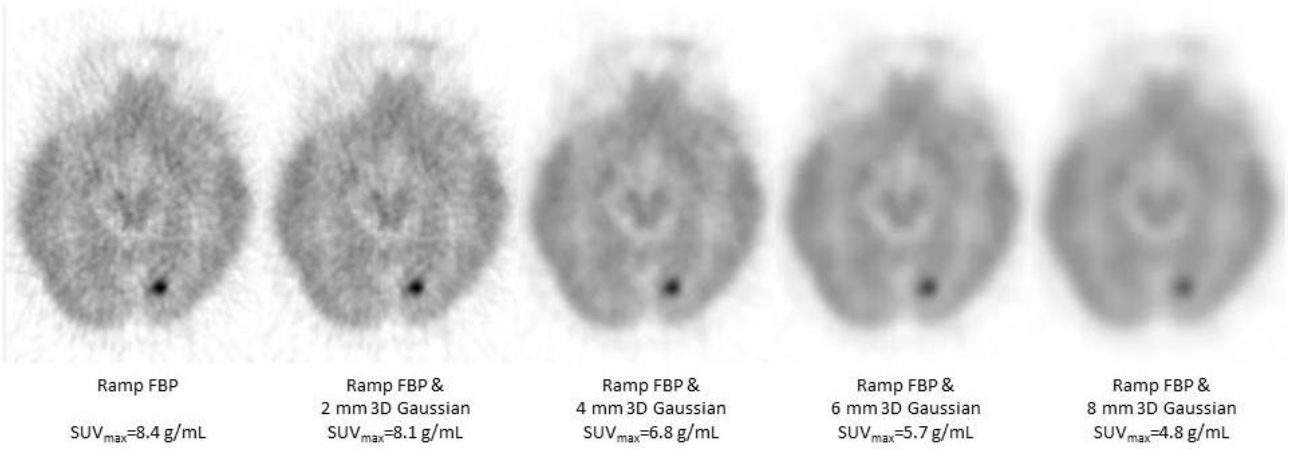

FIG. 20. Transverse slice from an FDG brain study showing the effect of image smoothing on SUV_{max}. All images are shown in a fixed inverse greyscale SUV from 0 to 8.

6.8. REGION AND VOLUME DEFINITION

The way regions and volumes are defined substantially affects quantitative measurements in PET, especially when for small objects such as small tumours or brain structures [130].

One commonly used method to reduce PVEs, especially in the estimation of tumour SUVs, is to estimate the activity of the object using a VOI (or ROI) inside the object. In this case, using a small VOI away from the edges can reduce the impact of PVEs. However, the measurement will be less precise (more sensitive to noise) since the activity concentration is averaged over a small number of voxels. On the other hand, using a larger region that is closer to the edges of the object will tend to make the bias introduced by PVE more severe, but reduce the impact of noise.

There is no universally accepted way to define a region. In PET/CT systems, the CT image can sometimes be used to define a region precisely before placing it on the PET image, after appropriate registration. However,

this assumes that the anatomical boundaries of the structure of interest are identical to the metabolic boundaries, which is not always true. Regions can be defined automatically or semi-automatically, for instance, by using an intensity threshold such that all voxels with a value above that threshold are included in the region [150]. However, the optimal threshold that yields a region matching the actual metabolic boundaries depends not only on the spatial resolution, but also on the actual object volume and on the surrounding activity. Thus determining the optimal threshold is difficult.

It should be noted that the SUV associated with a tumour depends strongly on the defined region and the calculation method (Fig. 21). The highest SUV (SUV_{max}) is calculated using the highest voxel value in the tumour; this might be misleading in the presence of noise or when the tumour has heterogeneous uptake. The mean SUV measured over a VOI is more robust to noise, but might be biased by PVEs if the tumour is small (typically less than 3 times the spatial resolution in the reconstructed images) and PVEs are not compensated for.

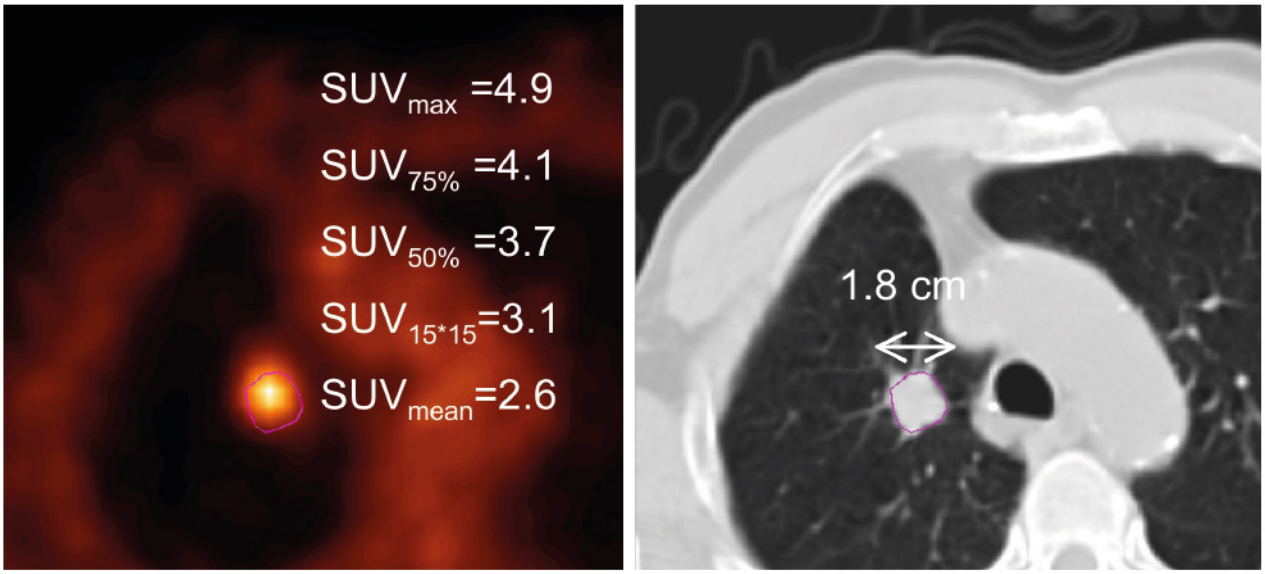

FIG. 21. Impact of the VOI used for estimating the SUV.

Region definition also impacts the estimate of the total activity within a region. In tumour imaging applications, the total activity is used to define the total lesion glycolysis, which is the product of the SUV by the tumour volume [154]. This will depend on how the tumour region is defined.

The problem of the delineation of metabolically active regions in the context of tumour imaging [2, 150] has been an active area of research focus. Accurate delineation of such regions could be useful for treatment planning in radiotherapy [155, 156]. Comparative evaluation of the accuracy of different methods in patients is needed in order to make sound recommendations about the method preferred for a given circumstance (e.g. location of the tumour, tumour size and contrast).

6.9. MOTION

Physiological (involuntary) motion (cardiac and respiratory) and voluntary motion (patient moving during the scan, coughing, etc.) adversely affect the quantitative accuracy of PET or PET/CT images. A well known example is the impact of respiratory motion on the appearance tumours have in PET images, which can result in an apparent increase in the tumour's volume and decrease in the tumour's uptake (see Fig. 22). These effects can be quite severe depending on the respiratory amplitude and tumour size, with SUV underestimation greater than 20% and tumour volume overestimation greater than 20% [157].

FIG. 22. Lung tumour as seen without motion correction (left) and after motion compensation (through respiratory gating).

In addition, respiratory motion can interfere with attenuation correction when using an attenuation map obtained with an X ray CT. Owing to long acquisition duration in PET compared to the respiratory period, PET images represent the averaged activity distribution and effects of attenuation over the whole respiratory cycle. On the other hand, the CT volume is typically acquired at a fixed time during the respiratory cycle, causing some mismatch between the boundaries of moving organs (e.g. the lungs or diaphragm) in the CT and PET images. Such misregistration can introduce errors in attenuation correction resulting in errors of the order of 30% in activity concentration estimates and of about 20% in volume estimates [158]. Accurate registration of CT and PET data before attenuation correction is therefore needed.

Compensating for respiratory motion requires monitoring of the respiratory motion during the PET data acquisition. This is most often performed using an external device that measures the motion of a relevant thoracic region. Several such devices have been described, such as a temperature sensitive device measuring the temperature of the exhaled air [159], an inductive respiration monitor that measures the changes in inductance of the coil formed by the fine flexible wire incorporated into an elasticized belt located around the patient's chest [160] or a real time position management system (Varian Medical Systems) that monitors the motion of the chest wall by tracking the vertical position of two passive reflective markers rigidly mounted on a lightweight plastic block and fixed on the patient's abdomen (using an infrared video camera mounted on the PET table) [161]. Alternatively, the respiratory signal can be extracted from the acquisition of a series of dynamic PET images acquired within a very short period of sampling (frame length of about 500 ms) [162]. However, this latter solution requires the reconstruction of many time frames and estimation of the motion from the resulting noisy images.

Images can be acquired using respiratory gating, consisting in sorting the acquired data as a function of the detection time during the respiratory cycle, to end up with a few frames (typically eight) each covering a small part of the respiratory cycle. Each of these frames includes less motion blur than is present in an ungated image, although even in these images residual motion blur is present. Respiratory gating can be performed either using phase or amplitude gating or even combining the two [163]. In phase gating, each respiratory cycle is divided into a number of time intervals, each with the same duration. This duration can be kept constant for all respiratory cycles or can vary from cycle to cycle, to take into account variations in the length of the respiratory cycle. In amplitude gating, the respiration amplitude is divided into a number of amplitude intervals of the same magnitude of the respiratory gating signal. This magnitude can also be the same for all cycles or vary from cycle to cycle. Comparative studies suggest that amplitude gating might be preferable [163, 164].

Most often, respiratory motion compensation in PET or PET/CT is limited to acquiring respiratory gated images and interpreting the resulting frames. However, each frame includes only a fraction of the total counts (if eight gates are acquired, each gate includes only about one-eighth of what would be acquired during an ungated acquisition). As a result, the benefit of motion deblurring is partly lost due to the amplification of noise. For the gated acquisition to yield good quality images compared to ungated acquisition, it has been shown that the acquisition duration should be increased by a factor of 3 [165].

Two approaches have been proposed to compensate for respiratory motion using respiratory gated data: image based and raw data based methods. In image based methods, a registration algorithm is used to realign the gated frames before summing them together. In the raw data based approaches, data are modified to account for motion between frames either before [166] or during [167] the reconstruction. In either approach, rigid or non-rigid registration models can be used. Four dimensional (4-D) reconstruction methods have also been described to reconstruct the series of gated images using a single reconstruction of the data corresponding to all gates [168]. By taking advantage of the time correlations existing between the gated frames, such methods offer the advantage of yielding gated images that have a signal to noise ratio similar to those of the ungated images.

Due to the relatively long duration of PET acquisition, involuntary motion can also affect the measured data, resulting in inconsistent projection data. Indeed, except for the 4-D reconstruction approaches mostly used when performing dynamic or gate PET, tomographic reconstruction always assumes that the tracer spatial distribution does not change during the scan duration. Any change introduces inconsistencies in the projections as then not all projections reflect the same activity distribution. Optical tracking systems have been proposed for tracking involuntary motion in brain imaging [169].

6.10. CALIBRATION

In PET or PET/CT, the calibration is performed as described in the NEMA-NU2–2012 standards [170]. The procedure gives the sensitivity of the scanner, which is then used to convert any count images into an activity image.

Variable detector efficiency, due to the different responses of the crystals that compose a PET machine, variable photomuliplier tube responses and geometric effects (photons coming from an annihilation occurring close to the edge of the transaxial field of view do not have the same probability of being detected as photons coming from an annihilation occurring at the centre of the field of view), is compensated for through a normalization procedure. A normalization map is calculated using a calibration procedure and is incorporated directly into the reconstruction process. This process is incorporated into the tomograph as part of factory calibration and QC procedures and applied as part of standard image reconstruction procedures. Thus, applying this calibration to images typically does not require activation of a special normalization procedure.

7. QUANTITATIVE IMAGING PROTOCOLS

7.1. NEED FOR PROTOCOLS

Protocols (or standard operating procedures) ensure consistency of data acquisition and processing. A protocol (or a set of protocols) should describe all the steps required to obtain satisfactory clinical data and measurements from them. A protocol should be written for any quantitative imaging task.

7.2. EXPERTISE AND TRAINING REQUIREMENTS

The expertise required for designing protocols differs from that required to implement them and different personnel may be required. Typically, the protocol can be written by a trained medical physicist and medical staff, while technologists can be trained to execute protocols.

7.2.1. Specification

The preparation of a protocol requires an understanding of the clinical question to be answered and an understanding of the capabilities of the resources available to achieve the answer. The clinical question and related biochemistry of the biological targeting agent and radiolabelling are beyond the scope of this publication. In general, the parts of the protocols concerned with imaging resources (camera preparation, data acquisition and processing) will require the expertise of a trained medical physicist. The physicist will prepare the protocol with an understanding of the available physical and human resources; the protocol must be unambiguous for the technician carrying out the procedures. The physicist need not necessarily be at the site where the data will be acquired or processed, but he or she must have an understanding of both the technical requirements of the procedure and the resources available at the site(s).

7.2.2. Execution

Most procedures are carried out by technologists or radiographers working under protocol. Technologists must be trained to a level where they can understand a protocol and carry out its instructions. For complex procedures (or those carried out infrequently) it is advantageous for the same technologist to undertake them on each occasion. Any deviation from the written protocol should be carefully documented.

7.3. ELEMENTS

The elements that need to be included in a protocol and recorded and reported in the image or study metadata will differ between modalities and procedures. Additionally, new techniques are continually being developed, meaning it will never be possible to guarantee that any list is exhaustive; that being said, the following elements should be considered in the preparation of a protocol.

7.3.1. Procedural

- Radiotracer;
- Tracer activity administered to the patient;
- Administration route;
- Time for the injection;
- Background measurement.

7.3.2. Technical

Emission acquisition

- Scintillation camera or PET scanner;
- Acquisition time;
- Collimator and associated characteristics (hole size and shape, thickness, septal thickness);
- 2-D or 3-D acquisition mode in PET and associated parameters (span, maximum ring difference, mashing parameters);
- Energy window setting;
- Field of view, number of bed positions and overlap between the bed positions;
- Orbit information;
- Pixel size in the projection data, or sinogram sampling in PET;
- Number of projections in SPECT, or sinogram sampling in PET;
- Acquisition duration (per bed position);
- Time sampling in case of dynamic scanning;
- External gating device if any (for respiratory or cardiac gating);
- Gating method if any (phase, amplitude, etc.);
- Number of gates;
- Acquisition format (frames or list mode);
- Output format (DICOM, Interfile, manufacturer format).

Calibration procedure

- Calibration phantom;
- Calibration phantom acquisition parameters (should be the same as patient study except perhaps for frequency of calibration phantom acquisitions (e.g. monthly, etc.);
- Sensitivity measurement protocol (source activity, source size, distance from collimators, if used, etc.);
- Frequency of sensitivity measurements (e.g. per patient, per day, etc.).

Transmission acquisition

- Acquisition duration (per bed position);
- Scanning geometry (scanning or tomographic);
- Source type (radionuclide or X ray tube);
- Source energy in kV or keV;
- Source strength in MBq or mAs;
- Duration of the transmission acquisition (per bed position);
- Acquisition format (frames or list mode);
- Spatial or angular sampling or both;
- Field of view;
- Breathing protocol;
- Output format (DICOM, Interfile, manufacturer format).

Processing

- Transmission data:
  - — Reconstruction algorithm used for the attenuation map, if any, with associated parameters;
  - — Scaling method for the attenuation map;
  - — Segmentation method for the attenuation map, if any.
- Emission data:
  - — Reconstruction algorithm and associated parameters (number of subsets, number of iterations, filter, parameter(s) of the filter, regularization parameter(s), post-filter, parameter of the post-filter);
  - — Voxel size in the reconstructed data;
  - — Attenuation correction, if any, and associated parameters;
  - — Scatter correction, if any, and associated parameters;
  - — Detector response correction, if any, and associated parameters;
  - — PVE correction, if any, and associated parameters;
  - — ROI definition (regions should be systematically stored if possible);
  - — Exact definition and calculation method of the quantitative index/indices of interest.

7.3.3. Quality assurance and quality control

Quality assurance and quality control (QA/QC) tasks should be performed at a specified frequency to ensure that the equipment is operating as intended. The schedule for QA/QC procedures should be specified in the protocol. QA/QC results should be systematically provided along with all data related to the protocol.

7.4. VALIDATION

There are well defined anthropomorphic phantoms available that can be used to validate activity quantification in large structures such as the liver and the heart as well as in spheres of different sizes.

An important parameter to validate is the measurement of the activity. A well counter properly calibrated for the particular radionuclide is therefore essential. Care should be taken when preparing a physical phantom for a validation study since errors in the preparation may be difficult to determine at a later date. For example, it may be difficult to ascertain whether a uniform background activity is really homogeneous or whether it is activity trapped to the surface of the phantom [171].

A common way to assess the quantitative accuracy that can be expected in certain conditions is the use of Monte Carlo simulation of patient or phantom studies. Simulation offers potential advantages in its flexibility and the possibility of evaluating potential degradations in image quality and accuracy for different simulated clinical situations and radiopharmaceuticals. It is essential that these programs in turn are validated against all locally available phantom measurements. Many of the MC programs can use voxel based software phantoms. Validations can then be made by acquiring CT scans of a locally available physical phantom and developing a digital version

of it for comparison between real measurements and simulations using an identical geometry. Such a comparison can then validate the results from simulation of more complicated but versatile software phantoms such as the NCAT/XCAT phantoms by Segars [172]. One should be aware that a Monte Carlo program is a model of a real system and may not always be able to fully mimic the image creation process.

In many cases, when using commercial systems it is difficult to get a full description of how a certain method is designed and implemented or what assumptions underlie a particular method. Writing one's own software may sometimes be the only solution to this problem but requires skilled staff and extensive time. Problems can arise when trying to collect sufficient relevant information about a particular acquisition that might be needed for an external software package. Thus, careful validation and cross-checking is essential.

REFERENCES

[1] NESTLE, U., WEBER, W., HENTSCHEL, M., GROSU, A.L., Biological imaging in radiation therapy: Role of positron emission tomography, Phys. Med. Biol. **54** (2009) R1–25.

[2] NESTLE, U., et al., Comparison of different methods for delineation of 18F-FDG PET-positive tissue for target volume definition in radiotherapy of patients with non-small cell lung cancer, J. Nucl. Med. **46** (2005) 1342–1348.

[3] BOELLAARD, R., et al., FDG PET and PET/CT: EANM procedure guidelines for tumour PET imaging: Version 1.0, Eur. J. Nucl. Med. Mol. Imaging **37** (2010) 181–200.

[4] ZASADNY, K.R., KORAL, K.F., SWAILEM, F.M., Dead time of an anger camera in dual-energy-window-acquisition mode, Med. Phys. **20** (1993) 1115–1120.

[5] ZASADNY, K.R., WAHL, R.L., Standardized uptake values of normal tissues at PET with 2-[fluorine-18]-fluoro-2-deoxy-d-glucose: Variations with body weight and a method for correction, Radiology **189** (1993) 847–850.

[6] KIM, C.K., GUPTA, N.C., CHANDRAMOULI, B., ALAVI, A., Standardized uptake values of FDG: Body surface area correction is preferable to body weight correction, J. Nucl. Med. **35** (1994) 164–167.

[7] SUGAWARA, Y., ZASADNY, K.R., NEUHOFF, A.W., WAHL, R.L., Reevaluation of the Standardized Uptake Value for FDG: Variations with body weight and methods for correction, Radiology **213** (1999) 521–525.

[8] ERSELCAN, T., TURGUT, B., DOGAN, D., OZDEMIR, S., Lean body mass-based standardized uptake value, derived from a predictive equation, might be misleading in PET studies, Eur. J. Nucl. Med. Mol. Imaging **29** (2002) 1630–1638.

[9] YEUNG, H.W., et al., Standardized uptake value in pediatric patients: an investigation to determine the optimum measurement parameter, J. Nucl. Med. Eur. J. Nucl. Med. Mol. Imaging **29** (2002) 61–66.

[10] SJÖGREEN, K., LJUNGBERG, M., A Patient-Weight-Based Method for Obtaining Attenuation Maps from X-Ray CT Scouts, for Planar Based Absorbed Dose Assessments in Radionuclide Therapy, Phys. Med. Biol. (2010).

[11] KUNYANSKY, L.A., A new SPECT reconstruction algorithm based on the Novikov explicit inversion formula, Inverse Probl. **17** (2001) 293.

[12] NOVIKOV, R., An inversion formula for the attenuated X-ray transformation, Ark. Mat **40** (2002) 145–167.

[13] QI, J., LEAHY, R.M., Iterative reconstruction techniques in emission computed tomography, Phys. Med. Biol. **51** (2006) R541–578.

[14] SHEPP, L.A., VARDI, Y., Maximum likelihood reconstruction for emission tomography, IEEE Trans. Med. Imaging **1** (1982) 113–122.

[15] LANGE, K., CARSON, R., EM reconstruction algorithms for emission and transmission tomography, J. Comput. Assist. Tomogr. **8** (1984) 306–316.

[16] HUDSON, H.M., LARKIN, R.S., Accelerated image reconstruction using ordered subsets of projection data, IEEE Trans. Med. Imaging **13** (1994) 601–609.

[17] SERET, A., The number of subsets required for OSEM reconstruction in nuclear cardiology, Eur. J. Nucl. Med. Mol. Imaging **33** (2006) 231.

[18] BROWNE, J., DE PIERRO, A.B., A row-action alternative to the EM algorithm for maximizing likelihood in emission tomography, IEEE Trans. Med. Imaging **15** (1996) 687–699.

[19] FESSLER, J.A., Mean and variance of implicitly defined biased estimators (such as penalized maximum likelihood): Applications to tomography, IEEE Trans. Image Process **5** (1996) 493–506.

[20] GEMAN, S., MCCLURE, D., "Bayesian Image Analysis: An Application to Single Photon Emission Tomography", Proceedings of the Statistical Computing Section, American Statistical Association, Washington, DC (1985) 12–18.

[21] GREEN, P.J., Bayesian reconstructions from emission tomography data using a modified EM algorithm, IEEE Trans. Med. Imaging **9** (1990) 84–93.

[22] DE PIERRO, A.R., YAMAGISHI, M.E.B., Fast EM-Like Methods for Maximum "a Posteriori" Estimates in Emission Tomography, IEEE Trans. Med. Imaging **20** (2001) 280–288.

[23] AHN, S., FESSLER, J.A., Globally convergent image reconstruction for emission tomography using relaxed ordered subsets algorithms, IEEE Trans. Med. Imaging **22** (2003) 613–626.

[24] CHANG, J.H., ANDERSON, J.M.M., VOTAW, J.R., Regularized image reconstruction algorithms for positron emission tomography, IEEE Trans. Med. Imaging **23** (2004) 1165–1175.

[25] HSIAO, I.T., RANGARAJAN, A., KHURD, P., GINDI, G., An accelerated convergent ordered subsets algorithm for emission tomography, Phys. Med. Biol. **49** (2004) 2145–2156.

[26] AHN, S., FESSLER, J.A., BLATT, D., HERO, A.O., Convergent incremental optimization transfer algorithms: Application to tomography, IEEE Trans. Med. Imaging **25** (2006) 283–296.

[27] DEFRISE, M., GULLBERG, G.T., Image reconstruction, Phys. Med. Biol. **51** (2006) R139–154.

[28] GULLBERG, G.T., HUESMAN, R.H., MALKO, J.A., PELC, N.J., BUDINGER, T.F., An attenuated projector-backprojector for iterative SPECT reconstruction, Phys. Med. Biol. **30** (1985) 799–816.

[29] TSUI, B.M.W., HU, H., GILLAND, D.R., GULLBERG, G.T., Implementation of simultaneous attenuation and detector response correction in SPECT, IEEE Trans. Nucl. Sci. **35** (1988) 778–783.
[30] LASSMANN, M., et al., EANM Dosimetry Committee series on standard operational procedures for pre-therapeutic dosimetry I: Blood and bone marrow dosimetry in differentiated thyroid cancer therapy, Eur. J. Nucl. Med. Mol. Imaging **35** (2008) 1405–1412.
[31] GAZE, M.N., et al., Feasibility of dosimetry-based high-dose 131I-meta-iodobenzylguanidine with topotecan as a radiosensitizer in children with metastatic neuroblastoma, Cancer Biother. Radio. **20** (2005) 195–199.
[32] VIOLET, University College, London, unpublished data.
[33] HINDORF, C., LINDEN, O., TENNVALL, J., WINGARDH, K., STRAND, S.E., Evaluation of methods for red marrow dosimetry based on patients undergoing radioimmunotherapy, Acta Oncol. **44** (2005) 579–588.
[34] VERBURG, F.A., et al., The absorbed dose to the blood is a better predictor of ablation success than the administered ^{131}I activity in thyroid cancer patients, J. Nucl. Med. Mol. Imaging **38** (2011) 673–680.
[35] LASSMANN, M., CHIESA, C., FLUX, G., BARDIES, M., EANM Dosimetry Committee guidance document: Good practice of clinical dosimetry reporting, Eur. J. Nucl. Med. Mol. Imaging **38** (2011) 192–200.
[36] CHITTENDEN, S.J., et al., Optimization of equipment and methodology for whole body activity retention measurements in children undergoing targeted radionuclide therapy, Cancer Biother. Radio. **22** (2007) 243–249.
[37] SORENSON, J.A., Methods for Quantitation of Radioactivity in Vivo by External Counting Measurements, University of Wisconsin, Madison, 1971.
[38] FLEMING, J.S., A technique for the absolute measurement of activity using a gamma camera and computer, Phys. Med. Biol. **24** (1979) 176.
[39] MINARIK, D., SJÖGREEN, K., LJUNGBERG, M., A new method to obtain transmission images for planar whole-body activity quantification, Cancer Biother. Radio. **20** (2005) 72–76.
[40] OGAWA, K., HARATA, Y., ICHIHARA, T., KUBO, A., HASHIMOTO, S., A practical method for position dependent Compton-scatter correction in single photon emission CT, IEEE Trans. Med. Imaging **10** (1991) 408–412.
[41] SIEGEL, J. A., WU, R.K., MAURER, A.H., The buildup factor: Effect on scatter on absolute volume determination, J. Nucl. Med. **26** (1985) 390–394.
[42] SJÖGREEN, K., LJUNGBERG, M., STRAND, S.E., An activity quantification method based on registration of CT and whole-body scintillation camera images, with application to 131I, J. Nucl. Med. **43** (2002) 972–982.
[43] LIU, A., WILLIAMS, L.E., RAUBITSCHEK, A.A., A CT assisted method for absolute quantitation of internal radioactivity, Med. Phys. **23** (1996) 1919–1928.
[44] HE, B., FREY, E.C., comparison of conventional, model-based quantitative planar, and quantitative SPECT image processing methods for organ activity estimation using In-111 agents, Phys. Med. Biol. **51** (2006) 3967–3981.
[45] CHIESA, C., et al., A practical dead time correction method in planar activity quantification for dosimetry during radionuclide therapy, Q J. Nucl. Med. Mol. Imaging **53** (2009) 658–670.
[46] HOBBS, R.F., et al., A gamma camera count rate saturation correction method for whole-body planar imaging, Phys. Med. Biol. **55** (2010) 817–831.
[47] ROSENTHAL, M.S., et al., Quantitative SPECT imaging: A review and recommendations by the Focus Committee of the Society of Nuclear Medicine Computer and Instrumentation Council, J. Nucl. Med. **36** (1995) 1489–1513.
[48] CHANG, L.T., A Method for Attenuation Correction in Radionuclide Computed Tomography, IEEE Trans. Nucl. Sci. **NS-25** (1978) 638–643.
[49] BELLINI, S., PIACENTINI, M., CAFFORIA, C., ROCCA, F., Compensation of Tissue Absorption in Emission Tomography, IEEE Trans. Acoust. Speech **27** (1979) 213–318.
[50] TRETIAK, O.J., METZ, C.E., The Exponential Radon Transform, SIAM J. Appl. Math. **39** (1980) 341–354.
[51] PAN, X., WONG, W.H., CHEN, C.-T., LIU, J., Correction for photon attenuation in SPECT: Analytical framework, average attenuation factors, and a new hybrid approach, Phys. Med. Biol. **38** (1993) 1219–1234.
[52] LALUSH, D.S., TSUI, B.M.W., Comparison of iterative filtered backprojection and weighted least-squares reconstruction methods, J. Nucl. Med. **35** (1994) 28P.
[53] MALKO, J.A., VAN HEERTUM, R.L., GULLBERG, G.T., KOWALSKY, W.P., SPECT liver imaging using an iterative attenuation correction algorithm and an external flood source, J. Nucl. Med. **27** (1986) 701–705.
[54] BAILEY, D.L., HUTTON, B.F., WALKER, P.J., Improved SPECT using simultaneous emission and transmission tomography, J. Nucl. Med. **28** (1987) 844–851.
[55] FREY, E.C., TSUI, B.M.W., PERRY, J.R., Simultaneous acquisition of emission and transmission data for improved thallium-201 cardiac SPECT imaging using a technetium-99m transmission source, J. Nucl. Med. **33** (1992) 2238–2245.
[56] TAN, P., et al., A scanning line source for simultaneous emission and transmission measurements in SPECT, J. Nucl. Med. **34** (1993) 1752–1760.
[57] TUNG, C.-H., GULLBERG, G.T., A simulation of emission and transmission noise propagation in cardiac SPECT imaging with non-uniform attenuation correction, Med. Phys. **21** (1994) 1565–1576.

[58] FLEMING, J.S., A technique for using CT images in attenuation correction and quantitation in SPECT, Nucl. Med. Comm. **10** (1989) 83–97.
[59] BEEKMAN, F.J., FREY, E.C., KAMPHUIS, C., TSUI, B.M.W., VIERGEVER, M.A., A new phantom for fast determination of the scatter response of a gamma camera, IEEE Trans. Nucl. Sci. **41** (1994) 1481–1488.
[60] LACROIX, K.J., TSUI, B.M.W., HASEGAWA, B.H., BROWN, J.K., Investigation of the use of X-ray CT images for attenuation compensation in SPECT, IEEE Trans. Nucl. Sci. **41** (1994) 2793–2799.
[61] LACROIX, K.J., Investigation of the Use of Single Energy X-ray CT Images for Attenuation Compensation in SPECT, The University of North Carolina at Chapel Hill, 1994.
[62] BROWN, S., BAILEY, D.L., WILLOWSON, K., BALDOCK, C., Investigation of the relationship between linear attenuation coefficients and CT Hounsfield units using radionuclides for SPECT, Appl. Radiat. Isotopes **66** (2008) 1206–1212.
[63] SEO, Y., WONG, K.H., HASEGAWA, B.H., Calculation and validation of the use of effective attenuation coefficient for attenuation correction in In-111 SPECT, Med. Phys. **32** (2005) 3628–3635.
[64] STONE, C.D., et al., Effect of registration errors between transmission and emission scans on a SPECT system using sequential scanning, J. Nucl. Med. **39** (1998) (abstract).
[65] GOETZE, S., BROWN, T.L., LAVELY, W.C., ZHANG, Z., BENGEL, F.M., Attenuation correction in myocardial perfusion SPECT/CT: Effects of misregistration and value of reregistration, J. Nucl. Med. **48** (2007) 1090–1095.
[66] FREY, E.C., TSUI, B.M.W., "The effects of out of field-of-view activity on iterative reconstruction-based scatter compensation in cardiac SPECT", J. Nucl. Med. **38**, 1997 (abstract).
[67] AXELSSON, B., MSAKI, P., ISRAELSSON, A., Subtraction of Compton-scattered photons in single-photon emission computerized tomography, J. Nucl. Med. **25** (1984) 490–494.
[68] FLOYD, C.E., JASZCZAK, R.J., GREER, K.L., COLEMAN, R.E., Deconvolution of Compton scatter in SPECT, J. Nucl. Med. **26** (1985) 403–408.
[69] YANCH, J.C., FLOWER, M.A., WEBB, S., A comparison of deconvolution and windowed subtraction techniques for scatter compensation in SPECT, IEEE Trans. Med. Imaging **7** (1988) 13–20.
[70] MEIKLE, S.R., HUTTON, B.F., BAILEY, D.L., A transmission-dependent method for scatter correction in SPECT, J. Nucl. Med. **35** (1994) 360–367.
[71] BEEKMAN, F.J., EIJKMAN, E.G.J., VIERGEVER, M.A., BORM, G.F., SLIJPEN, E.T.P., Object shape dependent PSF model for SPECT imaging, IEEE Trans. Nucl. Sci. **40** (1993) 31–39.
[72] FREY, E.C., JU, Z.W., TSUI, B.M.W., A fast projector-backprojector pair modeling the asymmetric, spatially varying scatter response function for scatter compensation in SPECT imaging, IEEE Trans. Nucl. Sci. **40** (1993) 1192–1197.
[73] FREY, E.C., TSUI, B.M.W., A practical method for incorporating scatter in a projector-backprojector for accurate scatter compensation in SPECT, IEEE Trans. Nucl. Sci. **40** (1993) 1107–1116.
[74] BEEKMAN, F.J., DEN HARDER, J.M., VIERGEVER, M.A., VANRIJK, P.P., Fully 3D iterative scatter compensation in non-uniform attenuating media for SPECT, J. Nucl. Med. **37** (1996) 979.
[75] FREY, E.C., TSUI, B.M.W., "A new method for modeling the spatially-variant, object shape dependent scatter response function in SPECT", Proc. IEEE Nuclear Science Symp. And Medical Imaging Conf, 1996, IEEE, Anaheim, CA (1996) 1082–1086.
[76] KADRMAS, D.J., FREY, E.C., TSUI, B.M.W., Application of reconstruction-based scatter compensation to thallium-201 SPECT: Implementations for reduced reconstructed image noise, IEEE Trans. Med. Imaging **17** (1998) 325–333.
[77] BEEKMAN, F.J., KAMPHUIS, C., FREY, E.C., Scatter compensation methods in 3D iterative SPECT reconstruction: A simulation study, Phys. Med. Biol. **42** (1997) 1619–1632.
[78] DU, Y., TSUI, B.M.W., FREY, E.C., Model-based compensation for quantitative ^{123}I brain SPECT imaging, Phys. Med. Biol. **51** (2006) 1269–1282.
[79] LJUNGBERG, M., et al., 3D absorbed dose calculations based on SPECT: evaluation for 111-In/90-Y therapy using Monte Carlo simulations, Cancer Biother. Radio **18** (2003) 99–107.
[80] HE, B., DU, Y., SONG, X.Y., SEGARS, W.P., FREY, E.C., A Monte Carlo and physical phantom evaluation of quantitative In-111 SPECT, Phys. Med. Biol. **50** (2005) 4169–4185.
[81] LJUNGBERG, M., et al., A 3-dimensional absorbed dose calculation method based on quantitative SPECT for radionuclide therapy: Evaluation for (131)I using monte carlo simulation, J. Nucl. Med. **43** (2002) 1101–1109.
[82] MINARIK, D., SJÖGREEN GLEISNER, K., LJUNGBERG, M., Evaluation of quantitative (90)Y SPECT based on experimental phantom studies, Phys. Med. Biol. **53** (2008) 5689–5703.
[83] DE JONG, H., SLIJPEN, E.T.P., BEEKMAN, F.J., Acceleration of Monte Carlo SPECT simulation using convolution-based forced detection, IEEE Trans. Nucl. Sci. **48** (2001) 58–64.
[84] BEEKMAN, F.J., DE JONG, H., VAN GELOVEN, S., Efficient fully 3-D iterative SPECT reconstruction with Monte Carlo-based scatter compensation, IEEE Trans. Med. Imaging **21** (2002) 867–877.
[85] BOWSHER, J.E., FLOYD, C.E., Treatment of Compton scattering in maximum-likelihood, expectation-maximization reconstructions of SPECT images, J. Nucl. Med. **32** (1991) 1285–1291.

[86] KADRMAS, D.J., FREY, E.C., KARIMI, S.S., TSUI, B.MW., Fast implementations of reconstruction-based scatter compensation in fully 3D SPECT image reconstruction, Phys. Med. Biol. **43** (1998) 857–873.
[87] KAMPHUIS, C., BEEKMAN, F.J., VAN RIJK, P.P., VIERGEVER, M.A., Dual matrix ordered subsets reconstruction for accelerated 3D scatter compensation in single-photon emission tomography, Eur. J. Nucl. Med. **25** (1998) 8–18.
[88] ZENG, G.L., GULLBERG, G.T., Unmatched projector/backprojector pairs in an iterative reconstruction algorithm, IEEE Trans. Med. Imaging **19** (2000) 548–555.
[89] KING, M.A., DOHERTY, P.W., SCHWINGER, R.B., PENNEY, B.C., A Wiener filter for nuclear medicine images, Med. Phys. **10** (1983) 876–880.
[90] KING, M.A., SCHWINGER, R.B., DOHERTY, P.W., PENNEY, B.C., Two-dimensional filtering of SPECT images using the Metz and Wiener filters, J. Nucl. Med. **25** (1984) 1234–1240.
[91] KING, M.A., SCHWINGER, R.B., PENNEY, B.C., Variation of the count-dependent Metz filter with imaging system modulation transfer function, Med. Phys. **13** (1986) 139–149.
[92] GILLAND, D.R., TSUI, B.M.W., McCARTNEY, W.H., PERRY, J.R., BERG, J., Determination of the optimal filter function for SPECT imaging, J. Nucl. Med. **29** (1988) 643–650.
[93] KING, M.A., PENNEY, B.C., GLICK, S.J., An image-dependent Metz filter for nuclear medicine images, J. Nucl. Med. **29** (1988) 1980–1989.
[94] APPLEDORN, C.R., An analytical solution to the nonstationary reconstruction problem, SPECT, Prog. Clin. Biol. Res. **363** (1991) 69–79.
[95] SOARES, E.J., BYRNE, C.L., GLICK, S.J., APPLEDORN, C.R., KING, M.A., "Implementation and evaluation of an analytical solution to the photon attenuation and nonstationary resolution reconstruction problem in SPECT" Conference Record of the 1991 IEEE (Proc. Nuclear Science Symp. and Medical Imaging Conf. 1991), Institute of Electrical and Electronics Engineers, Piscataway, NJ (1991) 1231–1237.
[96] GLICK, S.J., PENNEY, B.C., KING, M.A., Noniterative compensation for the distance-dependent detector response and photon attenuation in SPECT imaging, IEEE Trans. Med. Imaging **13** (1994) 363–374.
[97] PAN, X.C., METZ, C.E., CHEN, C.T., "A class of analytical methods that compensate for attenuation and spatially-variant resolution in 2D SPECT", IEEE Nuclear Science Symposium and Medical Imaging Conference Record, IEEE Service Center, Piscataway, NJ (1996) 2244–2254.
[98] ZENG, G.L., GULLBERG, G.T., Frequency domain implementation of the three-dimensional geometric point source correction in SPECT imaging, IEEE Trans. Nucl. Sci. **39** (1992) 1444–1453.
[99] GLICK, S.J., et al., "Characteristics of Reconstructed Point Response in Three-Dimensional Spatially Variant Detector Response Compensation in SPECT", Three-Dimensional Image Reconstruction in Radiology and Nuclear Medicine (GRANGEAT, P., AMANS, J.-L., Eds), Dordrecht, Kluwer Academic Publishers (1996) pp. 149–161.
[100] FREY, E., TSUI, B., "Collimator-detector response compensation in SPECT", Quantitative Analysis of Nuclear Medicine Images (ZAIDI, H., Ed.), Springer, New York (2006).
[101] METZ, C.E., ATKINS, F.B., BECK, R.M.,The geometric transfer function component for scintillation camera collimators with straight parallel holes, Phys. Med. Biol. **25** (1980) 1059–1070.
[102] HE, X., LINKS, J.M., FREY, E.C., An investigation of the trade-off between the count level and image quality in myocardial perfusion SPECT using simulated images: The effects of statistical noise and object variability on defect detectability, Phys. Med. Biol. **55** (2010) 4949–4961.
[103] HOFFMAN, E.J., HUANG, S.C., PHELPS, M.E., Quantitation in positron emission computed tomography: 1. Effect of object size, J. Comput. Assist. Tomogr. **3** (1979) 299–308.
[104] KESSLER, R.M., ELLIS, J.R., EDEN, M., Analysis of emission tomographic scan data: Limitations imposed by resolution and background, J. Comput. Assist. Tomogr. **8** (1984) 514–522.
[105] ZITO, F., GILARDI, M.C., MAGNANI, P., FAZIO, F., Single-photon emission tomographic quantification in spherical objects: Effects of object size and background, Eur. J. Nucl. Med. **23** (1996) 263–271.
[106] DEWARAJA, Y., LI, J., KORAL, K., Quantitative ^{131}I SPECT with triple energy window Compton scatter correction, IEEE Trans. Nucl. Sci. **45** (1998) 3109–3114.
[107] KORAL, K.F., DEWARAJA, Y., I-131 SPECT activity recovery coefficients with implicit or triple-energy-window scatter correction, SPECTNucl. Instrum. Meth. A **422** (1999) 688–692.
[108] GEWORSKI, L., KNOOP, B.O., DE CABREJAS, M.L., KNAPP, W.H., MUNZ, D.L., Recovery correction for quantitation in emission tomography: A feasibility study, Eur J. Nucl. Med. **27** (2000) 161–169.
[109] MÜLLER-GÄRTNER, H.W., et al., Measurement of radiotracer concentration in brain gray matter using positron emission tomography: MRI-based correction for partial volume effects, J. Cerebr. Blood. F. Met. **12** (1992) 571–583.
[110] MELTZER, C.C., et al., MR-based correction of brain PET measurements for heterogeneous gray matter radioactivity distribution, J. Cerebr. Blood. F. Met. **16** (1996) 650–658.
[111] DA SILVA, A.J., et al., Absolute quantification of regional myocardial uptake of 99m Tc-sestamibi with SPECT: Experimental validation in a porcine model, J. Nucl. Med. **42** (2001) 772–779.

[112] TANG, H.R., et al., Neuroblastoma imaging using a combined CT scanner-scintillation camera and ^{131}I-MIBG, J. Nucl. Med. **42** (2001) 237–247.
[113] ROUSSET, O.G., MA, Y.L., EVANS, A.C., Correction for partial volume effects in PET: Principle and validation, J. Nucl. Med. **39** (1998) 904–911.
[114] DU, Y., TSUI, B.M.W., FREY, E.C., Partial volume effect compensation for quantitative brain SPECT imaging, IEEE Trans. Med. Imaging **24** (2005) 969–976.
[115] HE, B., et al., Comparison of residence time estimation methods for radioimmunotherapy dosimetry and treatment planning — Monte Carlo simulation studies, IEEE Trans. Med. Imaging **27** (2008) 521–530.
[116] HE, B., FREY, E.C., Effects of shortened acquisition time on accuracy and precision of quantitative estimates of organ activity, Med. Phys. **37** (2010) 1807–1815.
[117] HE, B., et al., Evaluation of quantitative imaging methods for organ activity and residence time estimation using a population of phantoms having realistic variations in anatomy and uptake, Med. Phys. **36** (2009) 612–619.
[118] ASSIE, K., et al., Comparison between 2D and 3D dosimetry protocols in 90Y-ibritumomab tiuxetan radioimmunotherapy of patients with non-Hodgkin's lymphoma, Cancer Biother. Radio. **23** (2008) 53–64.
[119] HE, B., FREY, E.C., The impact of 3D Volume of interest definition on accuracy and precision of activity estimation in quantitative SPECT and planar processing methods, Phys. Med. Biol. **55** (2010) 3535–3544.
[120] SONG, N., HE, B., FREY, E.C., The effect of volume-of-interest misregistration on quantitative planar activity and dose estimation, Phys. Med. Biol. **55** (2010) 5483–5497.
[121] EISNER, R.L., et al., Use of cross-correlation function to detect patient motion during SPECT imaging, J. Nucl. Med. **28** (1987) 97–101.
[122] GERMANO, G., CHUA, T., KAVANAGH, P.B., KIAT, H., BERMAN, D.S., Detection and correction of patient motion in dynamic and static myocardial SPECT using a multi-detector camera, J. Nucl. Med. **34** (1993) 1349–1355.
[123] FULTON, R.R., HUTTON, B.F., BRAUN, M., ARDEKANI, B., LARKIN, R., Use of 3D reconstruction to correct for patient motion in SPECT, Phys Med. Biol. **39** (1994) 563–574.
[124] LINKS, J.M., et al., Combined corrections for attenuation, depth-dependent blur, and motion in cardiac SPECT: A multicenter trial, J. Nucl. Cardiol. **7** (2000) 414–425.
[125] MATSUMOTO, N., et al., Quantitative assessment of motion artifacts and validation of a new motion-correction program for myocardial perfusion SPECT, J. Nucl. Med. **42** (2001) 687–694.
[126] BOENING, G., et al., "Motion correction for cardiac SPECT using a RBI-ML partial-reconstruction approach", 2004 IEEE Nuclear Science Symposium Conference Record, (Proc. Conf. 2004 Rome), Institute of Electrical and Electronics Engineers, Piuscataway, NJ, (2004) 2849–2853.
[127] YOUNG, H., et al., Measurement of clinical and subclinical tumour response using [18F]-fluorodeoxyglucose and positron emission tomography: Review and 1999 EORTC recommendations. European Organization for Research and Treatment of Cancer (EORTC) PET Study Group, Eur. J. Cancer **35** (1999) 1773–1782.
[128] DELBEKE, D., et al., Procedure guideline for tumour imaging with 18F-FDG PET/CT 1.0, J. Nucl. Med. **47** (2006) 885–895.
[129] ZAIDI, H., Recent developments and future trends in nuclear medicine instrumentation, Z. Med. Phys. **16** (2006) 5–17.
[130] BOELLAARD, R., KRAK, N.C., HOEKSTRA, O.S., LAMMERTSMA, A.A., Effects of noise, image resolution, and ROI definition on the accuracy of standard uptake values: A simulation study, J. Nucl. Med. **45** (2004) 1519–1527.
[131] PARRA, L., BARRETT, H.H., List-mode likelihood: EM algorithm and image quality estimation demonstrated on 2-D PET, IEEE Trans. Med. Imaging **17** (1998) 228–235.
[132] READER, A.J., ERLANDSSON, K., FLOWER, M.A., OTT, R.J., Fast accurate iterative reconstruction for low-statistics positron volume imaging, Phys. Med. Biol. **43** (1998) 835–846.
[133] COLSHER, J.G., Fully three-dimensional positron emission tomography, Phys. Med. Biol. **25** (1980) 103–115.
[134] RA, J., LIM, C., CHO, Z., HILAL, S., CORRELL, J., A true three-dimensional reconstruction algorithm for the spherical positron emission tomograph, Phys. Med. Biol. **27** (1982) 37.
[135] KINAHAN, P.E., ROGERS, J.G., Analytic three-dimensional image reconstruction using all detected events, IEEE Trans. Nucl. Sci. **36** (1989) 964–968.
[136] DAUBE-WITHERSPOON, M.E., MUEHLLEHNER, G., Treatment of axial data in three-dimensional PET, J. Nucl. Med. **28** (1987) 1717–1724.
[137] LEWITTT, R.M., MUEHLLEHNER, G., KARPT, J.S., Three-dimensional image reconstruction for PET by multi-slice rebinning and axial image filtering, Phys. Med. Biol. **39** (1994) 321–339.
[138] DEFRISE, M., et al., Exact and approximate rebinning algorithms for 3-D PET data, IEEE Trans. Med. Imaging **16** (1997) 145–158.
[139] BACHARACH, S.L., BUVAT, I., Attenuation correction in cardiac positron emission tomography and single-photon emission computed tomography, J. Nucl. Cardiol. **2** (1995) 246–255.
[140] ZAIDI, H., HASEGAWA, B., Determination of the attenuation map in emission tomography, J. Nucl. Med. **44** (2003) 291–315.
[141] OSMAN, M.M., COHADE, C., NAKAMOTO, Y., WAHL, R.L., Respiratory motion artifacts on PET emission images obtained using CT attenuation correction on PET-CT, J. Nucl. Med. Mol. Imaging **30** (2003) 603–606.

[142] PAN, T., et al., Attenuation Correction of PET Images with Respiration-Averaged CT Images in PET/CT, J. Nucl. Med. **46** (2005) 1481–1487.
[143] HUANG, S.C., HOFFMAN, E.J., PHELPS, M.E., KUHL, D.E., Quantitation in positron emission computed tomography: 2. Effects of inaccurate attenuation correction, J. Comput. Assist. Tomo. **3** (1979) 804–814.
[144] KINAHAN, P.E., TOWNSEND, D.W., BEYER, T., SASHIN, D., Attenuation correction for a combined 3D PET/CT scanner, Med. Phys. **25** (1998) 2046–2053.
[145] YAU, Y.Y., et al., Application of intravenous contrast in PET/CT: Does it really introduce significant attenuation correction error?, J. Nucl. Med. **46** (2005) 283–291.
[146] CARNEY, J., BEYER, T., BRASSE, D., YAP, J., TOWNSEND, D., Clinical PET/CT scanning using oral CT contrast agents, J. Nucl. Med. **45** (2002) 57P.
[147] ZAIDI, H., KORAL, K.F., Scatter modelling and compensation in emission tomography, Eur. J. Nucl. Med. Mol. Imaging **31** (2004) 761–782.
[148] SUREAU, F., et al., Impact of image-space resolution modeling for the high-resolution research tomograph, J. Nucl. Med. (2008) **49** (2008) 1000–1008.
[149] SORET, M., BACHARACH, S.L., BUVAT, I., Partial-volume effect in PET tumour imaging, J. Nucl. Med. **48** (2007) 932–945.
[150] TYLSKI, P., et al., Comparative assessment of methods for estimating tumour volume and standardized uptake value in (18)F-FDG PET, J. Nucl. Med. **51** (2010) 268–276.
[151] LABBÉ, C., et al., "Absolute PET Quantification with correction for partial volume effects within cerebral structures", Quantitative Functional Brain Imaging with Positron Emission Tomography (CARSON, R.E., DAUBE-WITHERSPOON, M.E. and HERSCOVITSCH, P. Eds), Academic Pr, San Diego, CA (1998).
[152] BOUSSION, N., et al., A multiresolution image based approach for correction of partial volume effects in emission tomography, Phys. Med. Biol. **51** (2006) 1857–1876.
[153] BRASSE, D., et al., Correction methods for random coincidences in fully 3D whole-body PET: Impact on data and image quality, J. Nucl. Med. **46** (2005) 859–867.
[154] LARSON, S.M., et al., Tumour treatment response based on visual and quantitative changes in global tumour glycolysis using PET-FDG imaging. The visual response score and the change in total lesion glycolysis, Clin. Positron Imaging **2** (1999) 159–171.
[155] GREGOIRE, V., HAUSTERMANS, K., GEETS, X., ROELS, S., LONNEUX, M., PET-based treatment planning in radiotherapy: A new standard?, J. Nucl. Med. **48 Suppl 1** (2007) 68S–77S.
[156] FORD, E.C., HERMAN, J., YORKE, E., WAHL, R.L., 18F-FDG PET/CT for image-guided and intensity-modulated radiotherapy, J. Nucl. Med. **50** (2009) 1655–1665.
[157] NEHMEH, S.A., et al., Effect of respiratory gating on reducing lung motion artifacts in PET imaging of lung cancer, Med. Phys. **29** (2002) 366–371.
[158] BEYER, T., et al., Respiration artifacts in whole-body (18)F-FDG PET/CT studies with combined PET/CT tomographs employing spiral CT technology with 1 to 16 detector rows, Eur. J. Nucl. Med. Mol. Imaging **32** (2005) 1429–1439.
[159] BOUCHER, L., RODRIGUE, S., LECOMTE, R., BENARD, F., Respiratory gating for 3-dimensional PET of the thorax: Feasibility and initial results, J. Nucl. Med. **45** (2004) 214–219.
[160] LIVIERATOS, L., et al., Rigid-body transformation of list-mode projection data for respiratory motion correction in cardiac PET, Phys. Med. Biol. **50** (2005) 3313–3322.
[161] NEHMEH, S.A., et al., Reduction of respiratory motion artifacts in PET imaging of lung cancer by respiratory correlated dynamic PET: Methodology and comparison with respiratory gated PET, J. Nucl. Med. **44** (2003) 1644–1648.
[162] BUNDSCHUH, R.A., et al., Postacquisition detection of tumour motion in the lung and upper abdomen using list-mode PET data: A feasibility study, J. Nucl. Med. **48** (2007) 758–763.
[163] DAWOOD, M., BUTHER, F., LANG, N., SCHOBER, O., SCHAFERS, K.P., Respiratory gating in positron emission tomography: A quantitative comparison of different gating schemes, Med. Phys. **34** (2007) 3067–3076.
[164] WANG, J., BYRNE, J., FRANQUIZ, J., MCGORON, A., Evaluation of amplitude-based sorting algorithm to reduce lung tumour blurring in PET images using 4D NCAT phantom, Comput. Meth. Prog. Bio. **87** (2007) 112–122.
[165] VISVIKIS, D., et al., Evaluation of respiratory motion effects in comparison with other parameters affecting PET image quality, IEEE Nuclear Science Symposium Conference Record (Proc. Conf. 2004 Rome), Institute of Electrical and Electronics Engineers, Piuscataway, NJ (2004) 3668–3672.
[166] RAHMIM, A., et al., Motion compensation in histogram-mode and list mode EM reconstructions: beyond the event-driven approach, IEEE Trans. Nucl. Sci. **51** (2004) 2588–2596.
[167] QIAO, F., PAN, T., CLARK, J.W., JR., MAWLAWI, O.R., A motion-incorporated reconstruction method for gated PET studies, Phys. Med. Biol. **51** (2006) 3769–3783.
[168] GROTUS, N., et al., Fully 4D List-mode reconstruction applied to respiratory-gated PET scans, Phys. Med. Biol. **54** (2009) 1705–1721.

[169] BLOOMFIELD, P.M., et al., The design and implementation of a motion correction scheme for neurological PET, Phys. Med. Biol. **48** (2003) 959–978.
[170] NATIONAL ELECTRICAL MANUFACTURERS ASSOCIATION, Performance Measurements of Positron Emission Tomographs (PETs), NEMA Standards Publication NU 2–2012, NEMA, Rosslyn, VA (2012).
[171] PARK, M.A., et al., Adsorption of metallic radionuclides on plastic phantom walls, Med. Phys. **35** (2008) 1606–1610.
[172] SEGARS, W.P., Development and Application of a New Dynamic NURBS-based Cardiac-Torso (NCAT) Phantom, Universiy of North Carolina (2001).

ABBREVIATIONS

CDR	collimator–detector response
COV	coefficient of variation
CT	computed tomography
DF	decay factor
EM	expectation maximization
FDG	fluorodeoxyglucose
FWHM	full width at half maximum
GTM	geometric transfer matrix
IV	intravenous
LEHR	low energy high resolution
LOR	line of response
MAP	maximum a posteriori
ML	maximum likelihood
MIBG	metaiodobenzylguanidine
ML-EM	maximum likelihood expectation maximization
MR	magnetic resonance
OS-EM	ordered subset expectation maximization
PET	positron emission tomography
PL	penalized likelihood
PSF	point spread function
PV	partial volume
PVC	partial volume correction
PVE	partial volume effect
QA	quality assurance
QC	quality control
RAMLA	row-action maximum-likelihood algorithm
RMSE	root mean square error
ROI	region of interest
SPECT	single photon emission computed tomography
SUV	standardized uptake value
TAC	time–activity curve
TEW	triple energy window
VOI	volume of interest

CONTRIBUTORS TO DRAFTING AND REVIEW

Buvat, I.	National Centre of Scientific Research, France
du Raan, H.	University of the Free State, South Africa
Frey, E.C.	Johns Hopkins University, United States of America
Green, A.J.	National Physical Laboratory, United Kingdom
Hutton, B.	University College London, United Kingdom
Ljungberg, M.	Lund University, Sweden
Palm, S.	International Atomic Energy Agency
Poli, G.L.	International Atomic Energy Agency

IAEA
International Atomic Energy Agency

No. 23

ORDERING LOCALLY

In the following countries, IAEA priced publications may be purchased from the sources listed below or from major local booksellers.

Orders for unpriced publications should be made directly to the IAEA. The contact details are given at the end of this list.

AUSTRALIA
DA Information Services
648 Whitehorse Road, Mitcham, VIC 3132, AUSTRALIA
Telephone: +61 3 9210 7777 • Fax: +61 3 9210 7788
Email: books@dadirect.com.au • Web site: http://www.dadirect.com.au

BELGIUM
Jean de Lannoy
Avenue du Roi 202, 1190 Brussels, BELGIUM
Telephone: +32 2 5384 308 • Fax: +32 2 5380 841
Email: jean.de.lannoy@euronet.be • Web site: http://www.jean-de-lannoy.be

CANADA
Renouf Publishing Co. Ltd.
5369 Canotek Road, Ottawa, ON K1J 9J3, CANADA
Telephone: +1 613 745 2665 • Fax: +1 643 745 7660
Email: order@renoufbooks.com • Web site: http://www.renoufbooks.com

Bernan Associates
4501 Forbes Blvd., Suite 200, Lanham, MD 20706-4391, USA
Telephone: +1 800 865 3457 • Fax: +1 800 865 3450
Email: orders@bernan.com • Web site: http://www.bernan.com

CZECH REPUBLIC
Suweco CZ, spol. S.r.o.
Klecakova 347, 180 21 Prague 9, CZECH REPUBLIC
Telephone: +420 242 459 202 • Fax: +420 242 459 203
Email: nakup@suweco.cz • Web site: http://www.suweco.cz

FINLAND
Akateeminen Kirjakauppa
PO Box 128 (Keskuskatu 1), 00101 Helsinki, FINLAND
Telephone: +358 9 121 41 • Fax: +358 9 121 4450
Email: akatilaus@akateeminen.com • Web site: http://www.akateeminen.com

FRANCE
Form-Edit
5 rue Janssen, PO Box 25, 75921 Paris CEDEX, FRANCE
Telephone: +33 1 42 01 49 49 • Fax: +33 1 42 01 90 90
Email: fabien.boucard@formedit.fr • Web site: http://www.formedit.fr

Lavoisier SAS
14 rue de Provigny, 94236 Cachan CEDEX, FRANCE
Telephone: +33 1 47 40 67 00 • Fax: +33 1 47 40 67 02
Email: livres@lavoisier.fr • Web site: http://www.lavoisier.fr

L'Appel du livre
99 rue de Charonne, 75011 Paris, FRANCE
Telephone: +33 1 43 07 50 80 • Fax: +33 1 43 07 50 80
Email: livres@appeldulivre.fr • Web site: http://www.appeldulivre.fr

GERMANY
Goethe Buchhandlung Teubig GmbH
Schweitzer Fachinformationen
Willstätterstrasse 15, 40549 Düsseldorf, GERMANY
Telephone: +49 (0) 211 49 8740 • Fax: +49 (0) 211 49 87428
Email: s.dehaan@schweitzer-online.de • Web site: http://www.goethebuch.de

HUNGARY
Librotade Ltd., Book Import
PF 126, 1656 Budapest, HUNGARY
Telephone: +36 1 257 7777 • Fax: +36 1 257 7472
Email: books@librotade.hu • Web site: http://www.librotade.hu

INDIA
Allied Publishers
1st Floor, Dubash House, 15, J.N. Heredi Marg, Ballard Estate, Mumbai 400001, INDIA
Telephone: +91 22 2261 7926/27 • Fax: +91 22 2261 7928
Email: alliedpl@vsnl.com • Web site: http://www.alliedpublishers.com

Bookwell
3/79 Nirankari, Delhi 110009, INDIA
Telephone: +91 11 2760 1283/4536
Email: bkwell@nde.vsnl.net.in • Web site: http://www.bookwellindia.com

ITALY
Libreria Scientifica "AEIOU"
Via Vincenzo Maria Coronelli 6, 20146 Milan, ITALY
Telephone: +39 02 48 95 45 52 • Fax: +39 02 48 95 45 48
Email: info@libreriaaeiou.eu • Web site: http://www.libreriaaeiou.eu

JAPAN
Maruzen Co., Ltd.
1-9-18 Kaigan, Minato-ku, Tokyo 105-0022, JAPAN
Telephone: +81 3 6367 6047 • Fax: +81 3 6367 6160
Email: journal@maruzen.co.jp • Web site: http://maruzen.co.jp

NETHERLANDS
Martinus Nijhoff International
Koraalrood 50, Postbus 1853, 2700 CZ Zoetermeer, NETHERLANDS
Telephone: +31 793 684 400 • Fax: +31 793 615 698
Email: info@nijhoff.nl • Web site: http://www.nijhoff.nl

Swets Information Services Ltd.
PO Box 26, 2300 AA Leiden
Dellaertweg 9b, 2316 WZ Leiden, NETHERLANDS
Telephone: +31 88 4679 387 • Fax: +31 88 4679 388
Email: tbeysens@nl.swets.com • Web site: http://www.swets.com

SLOVENIA
Cankarjeva Zalozba dd
Kopitarjeva 2, 1515 Ljubljana, SLOVENIA
Telephone: +386 1 432 31 44 • Fax: +386 1 230 14 35
Email: import.books@cankarjeva-z.si • Web site: http://www.mladinska.com/cankarjeva_zalozba

SPAIN
Diaz de Santos, S.A.
Librerias Bookshop • Departamento de pedidos
Calle Albasanz 2, esquina Hermanos Garcia Noblejas 21, 28037 Madrid, SPAIN
Telephone: +34 917 43 48 90 • Fax: +34 917 43 4023
Email: compras@diazdesantos.es • Web site: http://www.diazdesantos.es

UNITED KINGDOM
The Stationery Office Ltd. (TSO)
PO Box 29, Norwich, Norfolk, NR3 1PD, UNITED KINGDOM
Telephone: +44 870 600 5552
Email (orders): books.orders@tso.co.uk • (enquiries): book.enquiries@tso.co.uk • Web site: http://www.tso.co.uk

UNITED STATES OF AMERICA
Bernan Associates
4501 Forbes Blvd., Suite 200, Lanham, MD 20706-4391, USA
Telephone: +1 800 865 3457 • Fax: +1 800 865 3450
Email: orders@bernan.com • Web site: http://www.bernan.com

Renouf Publishing Co. Ltd.
812 Proctor Avenue, Ogdensburg, NY 13669, USA
Telephone: +1 888 551 7470 • Fax: +1 888 551 7471
Email: orders@renoufbooks.com • Web site: http://www.renoufbooks.com

United Nations
300 East 42nd Street, IN-919J, New York, NY 1001, USA
Telephone: +1 212 963 8302 • Fax: 1 212 963 3489
Email: publications@un.org • Web site: http://www.unp.un.org

Orders for both priced and unpriced publications may be addressed directly to:

IAEA Publishing Section, Marketing and Sales Unit, International Atomic Energy Agency
Vienna International Centre, PO Box 100, 1400 Vienna, Austria
Telephone: +43 1 2600 22529 or 22488 • Fax: +43 1 2600 29302
Email: sales.publications@iaea.org • Web site: http://www.iaea.org/books

INTERNATIONAL ATOMIC ENERGY AGENCY
VIENNA
ISBN 978–92–0–141510–3
ISSN 2074–7667